Nanostructured Gel-Phase Materials for Arsenic Removal from Water

Matthew Jack Fogarty

MSc By Research

University of York

Chemistry

January 2019

Abstract

Arsenic is present naturally in groundwater in many countries around the world; it affects over 140 million people in the world. Consumption of arsenic contaminated water has resulted in arsenic been named by the World Health Organisation (WHO) as one of the top 10 chemicals of public health concern, due to the toxicity of arsenic contaminated drinking water. Current commercial arsenic adsorbents such as activated carbon have low adsorption capacities.

In this work, self-assembled cationic C16-DAPMA micelles based on palmitic acid and 3,3'-diamino-*N*-methyldipropylamine were investigated for interactions with arsenite (As III) and arsenate (As V). The properties of a gelator based on dibenzylidene sorbitol functionalized with hydrazide groups (DBS-$CONHNH_2$) was investigated as a support for the micelles. The embedding of C16-DAPMA micelles into DBS-$CONHNH_2$ hydrogels was investigated to determine whether it was suitable for use as an arsenic removal system.

It was found that the C16-DAPMA micelles could bind arsenate through electrostatic interactions, due to the fact that arsenate exists as an anion in water. It was found that at 3.49 mM of arsenate, aggregation between arsenate and C16-DAPMA micelles occurred. It was found that C16-DAPMA micelles could be embedded into DBS-$CONHNH_2$ hydrogels. The presence of C16-DAPMA micelles within DBS-$CONHNH_2$ resulted in stiffer hydrogels, as C16-DAPMA micelles limited the entanglement of the self-spanning network and reduced its flexibility. It was found that C16-DAPMA micelles embedded within the DBS-$CONHNH_2$ hydrogels (with agarose for added stability) were able to reduce the concentration of arsenate from 298 ppb to an estimated value of between 80 to 100 ppb.

This work demonstrated that C16-DAPMA micelles embedded within DBS-$CONHNH_2$ hydrogels have potential to be used as an alternative water filtration system due to cheap nature of the materials compared to commercial adsorbents. However, further work is required to prevent leaching of the micelles from the hydrogel network.

Table Contents

List of Tables

List of Figures

List of Schemes

Acknowledgements

I would like to thank my supervisor Professor David Smith for the supervision throughout my masters and helping me develop, in both my scientific knowledge and as a person, for which I will be forever grateful. I would also like to thank all technical staff at the University of York for all the hard work they do.

I would like to thank all the Smith group members, for everything they have done from helping me to develop as a person. I would like to thank Kirsten, Phill and Anna each individually for everything they have done from teaching me squash, to taking me to the pharmacy when I needed to go, but most importantly being great friends. I would also like to thank Dr. Petr Slavik, Dr. Carmen Piras, Dr. Ana Rodrigo and Dr. Buthaina Albanyan for not only being postdocs within the group but being friends as well.

I would also like to thank friends in the Paul Clarke group for friendship and cakes throughout my masters.

Finally I would like to thank my mum and dad and the rest of my family, for being so supportive, not just during my masters but my entire lifetime, for which I am ever grateful.

Declaration

I declare that this thesis is a presentation of original work and I am the sole author. This work has not previously been presented for an award at this, or any other, University. All sources are acknowledged as References.

1.0 Introduction

1.1 Supramolecular Gels

Supramolecular chemistry is a key area of modern chemistry. It uses non-covalent interactions between molecules such as electrostatic interactions, van der Waals forces, hydrogen bonds, π – π interactions and hydrophilic / hydrophobic interactions.[1,2]

Supramolecular chemistry has gained a lot of attention over the past few years after supramolecular chemists won the Nobel Prize for chemistry in 1987 and 2016.[3,4] In 2016 Jean-Pierre Sauvage, Fraser Stoddart and Bernard Feringa won the Nobel Prize for their work on the design and production of molecular machines.[4] In 1983 Jean-Pierre Sauvage designed catenanes, which have two or more macrocycles interlocked together. In 1991, Fraser Stoddart designed rotaxanes, in which a macrocycle was threaded onto an axle and able to move along the axle with external stimuli but was prevented from untethering by the presence of bulky stoppers. The work by Sauvage and Stoddart used supramolecular interactions as a key strategy for achieving molecular interlocking.

The Nobel Prize was awarded to Donald Cram, Jean-Marie Lehn and Charles Pedersen in 1987 for using supramolecular interactions in their development and use of molecular receptors for the host guest binding of cations, anions and neutral molecules.[3] For example, Charles Pederson in 1967 discovered crown ethers, and it was shown that depending on the size of the crown ether, there was preferential binding of metal cations depending on their own size, *via* electrostatic interactions with the oxygen present in the crown either. The reason for preferential binding was due to optimal spatial fit.

Supramolecular molecules are often designed so that the molecules will spontaneously self-assemble into a complex or higher order structures under a defined set of conditions.[5,6] These complex or higher order structures are held together *via* non-covalent interactions such as those mentioned above.[6] An example of self-assembly is cryptands, first discovered by the Lehn group.[7] Cryptands are a type of molecule that have a cavity; within the cavity it is possible to capture and encapsulate certain species

such as metal ions, hence creating a higher order structure.[7,8] Micelles are cluster molecules that self-assemble; they self-assemble in liquids, for example water.[9,10] An amphiphile, which is a molecule that contains a hydrophobic and hydrophilic part within the same molecule, can form micelles. Usually the molecules which form micelles will contain a hydrophobic tail which aggregate together due to hydrophobic interactions and a hydrophilic head group which encapsulates the hydrophobic tails.[9,10] Work by Aggeli *et al.* investigated the use of peptide β-sheets in the design of oligopeptides that self-assemble into β-sheet tapes, which then become entangled forming gels.[11]

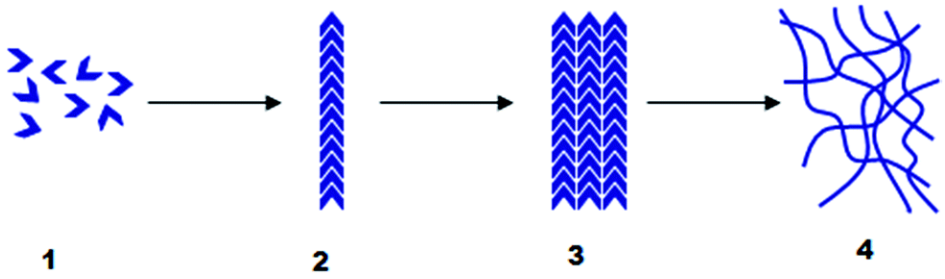

Figure 1.1.1 Schematic representation showing how supramolecular gels forms. LMWGs molecules (1), assemble into fibrils (2), bundle into fibres (3), then entangle to form a gel network (4).[12]

Supramolecular gels are a class of self-assembled supramolecular materials that have been the focus of much recent research. A gel is defined as a viscoelastic solid-like material made up of a crosslinked network, which entraps liquid within the network.[13,14] They form gel-phase materials from Low Molecular Weight Gelators (LMWGs).[15] LMWGs self-assemble as shown in Figure 1.1.1 into gel networks using supramolecular interactions as mentioned above.[12] Initially they form fibrils through non-covalent interactions. These then bundle into fibres that ultimately form a sample-spanning network.

Hydrogels are gels in which the liquid component is water. LMWGs and polymers are able to form hydrogels. There has been more research conducted into polymer based gels compared to LMWGs gels.[16] Polymeric gels have a greater mechanical strength when compared to LMWGs gels, however they are less tuneable and are less responsive to external stimuli. The advantages of LMWGs gels compared to polymeric gels are due to LMWGs being small molecules that assemble into a higher order structures to form gels, LMWGs molecules can be easily changed.[17] This then results in a change in the properties

of the gels.[18] LMWGs can form gels *via* many different ways, including a heat-cool cycle and pH-switching. Gels that form *via* pH-switching are reversible, which is another advantage of using LMWGs gels compared with polymeric gels.

LMWGs have numerous applications; they can be used for tissue engineering due to tissue compatibility. Supramolecular gels can also be used for sensing of certain elements due to the design of LMWGs, they can undergo a transition between gel phase and liquid phase in the presence of certain elements.[18]

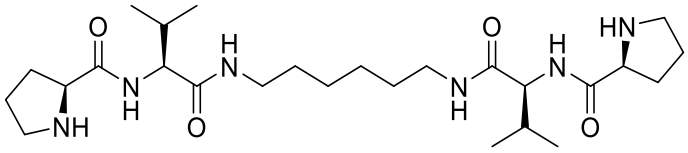

Figure 1.1.2 Structure of L-proline-L-valine dipeptide derivative gelator developed by Escuder and co-workers.[19]

Supramolecular gels can also be used as catalysts. For example, Escuder and co-workers synthesised an L-proline-L-valine dipeptide derivative (Figure 1.1.2), which self-assembled into an organogel in toluene.[19] The organogel was shown to be a good catalyst for the conjugate addition of cyclohexanone to trans-β-nitrostyrene that gave a product yield of 99 % and 34 % enantiomeric excess. The use of the chiral gel leads to the stereoselectivity.

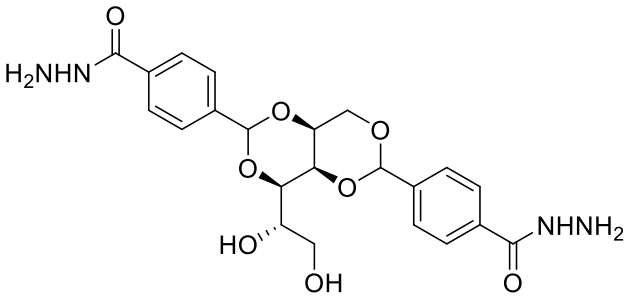

Figure 1.1.3 Structure of DBS-CONHNH$_2$

LMWGs such as p,p'-dihydraza-1,3: 2,4-dibenzylidene-D-Sorbitol (DBS-CONHNH$_2$) shown in Figure 1.1.3 self-assemble *via* non-covalent interactions to form gels. Work by the Smith group investigated the encapsulation and release of mesalazine, naproxen and ibuprofen (Figure 1.1.4) pharmaceutical ingredient, from DBS-CONHNH$_2$ hydrogels.[20]

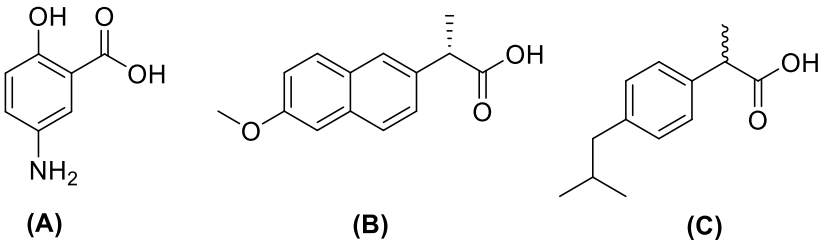

Figure 1.1.4 Structures of mesalazine (A), naproxen (B) and ibuprofen (C)

Later work by Chivers and Smith investigated the release of naproxen (Figure 1.1.4) at different pH values, for potential use as a topical drug release medium.[16] The DBS-$CONHNH_2$ hydrogels were found to incorporate > 92 % of naproxen, which was bound to the self-assembled DBS-$CONHNH_2$ hydrogel nanofibers. When the DBS-$CONHNH_2$ hydrogel with naproxen incorporated was exposed to pH 5.5 buffered solution, 80-90 % of naproxen was released. This shows its feasibility for transdermal drug delivery as the pH of skin is 5.4 – 5.9.

1.2 Environmental Remediation using Supramolecular Gels

Supramolecular gels can also be used for environmental remediation. LMWGs gels have many reasons why they may be suitable for use in environmental remediation. They have a relatively of the low cost of synthesis and the gels are porous materials that allow water to diffuse through the network.[18] This means that using specific interactions between the pollutant and the gel, the pollutant could be immobilised onto the gel network. The final advantage is that due to the gels being porous, they have a large surface area which means they could have high adsorption capacity for the uptake of pollutants.

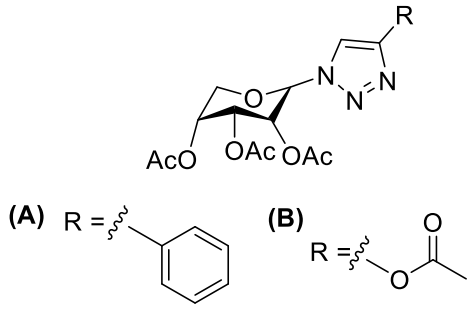

Figure 1.2.1 Structures of triazolylarabinoside derivatives developed by Rajkamal *et al.* [21]

As an example Rajkamal *et al.* designed two different triazolylarabinoside derivatives LMWGs (Figure 1.2.1), which showed the ability to extract petrol from water. They were able to achieve this by forming a gel only with petrol in a mixture of water and petrol.[21] Gelation occurred when a hot solution of the LMWGs and was added to the biphasic system. This system has the potential application of using supramolecular gels for environmental remediation of crude oil from water. This requires the gel to have enough mechanical strength to be removed intact from the water and to withstand environmental conditions.

1.2.1 Using Supramolecular Gels for the Removal of Dyes

There have been numerous examples of the removal of dyes and metals using supramolecular gels in a controlled laboratory environment. These systems have the potential to act as a water filtration system purifying water within industrial processes. If the dyes were to be released into the environment they would have a negative impact on humans and the environment, therefore it is an important area of research. Dyes are commonly used in industries such as textiles, leather, cosmetics and many more; there are over 700,000 tonnes a year of dyes produced a year.[22,23] It is estimated that of the 700,000 tonnes produced, 50,000 tonnes is released into the environment every year.[24] The dyes that are released into the environment contribute to water contamination, which has become a global issue due to industrial development.[24] Once in water, these dyes affect aquatic ecosystems, the ecology as a whole and also the human body in regard to the immune system and reproductive system.[22,25] Metal ions in water can also be toxic to biological systems.[26] Systems for environmental remediation need to be simple to use, low cost, have a high adsorption capacity and have a fast removal rate of

the contaminant.[24] Supramolecular gels fit many of these criteria due to the cheap nature of the material, as well as the possibility to have high adsorption capacities.

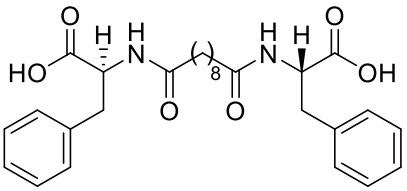

Figure 1.2.2 Structure of phenylalanine-based bolaamphiphile hydrogelator developed by Ray *et al.*[27]

The use of supramolecular gels for environmental remediation has been an area of study for over 10 years. Early examples include work by Ray *et al.* in 2006, who synthesised a phenylalanine-based bolaamphiphile hydrogelator (Figure 1.2.2) which formed hydrogels between pH values 6.5 – 7.2 in the presence of divalent salts ($MnCl_2$, $CoCl_2$, $CuSO_4$, and $NiCl_2$) after sonication.[27] The gels had the ability to remove dyes from a contaminated environment. Absorption by the hydrogel was investigated, by placing a dried hydrogel (xerogel) in 7 mL of buffered solution at pH 6.5. The dyes investigated were Crystal Violet (a cationic dye) and Naphthol Blue Black (an anionic dye) (Figure 1.2.3). Most of the dye solution was adsorbed onto the xerogel after 24 hours. The maximum adsorption capacities for Crystal Violet and Naphthol Blue Black were 63 mg g^{-1} and 84 mg g^{-1} respectively (reported in milligrams of pollutant adsorbed per gram of adsorbent). One disadvantage of this early use in environmental remediation was that dye adsorption was carried out in buffered solution, which may have facilitated the process and is not representative of the dye in water. Another issue was the low adsorption capacity of the hydrogel. However, despite these issues, the work by Ray *et al.* proved the principle that supramolecular hydrogels could adsorb both cationic and anionic dyes.

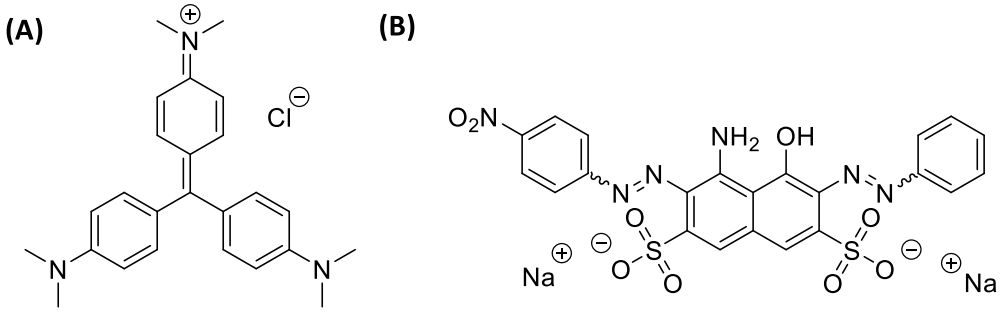

Figure 1.2.3 Structures of dyes Crystal Violet (A) and Naphthol Blue Black (B)

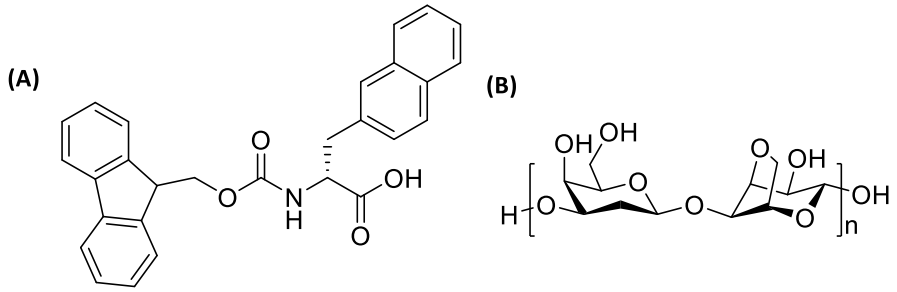

Figure 1.2.4 Structures of hybrid hydrogel used by Wang *et al.* used to investigate the removal of Methyl Violet using fmoc-3-(2-naphthyl)-D-alanine hydrogelator (A) and agarose polymeric gelator (B).[28]

Wang *et al.* used an fmoc-3-(2-naphthyl)-D-alanine gelator combined with agarose (Figure 1.2.4), a polymeric gelator, to form a hydrogel with good mechanical strength.[28] The removal of Methyl Violet (Figure 1.2.5) (an cationic dye) was investigated. It was found after 48 hours that 96 % of the dye was removed without any external stimuli. The adsorption of Methyl Violet using just the hydrogel without agarose present was 95.1 %, which showed that the presence of agarose has little effect on the adsorption of the dye. The adsorption capacity of the hybrid hydrogel was shown to be 1080 mg g^{-1}, which represents a high adsorption capacity. It was found that on stirring for after 24 hours, the adsorption onto the hybrid hydrogel was increased to 98 %. This work only investigated the uptake of cationic dyes and not anionic dyes.

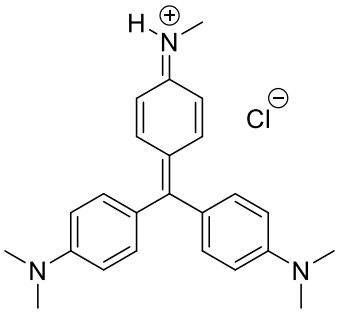

Figure 1.2.5 Structure of Methyl Violet Dye

Hao *et al.* investigated the adsorption of anionic dyes using a hybrid hydrogel of folic acid LMWGs (Figure 1.2.6) and gelatin, which is a polymeric gel.[2] The hybrid hydrogel was formed in a mixture of *N*-methylpyrrolidine (NMP) and H_2O in a ratio of 1:1. The self-assembly process showed the interactions between both molecules were hydrogen bonding and π-π interactions. Dye adsorption using this hybrid hydrogel was investigated

using Congo Red (anionic dye), Methyl Blue (anionic dye) and Methyl Orange (anionic dye) (Figure 1.2.7).

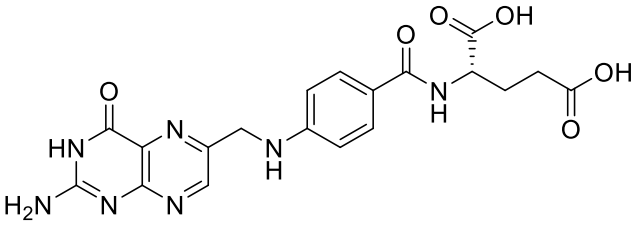

Figure 1.2.6 Structure of folic acid gelator used by Hao *et al.* [2]

The hybrid hydrogel adsorbed 64 % of Congo Red, 68 % of Methyl Blue and 44 % of Methyl Orange. This gave the folic acid gel, dye adsorption capacities for Congo Red of 372 mg g^{-1} and Methyl Blue of 433 mg g^{-1}. However the use of NMP in gel formation is not desirable owing to the toxicity of this solvent.

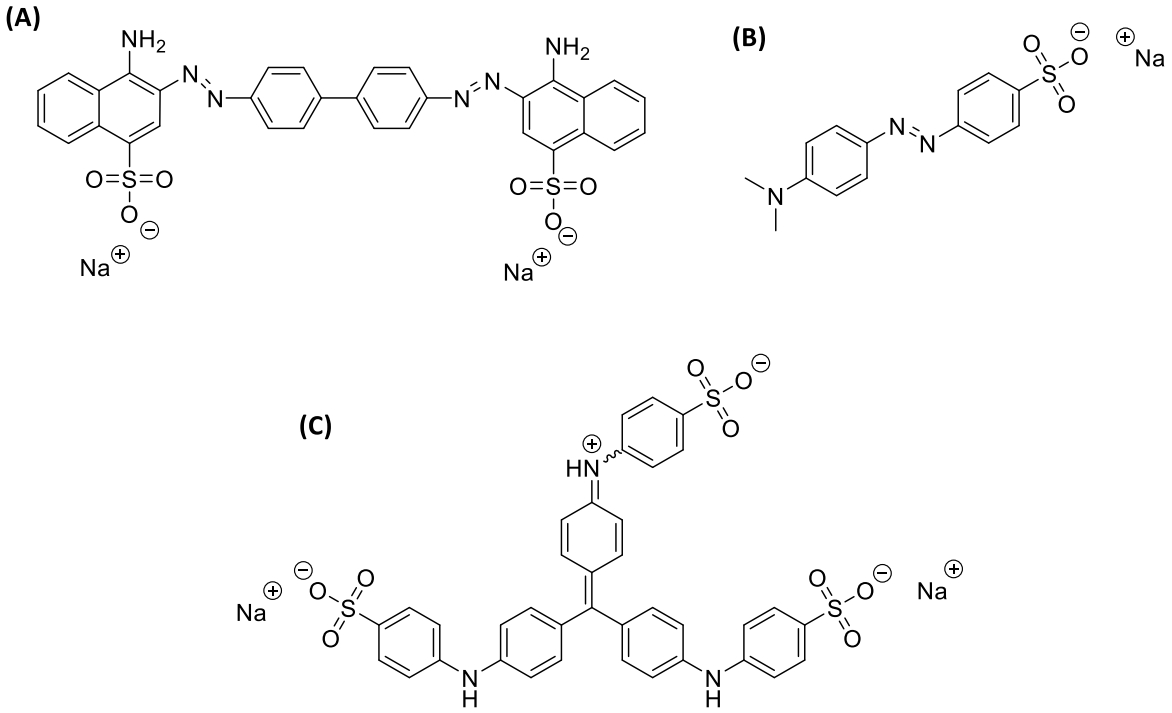

Figure 1.2.7 7 Structures of dyes Congo Red (A), Methyl Orange (B) and Methyl Blue (C)

Hayes and co-workers developed a pH-responsive bisaromatic hydrogelator (Figure 1.2.8) that, as well as being able to form hydrogels when the pH is changed, can also form hydrogels *via* a heat cool-cycle in the presence of a small amount of methanol or DMSO.[29]

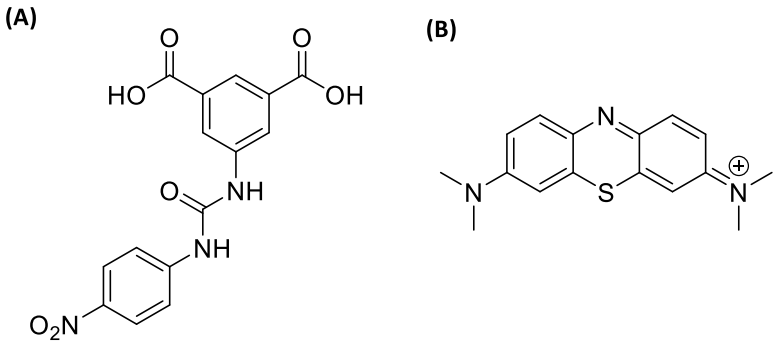

Figure 1.2.8 Structure of hydrogelator developed by Hayes and co-workers based on bisaromatic (A) and Methylene Blue (B).[29]

The adsorption of Methylene Blue (cationic dye) (Figure 1.2.8) and Methyl Violet (cationic dye) (Figure 1.2.5) was investigated; it was found that 98 % and 97 % respectively of the dye solutions were adsorbed after 48 hours. The disadvantage of work by Hayes and co-workers is that the adsorption of the dye onto the hydrogel was over a long time frame (48 hours). In this study a 1 mL hydrogel was used to investigate the dye adsorption of a 1 mL solution. Hayes and co-workers also investigated the uptake of Indigo Carmine (an anionic dye) (Figure 1.2.9) onto the hydrogel. When the uptake of this dye onto the hydrogel was studied it was found that less than 1 % was adsorbed. As a result, it could potentially be used for selective uptake of cationic dyes from a mixture of anionic and cationic dyes.

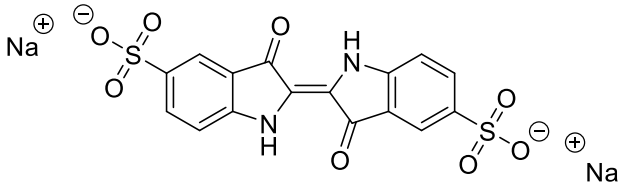

Figure 1.2.9 Structure of Indigo Carmine dye

Han *et al.* designed two different dual component gelators to investigate the preferential uptake of anionic or cationic dyes depending on which gelator used.[30] (Figure 1.2.10) The two different hydrogels had different morphologies when imaged, as well as having different zeta potentials with opposite electrical charges as a result of having either carboxylate or ammonium groups.

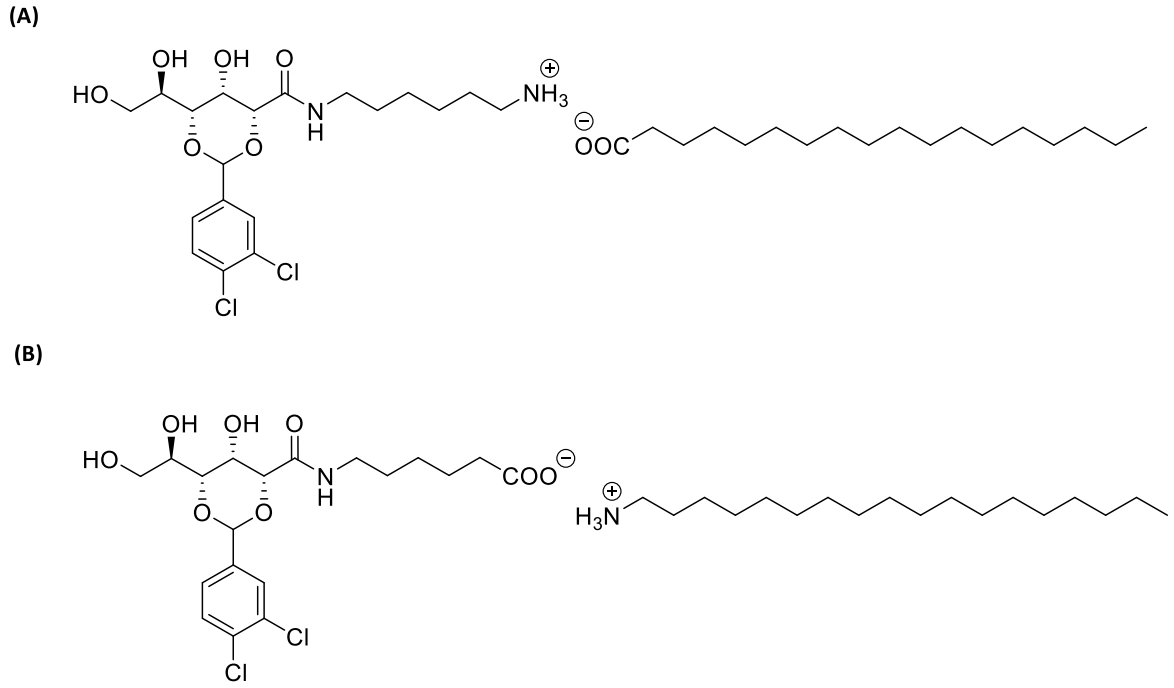

Figure 1.2.10 Structures of gelators designed by Han *et al.* C6 – A16 (A) and D6 – B16 (B).[30]

The dye adsorptions of both xerogels (dried gel network where solvent has been removed) were investigated using the cationic dyes Methyl Orange (Figure 1.2.7), Eosin Y (Figure 1.2.11), Acid Fuchsin (Figure 1.2.11) and the anionic dyes Crystal Violet (Figure 1.2.3), Methylene Blue (Figure 1.2.8) and Rhodamine 6G (Figure 1.2.11). It was shown that for D6 – B16 all of the anionic dyes had been adsorbed after 24 hours but the cationic dyes were not all adsorbed. The C6 – A16 xerogel was shown to adsorb some of cationic dyes but all of Crystal Violet was adsorbed. This showed that the xerogels had selective removal of dyes depending of which gelator combination was chosen. The maximum adsorption capacities for C6 – A16 with Crystal Violet were 1094 mg g^{-1} and for D6 – B16 with Eosin Y was 841 mg g^{-1}. The recyclability of the xerogels was also investigated by washing with acetonitrile to remove the dyes. Even after 4 cycles the xerogel still had adsorption capacities in certain cases of above 95 %.

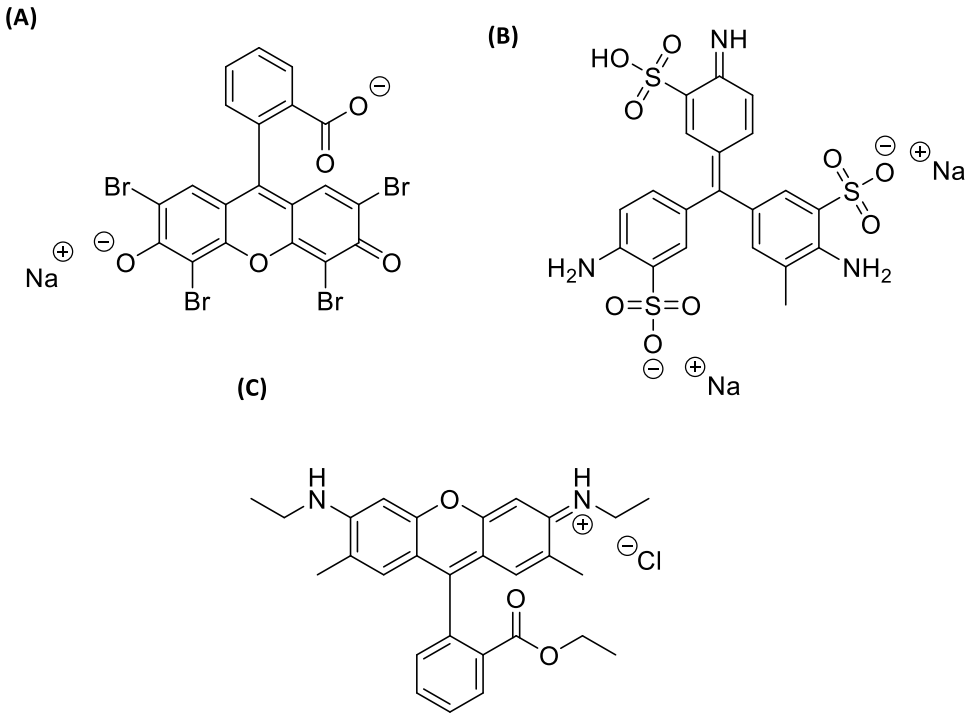

Figure 1.2.11 Structures of dyes Eosin Y (A), Acid Fuchsin (B) and Rhodamine 6G(C)

1.2.2 Using Supramolecular Gels for the Removal of Metals

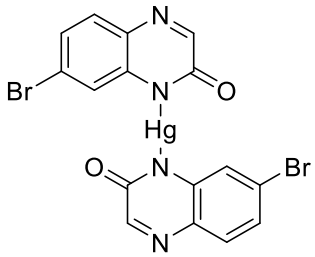

Figure 1.2.12 Structure of gelator designed by Carter *et al.*[31]

Supramolecular gels have applications for environmental remediation other than removal of dyes, such as the removal of metal ions. Carter *et al.* used supramolecular gels for the extraction of mercury (II) ions from water.[31] It was found that when a solution of mercury (II) was added to the gelator (Figure 1.2.12) in methanol, gelation occurred and extracted > 98 % of mercury. In the absence of mercury (II), gelation in water did not occur.

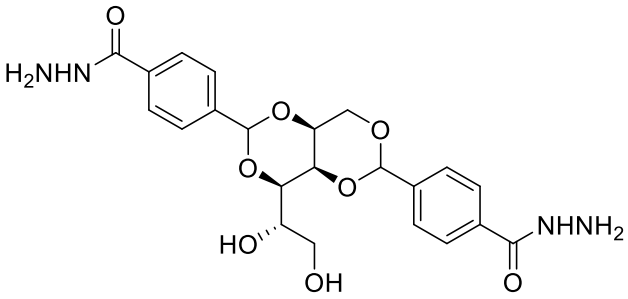

Figure 1.2.13 Structure of DBS-CONHNH$_2$ developed by Smith and co-workers.[32]

Work by Smith and co-workers used DBS-CONHNH$_2$ (Figure 1.2.13) to investigate the extraction of metals from water after 48 hours.[32] Investigation of the extraction of gold and silver salts found that DBS-CONHNH$_2$ had an extraction capacity for gold and silver of 2000 mg g^{-1} and 900 mg g^{-1} respectively (reported in milligrams of metal ion adsorbed per gram of adsorbent e.g. gelator) It was found that the hydrazide on DBS-CONHNH$_2$ reduced the metals within the gel network to form nanoparticles in situ, with a diameter of 5-10 nm. The incorporation of nanoparticles into the gel network showed electrochemical activity, which could have potential for a high value application.

Slavik *et al.* used DBS-CONHNH$_2$ (Figure 1.2.13) and agarose, a polymeric hydrogel for added mechanical stability, to investigate the extraction of palladium from aqueous solution.[33] It was found that after 48 hours, the DBS-CONHNH$_2$ hydrogel was capable of efficiently extracting palladium from aqueous solution, reducing it to form nanoparticles. It was shown that the gel with incorporated palladium nanoparticles was capable of being used as a catalyst for Suzuki reactions.

Work by Okesola and Smith on the extraction of metals using DBS-CONHNH$_2$, found it is capable of removing Cd^{2+}, Pb^{2+}, Hg^{2+} and As^{3+} from pH 6.5 solution.[34] The adsorption capacities for Cd^{2+}, Pb^{2+}, Hg^{2+} and As^{3+} were 312 mg g^{-1}, 458 mg g^{-1}, 760 mg g^{-1}, and 156 mg g^{-1} respectively. All the metals except As^{3+} had high adsorption capacities; this was probably due to all of the metals being cationic in pH 6.5 solution, except for As^{3+} which exists as an anion. It was thus shown that DBS-CONHNH$_2$ had the ability to adsorb a variety of cationic metals from pH 6.5 solution with high adsorption capacities, whereas adsorbing anionic metal ions resulted in the low adsorption capacities.

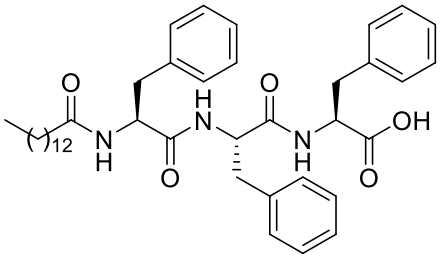

Figure 1.2.14 Structure of gelator Designed By Basak *et al.*[25]

Basak *et al.* designed a triphenylalanine based gelator (Figure 1.2.14), that formed gels in water; the gel was shown to shrink and expel water due to its hydrophobic nature, which limited the use as a water filtration system.[25]

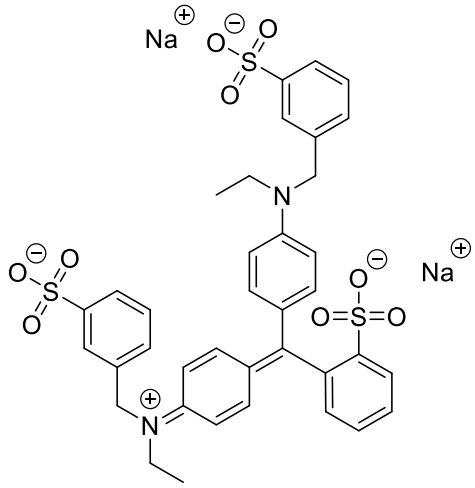

Figure 1.2.15 Structure of Brilliant Blue

The ability of the gel to remove Methylene Blue (cationic dye) (Figure 1.2.8), Brilliant Blue (anionic dye) (Figure 1.2.15) and Pb^{2+} ions was investigated. It was found that when the solution of Pb^{2+} ions and gelator was heated, on gelation the solution expelled from the gel contained 98 % less lead. The amount of dye removed using the gel was found to be > 99.5 %. However, as the solution needed to be heated for the removal of Pb^{2+} to occur, this could limit the effectiveness for waste water treatment.

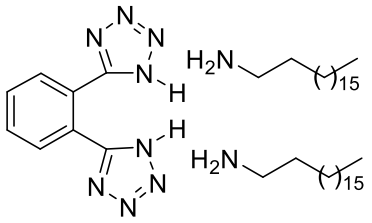

Figure 1.2.16 Structure of organogelator developed by Yan *et al.*[26]

Yan *et al.* developed a two component supramolecular gel (Figure 1.2.16) using a tetrazolyl derivative with octadecylamine, which was found to form gels in cyclohexane.[26] An investigation of removal of Cu^{2+} and Fe^{2+} from aqueous solution was conducted. It was found that the adsorption capacities for the gel for Cu^{2+} and Fe^{2+} were 1105 mg g^{-1} and 238 mg g^{-1} respectively. The gel was also shown to remove cationic and anionic dyes as well as a combination of dyes and metal at the same time.

There is a reasonable amount of literature (some mentioned above) regarding the use of supramolecular gels for environmental remediation for the removal of cationic and anionic dyes with high adsorption capacities. The removal of several metal ions has also been demonstrated, although these were mostly cations and not anions. Work by Okesola and Smith showed the adsorption of arsenic as an anion but with a low adsorption capacity. Indeed, arsenic remediation remains a significant environmental problem.

1.3 Arsenic Remediation using Supramolecular Chemistry

Arsenic is present naturally in groundwater in many countries, such as Argentina, Chile, Mexico, China, Bangladesh and India.[35] The most common arsenic species in water are arsenite (As (III)) and arsenate (As (V)) (Figure 1.3.1).[36]

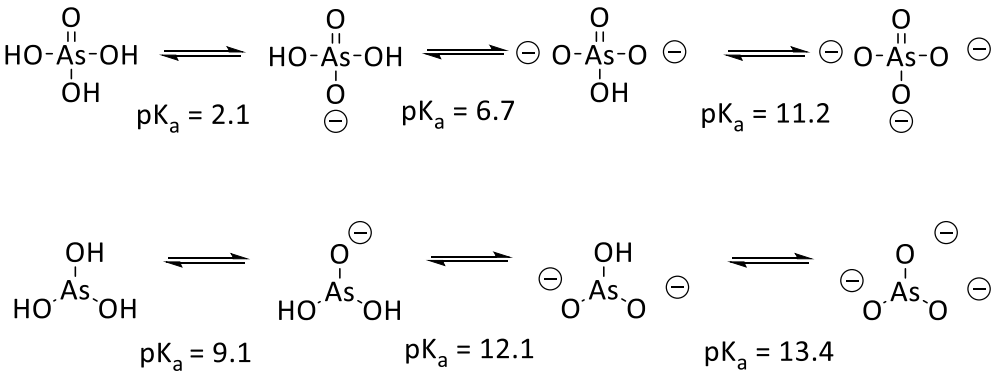

Figure 1.3.1 Showing speciation of arsenic present in water, arsenate (As (V)) (A) and arsenite (As (III)) (B) with associated pK$_a$ values.[36]

The concentration of arsenic present in groundwater depends on the location, with the range of arsenic present varying from 0.5 parts per billion (ppb) to over 5000 ppb.[35] Prior to January 2006, the World Health Organisation (WHO) had a recommended maximum limit of arsenic in drinking water of 50 ppb. Since then, the maximum limit of arsenic in drinking water has been lowered to 10 ppb.[37,38] There are several ways for arsenic to enter water *via* geological activity such as weathering of rocks, oxidation and leaching; however, arsenic is also found in water due to industrial processes such as mining.[35,39] The normal concentration of arsenic in water is below 10 ppb; but in a region of India near Bangladesh, reported concentrations of arsenic in water are up to 295 ppb.[35,40] It is estimated that worldwide over 140 million people are affected by arsenic contaminated drinking water with concentrations of above 10 ppb.[41] Arsenic contaminated water is a significant problem due to the toxicity of arsenic to humans. Long term consumption of contaminated drinking water causes chronic diseases such as lung, kidney and prostate cancer, as well as cardiovascular, neurological, respiratory and bladder problems.[39,42] For this reason, the WHO has placed arsenic on the list of 10 chemicals of major public health concern.[43,44] Currently, arsenic is most commonly removed from water *via* 3 methods; oxidation / precipitation, coagulation / co-precipitation, ion-exchange and adsorption.[45] For an arsenic removal system to be effective, it should a have fast removal process, high adsorption capacities and be relativity simple and inexpensive.[43,45] However, current commercial adsorbents for arsenic removal, such as activated carbon, activated alumina and zeolites, have adsorption capacities of less than 100 mg g^{-1}.[43]

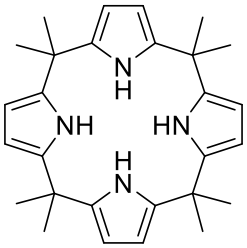

Figure 1.3.2 Structure of calix[4]pyrrole used by Danil de Namor *et al.*[46]

There have been a number of reports describing supramolecular chemistry for arsenic removal. One example from Danil de Namor *et al.* used calix[4]pyrrole (Figure 1.3.2) to investigate the removal of arsenite and arsenate from solution. It was found that due to the limited solubility of calix[4]pyrrole, it could be used as a solid-phase support for the removal.[46] The calix[4]pyrrole was able to adsorb arsenate and arsenite, with the binding site being the hydrogen bond donor NH group on the calix[4]pyrrole. The adsorption capacity of calix[4]pyrrole for arsenite and arsenate was 14 mg g^{-1} and 15 mg g^{-1} respectively. The ability for the calix[4]pyrrole to adsorb arsenate in competition with other anions such as phosphate and fluoride, which are present in water, was also investigated. It was found that the amount of arsenate adsorbed onto the calix[4]pyrrole changed from 98 % to 30 % when in competition with other anions. This work therefore showed it was possible to adsorb arsenic using supramolecular chemistry, but compared to commercial adsorbents the adsorption capacity was much lower.

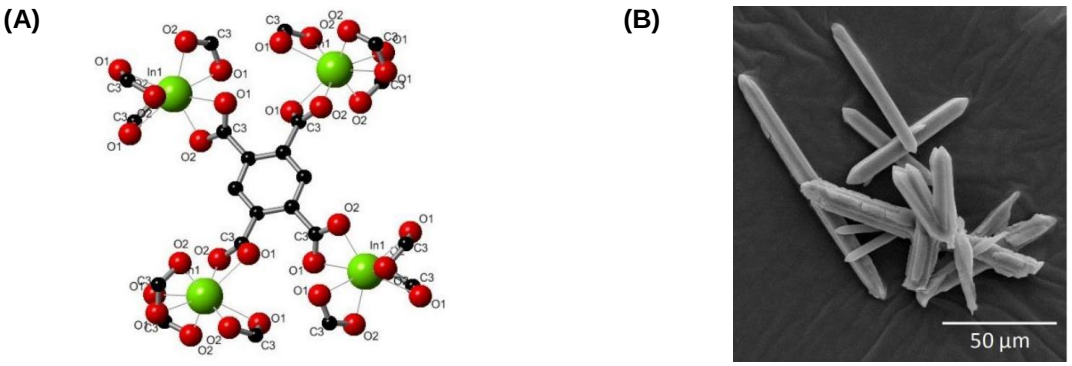

Figure 1.3.3 Crystal structure of indium based MOF (A) and TEM images of indium based MOF (B) developed by Atallah *et al.*[43]

Atallah *et al.* investigated the removal of arsenic from water using an indium based Metal-Organic Framework (MOF) with a pyromellitic acid as a ligand (Figure 1.3.3).[43] The MOF was able to adsorb arsenate from water after 12 hours of being shaken. It was reported to have an adsorption capacity of 103 mg g^{-1}, but this adsorption capacity was

calculated using 180,000 ppb of arsenate in water. This is a higher concentration of arsenate than found in a majority of contaminated water. At lower concentrations of arsenate it was calculated that the adsorption capacity of the MOF was 37 mg g^{-1}. It was demonstrated that the MOF could be recycled multiple times, however the disadvantage for potential use as an arsenic removal system is the low adsorption capacities at low concentrations.

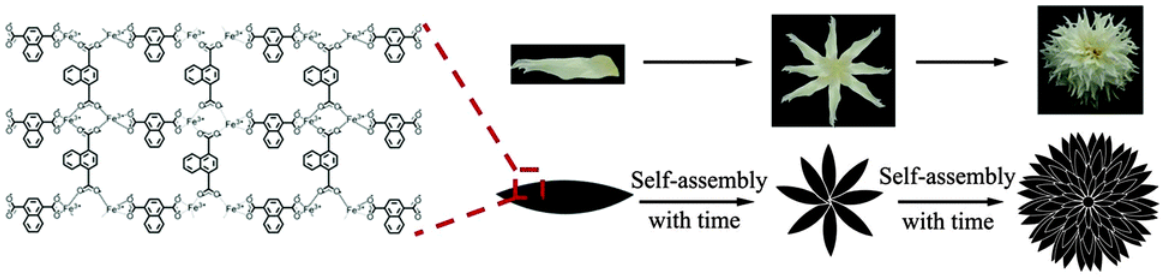

Figure 1.3.4 Schematic representation showing the formation of nanosheets of Fe^{3+} and naphthalenedicarboxylic MOG developed by Sui *et al.*[47]

Sui *et al.* used iron and naphthalenedicarboxylic acid for the formation of a Metal-Organic Gel (MOG) (Figure 1.3.4) for arsenic removal.[47] It was found that the MOG formed gels in ethanol; gel formation occurred *via* metal coordination interactions and π – π interactions. The rheological properties of the MOG were investigated; it was found that with increasing concentrations of Fe^{3+} the mechanical strength of the gel increased. The removal of arsenate from water was investigated using a xerogel. The removal rate was shown to be above 94 % from a solution containing 2000 ppb of arsenate after 8 hours. The adsorption capacity of the MOG was calculated to be 144 mg g^{-1}, which is higher than commercial adsorbents.[43] The disadvantage was that gel formation took 36 hours which potentially could be an inconvenience for an arsenic removal system.

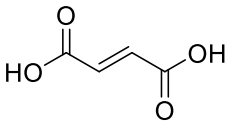

Figure 1.3.5 Structure of fumaric Acid used as a bidentate ligand to Fe^{3+} used by Gao *et al.*[48]

Gao *et al.* investigated the removal of arsenate from water using a MOG based on Fe^{3+} and fumaric acid (Figure 1.3.5).[48] It was demonstrated that the combination of Fe^{3+} with fumaric acid formed gels in ethanol; it was also demonstrated that the gel had good conductivity and self-healing properties. The removal of arsenate was investigated using a

xerogel, from arsenate solutions using a number of different concentrations ranging from 2000 ppb – 200,000 ppb. It was found that after 90 minutes, the adsorption capacity of the MOG was 232 mg g^{-1}. The disadvantage of this work is the unreasonable amount of arsenate used for the removal study, which is not comparable to genuine levels of arsenic contamination of 295 ppb. As seen in the work by Atallah *et al.* it is expected that the lower concentration of arsenic present in water will lead to a lower adsorption capacity.[43]

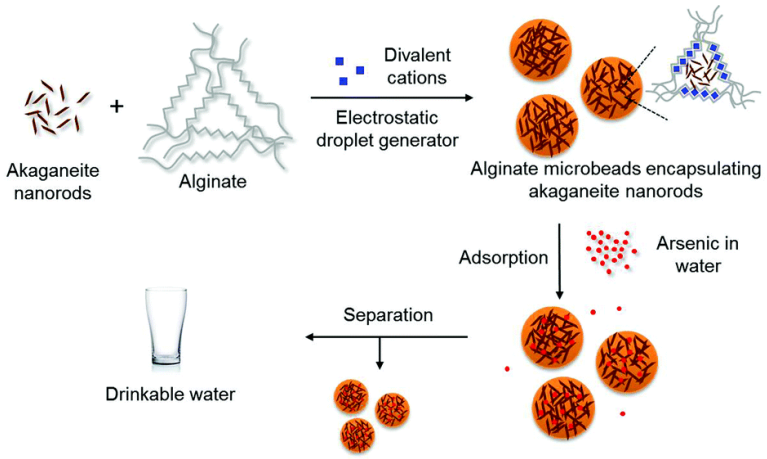

Figure 1.3.6 A graphic representation of alginate microbeads encapsulated with akaganeite nanorods used by Cho *et al.* for the investigation for the potential application of arsenic removal.[45]

Work by Cho *et al.* was conducted using a realistic amount of arsenic of 100 ppb in water during their study on the removal of arsenic using akaganeite nanorods encapsulated within alginate gel microbeads (Figure 1.3.6).[45] Akaganeite has a complex mineral structure but it is related to iron oxyhydroxysulfate.[49,50] The akaganeite synthesis was achieved *via* hydrolysis with ferric ions. The akaganeite nanorods were then encapsulated into alginate microbeads. It was found that after 10 mins of the akaganeite nanorods encapsulated within alginate microbeads being placed in solution, the arsenate concentration was halved to 50 ppb. It was found that with higher loading of akaganeite nanorods, the solution could be reduced from 100 ppb to 0.9 ppb, below the WHO recommended limit of arsenic present in water.

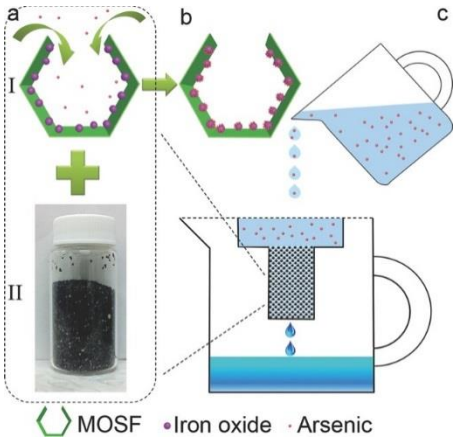

Figure 1.3.7 A schematic representation of ϒ-Fe_2O_3 nanoparticles embedded onto siliceous foam (I) (a) used by Yang *et al.* for the investigation for arsenic removal. A photo of a commercial adsorbent available for arsenic removal (II) (a), both ϒ-Fe_2O_3 nanoparticles embedded onto siliceous foam and the commercial adsorbent were used for the investigation of the removal of 1 L of arsenate contaminated water of 50 ppb. A representation of arsenic adsorbed onto the ϒ-Fe_2O_3 nanoparticles embedded onto siliceous foam. (b) A graphical representation for the setup for the 1 L arsenate removal experiment (c).[38]

Work by Yang *et al.* investigated arsenate and arsenite removal using iron oxide nanoparticles embedded onto siliceous foam.[38] It was found that using ϒ-Fe_2O_3 nanoparticles embedded onto siliceous foam had the ability to remove arsenite and arsenate from solution. The concentration of the solution containing arsenite and arsenate decreased from 100 ppb to 2 ppb. The work by Yang *et al.* showed potential application for an arsenic removal system, when used in a configuration as seen in Figure 1.3.7 (c) using a commercial adsorbent combined with iron oxide nanoparticles embedded onto siliceous foam. However the removal of 50 ppb arsenate contaminated water (1 L) resulted in a final arsenate concentration of 30 ppb, which is above the WHO recommended limit. These results would have been higher without the presence of the commercial adsorbent which would have helped reduce the concentration of arsenate.

1.4 Research Aims

Except for work by Okesola and Smith (Section 1.2) the suitability of supramolecular gels for arsenic removal has yet to be explored.[34] Arsenate exists as an anionic species in water; so cationic supramolecular systems might offer a way of binding arsenate. In recent years Smith and co-workers have reported self-assembled cationic micelles, which were investigated for the binding of DNA and heparin for the potential use of gene delivery and coagulation control.[51] They reported their micelles were based on palmitic acid with different amine ligands; one of these micelles was C16-DAPMA. Later they reported, the C16-DAPMA micelles had interactions with anions other than DNA and heparin, such as phosphate, which lead to aggregation.[52] The similarity between phosphate and arsenate led to the concept that C16-DAPMA cationic micelles suspended in a gel may be an effective arsenic remediation system.

The investigation of the properties of DBS-$CONHNH_2$ hydrogels, which has already been used for the extraction of a variety of metal ions from water (Section 1.2) would be conducted. In particular it was key importance whether C16-DAPMA micelles had affinity for arsenic. C16-DAPMA micelles incorporated within DBS-$CONHNH_2$ has already been shown to be possible in work undertaken by Vieira *et al*.[53] The effect the presence of C16-DAPMA micelles has on DBS-$CONHNH_2$ hydrogels would be investigated. The combination of DBS-$CONHNH_2$ hydrogels and C16-DAPMA micelles and its potential use for arsenic extraction from water would then be studied.

2.0 Results and discussion

2.1 C16-DAPMA micelles

2.1.1 Synthesis Of C16-DAPMA

The first target was to synthesize C16-DAPMA (Figure 2.1.1) cationic micelles and to investigate their ability to bind anionic arsenic species within supramolecular materials.

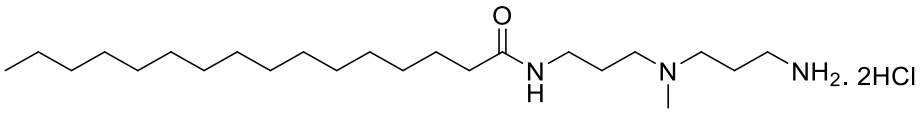

Figure 2.1.1 Structure of C16-DAPMA

C16-DAPMA was synthesised, following the literature procedure, in a three step process as shown in Scheme 2.1.1.[51] Firstly Mono-Boc DAPMA ***(3)*** was prepared by a condensation reaction with 5 equivalents of 3,3'-diamino-*N*-methyldipropylamine (DAPMA) ***(1)*** with di-*tert*-butyl dicarbonate (Boc_2O) ***(2)***. Five equivalents of DAPMA were used to avoid di-Boc DAPMA being formed. Mono-Boc DAPMA was washed and dried to give a yield of 13%. Then, Mono-Boc C16-DAPMA ***(5)*** was prepared by a condensation reaction of Mono-Boc DAPMA ***(3)*** with palmitic acid ***(4)*** in the presence of 1 equivalent of TBTU (acting as coupling reagent) and triethylamine (Et_3N). Mono-Boc C16-DAPMA ***(5)*** was washed and dried to give a yield of 81%. Finally C16-DAPMA ***(6)*** was prepared by Boc-deprotection of Mono-Boc C16-DAPMA ***(5)*** with 15 equivalents of HCl in dioxane (4M). C16-DAPMA was dried to give the target compound in a yield of 83%.

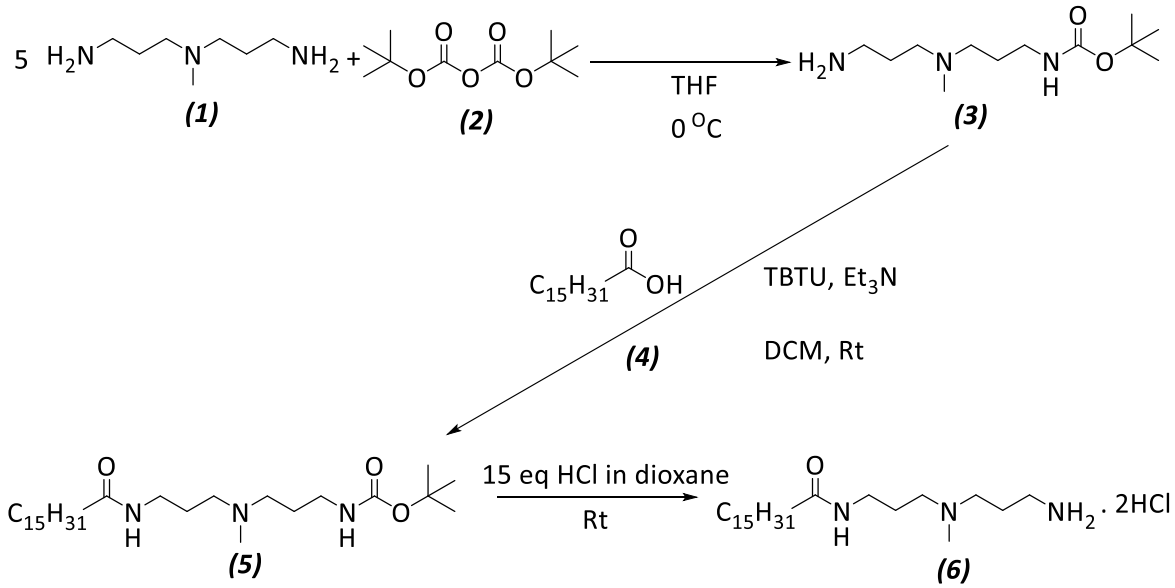

Scheme 2.1.1 Reaction scheme for the synthesis of C16-DAPMA

C16-DAPMA was fully characterized and all data were in agreement with previous literature reports.[51]

2.1.2 Dynamic Light Scattering – (DLS)

Dynamic Light Scattering (DLS) studies were carried out on C16-DAPMA (2.60 mM) micelles in Tris-HCl buffer (10 mM) and NaCl (150 mM), pH 7.4, to check that the C16-DAPMA self-assembled and the resulting micelles were consistent with the literature. C16-DAPMA micelles have been reported to have a diameter of 6.9 ± 0.1 nm.[52] C16-DAPMA micelles were formed by placing C16-DAPMA (2.60 mM) in Tris-HCl buffer (10 mM) and NaCl (150mM) and sonicating for 15 minutes.

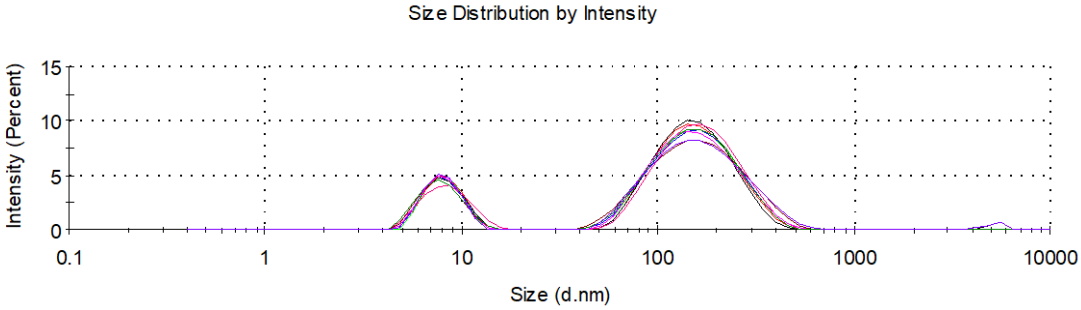

Figure 2.1.2 DLS size distribution by intensity of C16-DAPMA (2.60 mM) in Tris-HCl buffer (10 mM) and NaCl (150 mM), measured at 70 ˚C

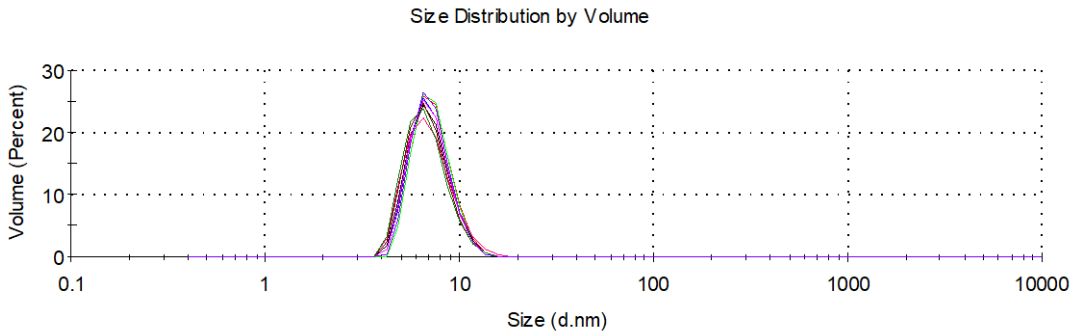

Figure 2.1.3 DLS size distribution by volume of C16-DAPMA (2.60 mM) in Tris-HCl buffer (10 mM) and NaCl (150 mM), measured at 70 ˚C

The DLS produced two different graphs of size distribution: (1) by intensity and (2) by volume. The size distribution by intensity is a measure of the intensity of back scattered light. The size distribution by volume corrects the measure of the back scattered intensity of light for the actually number of species present of each size. The graphs are shown in Figures 2.1.2 and Figure 2.1.3.

As shown in the size distribution of intensity, (Figure 2.1.2) there are two peaks. One peak represents a large aggregate, having a diameter of about 150 nm, with a higher percentage intensity. The other is a smaller diameter object of about 7 nm diameter with a smaller percentage intensity.

Comparing to the size distribution by volume (Figure 2.1.3), the normalization process indicates that in fact, very few of the larger aggregate with a diameter of 150 nm are present and that the smaller object with a diameter of 7 nm dominates.

Table 2.1.1 Showing average diameter by size distribution by volume for each run of C16-DAPMA (2.60 mM) in Tris-HCl buffer (10 mM) and NaCl (150 mM), measured at 70 ˚C

Run	Average Diameter / nm
1	7.36
2	7.33
3	7.14
4	7.09
5	7.07
6	7.11
7	6.93
8	6.81
9	7.20

From 9 repeat measurements (Table 2.1.1) it was calculated that the average micelle diameter of C16-DAPMA micelles was 7.1 ± 0.2 nm. This was consistent with the literature

value of C16-DAPMA micelles of 6.9 ± 0.1 nm.[52] The presence of small amount of a larger aggregate as indicated in Figure 2.1.2 was also consistent with the literature.

DLS was also used to collect zeta potential data (Table 2.1.2), which reflected the charge on the surface of the micelles.

Over ten repeat measurements the average zeta potential of C16-DAPMA micelles was calculated to be + 47.1 ± 6.7 mV. This shows that the surface of C16-DAPMA micelles is positively charged due to C16-DAPMA molecule being protonated. This is close to the literature value of zeta potential for C16-DAPMA micelles in Tris-HCl buffer (10 mM) and NaCl (150 mM) measured at 25 ˚C which was + 57.2 ± 2.6 mV.[52] The difference could be due to the absence of NaCl in the measurements made here. It is well known that the presence of salt can impact significantly on the self-assembly of charged micelles, as it can act to help screen the surface charge.[54]

Table 2.1.2 Zeta potential of C16-DAPMA (2.60 mM) in Tris-HCl buffer (10 mM) measured at 25 ˚C

Run	Zeta potential / mV
1	+ 44.7
2	+ 39.8
3	+ 36.8
4	+ 40.4
5	+ 46.6
6	+ 53.2
7	+ 56.6
8	+ 53.9
9	+ 51.7
10	+ 46.8

2.1.3 Transmission Electron Microscopy (TEM) of C16-DAPMA

Transmission Electron Microscopy (TEM) images were recorded of C16-DAPMA (2.60 mM) micelles in Tris-HCl buffer (10 mM) and NaCl (150 mM). The sample was placed onto a copper grid, washed with ultra-pure water and excess water removed by gentle blotting with filter paper. A negative stain (1% uranyl acetate) was applied and left to dry for 30 minutes; this process was used to avoid salt crystals being formed.

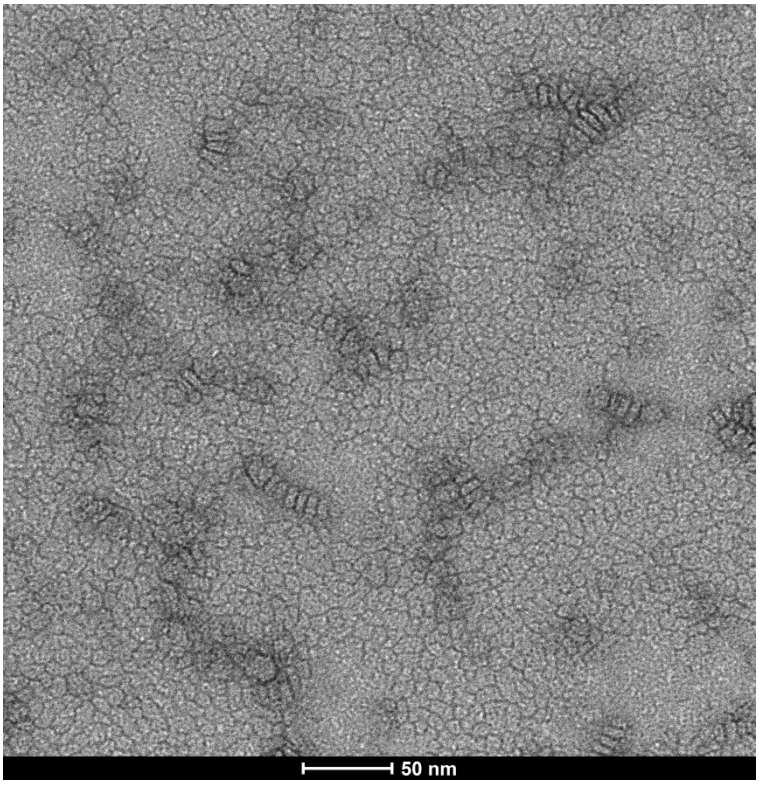

Figure 2.1.4 TEM image of C16-DAPMA (2.60 mM) micelles in Tris-HCl buffer (10 mM) at 98 k magnification

Figure 2.1.4 shows a TEM image recorded of C16-DAPMA (2.60 mM) micelles clearly indicating the presence of the micelles. The average micelle diameter was calculated using ImageJ, by measuring a number of micelle diameters and taking an average. The average micelle diameter was 7.3 nm, which is in agreement with the DLS data (Table 2.1.1). The TEM image (Figure 2.1.4) shows no evidence of larger aggregates of 150 nm, confirming the DLS size distribution by volume (Figure 2.1.3) is a more accurate representation compared to DLS size distribution by intensity (Figure 2.1.2).

2.1.4 Nile Red Assay of C16-DAPMA

The Critical Micelle Concentration (CMC) of C16-DAPMA micelles was characterized using a Nile Red dye (Figure 2.1.5) assay. The CMC is the lowest concentration at which micelles will form; below this concentration micelles do not form. Below the CMC, Nile Red is almost non-fluorescent due to being in a polar environment, but in a non-polar environment undergoes a fluorescence enhancement. Above the CMC, Nile Red dissolves into the hydrophobic domain of micelles. The hydrophobic domain of the of the micelles

being a non-polar environment, Nile Red will have excitation-dependant emission.[55] Using this effect, fluorescence can be employed to calculate the CMC of C16-DAPMA micelles.

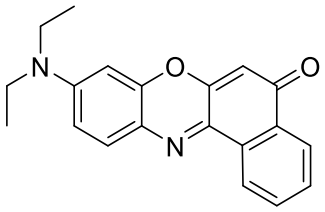

Figure 2.1.5 Structure of Nile Red Dye

A number of solutions of C16-DAPMA micelles in Tris-HCl buffer (10 mM) and NaCl (150 mM) were made up at concentrations of 100 µM and below. Nile Red (2.5 µM) was added and fluorescence spectroscopy was used to measure the intensity of light emitted at 635 nm, with an excitation wavelength of 550 nm.

The concentration at which the emission intensity starts to increase rapidly yields the critical micelle concentration of C16-DAPMA micelles as 42 ± 2 µM (Figure 2.1.6). This is a close match to the literature CMC value which is 40 ± 1 µM.[52]

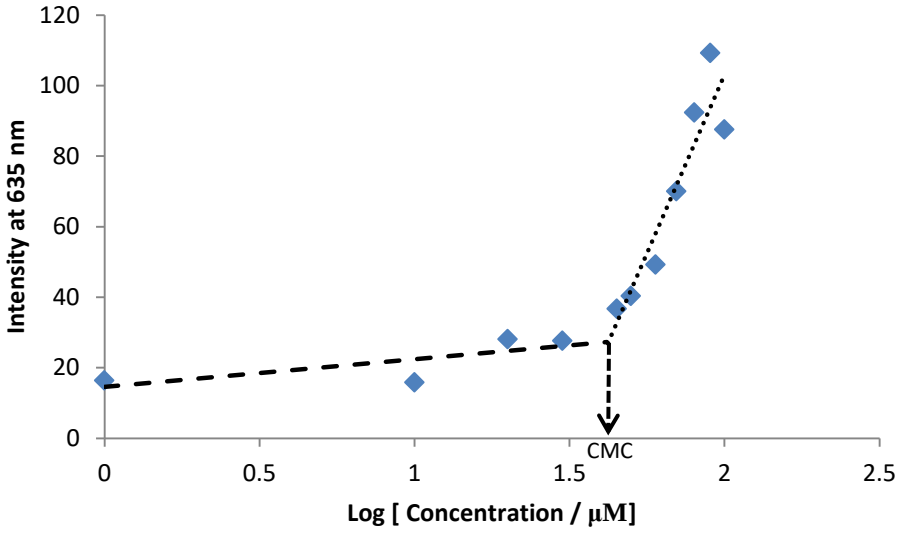

Figure 2.1.6 Plot of emission intensity at 635 nm for Nile Red (2.5 µM) in varying concentrations of C16-DAPMA in Tris-HCl buffer (10 mM) and NaCl (150 mM) used to work out critical micelle concentration. Excitation wavelength of 550nm.

2.1.5 Nuclear Magnetic Resonance (NMR)Spectroscopy of C16-DAPMA micelles

NMR spectroscopy was used to investigate if when the C16-DAPMA molecules self-assembled into micelles, the C16-DAPMA micelles still have molecular motion in solution to tumble fast enough to give a sharp 1H NMR spectrum. C16-DAPMA micelles (1000 mM) were prepared in deuterium oxide (D_2O) with an internal standard of 5 µL of dioxane.

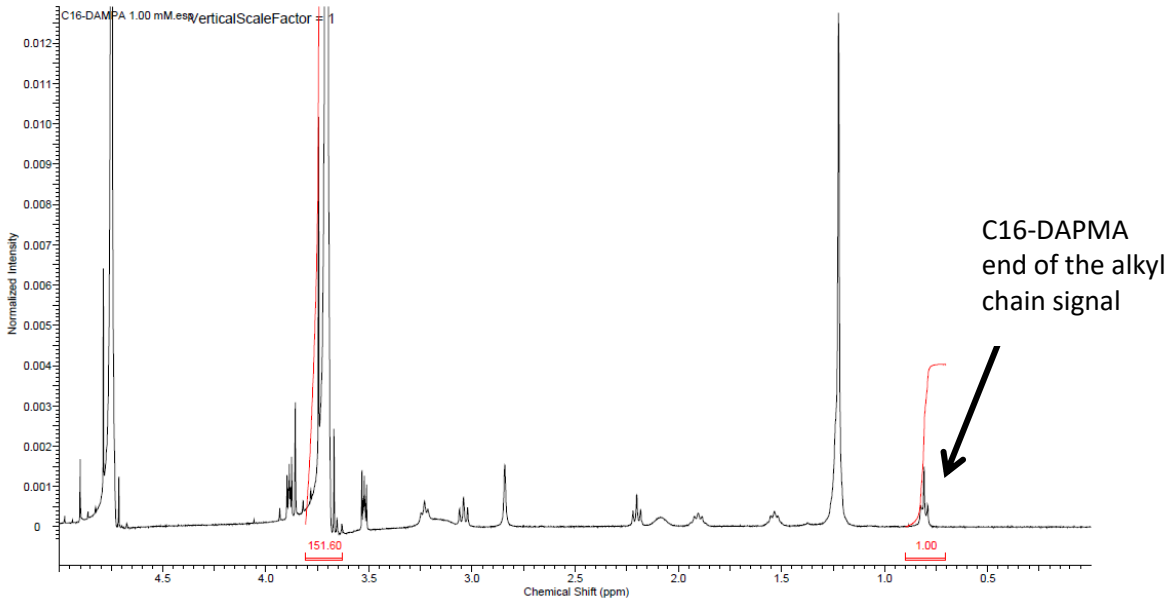

Figure 2.1.7 NMR Spectrum of C16-DAPMA Micelles in D_2O with a 5 µL internal spike of dioxane.

Figure 2.1.7 shows an NMR spectrum of C16-DAPMA micelles in D_2O. Results were calculated by using an internal spike of dioxane (5 µL) and comparing the integrations on the NMR spectrum of the internal spike against a known peak of C16-DAPMA micelles. It was found that all of the C16-DAPMA molecules are seen in the NMR spectrum to give a sharp 1H spectra, when they self-assemble into micelles.

2.2 C16-DAPMA micelles with arsenic

2.2.1 Theory of interaction between C16-DAPMA and arsenic

C16-DAPMA micelles have previously been reported to have interactions with anionic buffer components such as phosphate ***(7)***.[52]

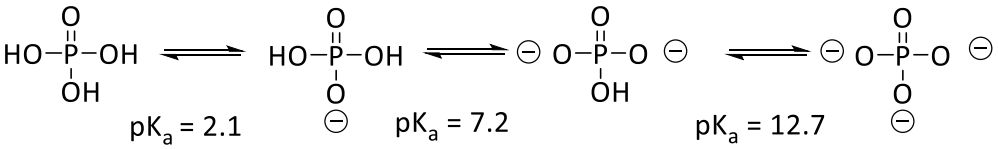

(7)

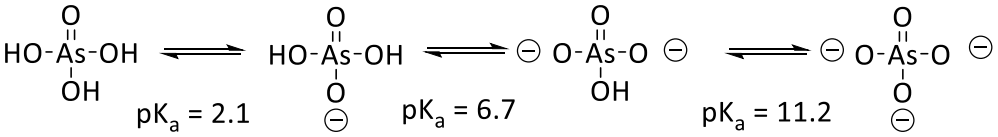

(8)

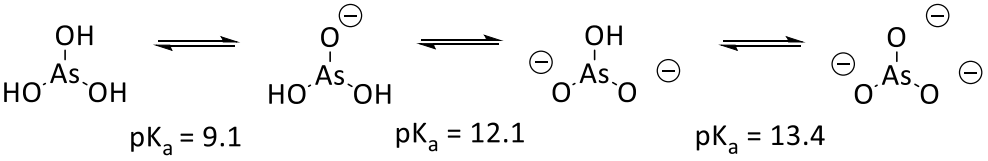

(9)

Figure 2.2.1 Showing speciation structures of phosphate (7), arsenate (8) and arsenite (9) with associated pK_a values.[39]

Shown in Figure 2.2.1 are the different structures which phosphate ***(7)***, arsenate ***(8)*** and arsenite ***(9)*** have over a range of pH values. Arsenate ***(8)*** and arsenite ***(9)*** were chosen to investigate the potential interactions with cationic C16-DAPMA micelles. Arsenate ***(8)*** and arsenite ***(9)*** are the most common species of arsenic in water; and exist as anions at certain pH values.[39] Potentially cationic C16-DAPMA micelles could have electrostatic interactions with arsenate ***(8)*** in neutral water, whereas arsenite ***(9)*** predominantly exists as an anion at higher pH values.

2.2.2 Dynamic Light Scattering of arsenite with C16-DAPMA micelles

The ability of C16-DAPMA micelles to bind arsenite ***(9)*** was investigated using DLS. It was hypothesized that C16-DAPMA micelles could potentially bind to arsenite and may form a larger diameter aggregate that could be observed using DLS.

Using As_2O_3 (75.82 mM) in a solution of C16-DAPMA micelles (2.60 mM) with Tris-HCl buffer (10 mM) and NaCl (150 mM), pH 7.4, after incubating at 60 ˚C, As_2O_3 failed to fully dissolve. The solution was then passed through a nylon syringe filter (0.22 µm) which created a saturated solution of arsenite ***(9)***. The diameter of C16-DAPMA micelles (2.60 mM) with Tris-HCl buffer (10 mM) and NaCl (150 mM) measured at 70 ˚C was monitored, while adding increments of a saturated solution of arsenite ***(9)*** (As_2O_3)**.** No increase in the diameter of C16-DAPMA micelles was observed indicating if there was any binding of arsenite ***(9)*** to C16-DAPMA micelles it didn't produce any aggregation or there is no binding of C16-DAPMA micelles to arsenite.

The pK_a values of arsenite ***(9)*** (Figure 2.2.1) indicate that arsenite stays as a neutral molecule until pH 9.1, at > pH 9.1 after which arsenite becomes anionic. The pH of C16-DAPMA (2.60 mM) with Tris-HCl buffer (10 mM) and NaCl (150 mM) is below this value. Arsenite ***(9)*** in the presence of C16-DAPMA (2.60 mM) micelles with Tris-HCl buffer (10 mM) and NaCl (150 mM) is therefore a neutral molecule and there will not be any electrostatic interactions between cationic C16-DAPMA and neutral arsenite ***(9)***. This explains why addition of arsenite ***(9)*** to a C16-DAPMA micelle solution resulted in no size increase.

2.2.3 Dynamic Light Scattering of an arsenate solution with C16-DAPMA micelles

2.2.3.1 Aggregate Size

Arsenate ***(8)*** becomes anionic at pH > 2.1 and has other pK_a values at 6.7, 11.2 which means that it may have interactions with cationic C16-DAPMA micelles. The ability for arsenate ***(8)*** to bind to C16-DAPMA micelles was investigated using DLS to investigate if micellar aggregation occurs. A solution of C16-DAPMA micelles (2.60 mM) was prepared in the presence and absence of arsenate (12.82 mM) and passed through a nylon syringe filter (0.22 µm). The diameter of micelles within these solutions was investigated using DLS.

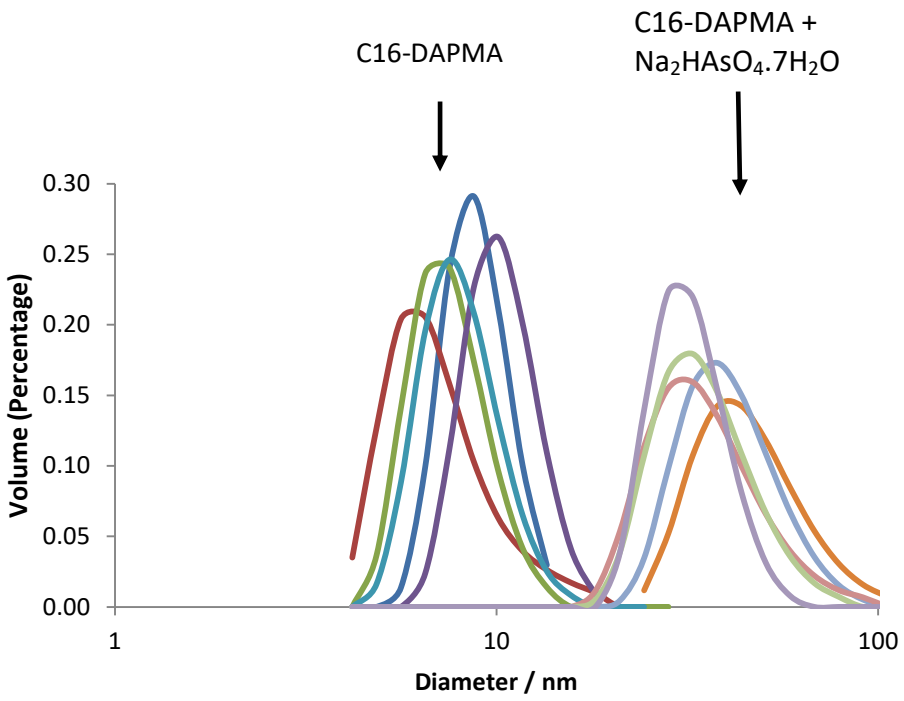

Figure 2.2.2 Size distribution by volume comparing diameter of C16-DAPMA (2.60 mM) and C16-DAPMA (2.60 mM) with $Na_2HAsO_4.7H_2O$ (12.82 mM) in Tris-HCl buffer (10 mM) and NaCl (150 mM) measured at 70 ˚C

Table 2.2.1 Showing average diameter by size distribution by volume for each run of C16-DAPMA (2.60 mM) and C16-DAPMA with $Na_2HAsO_4.7H_2O$ (12.82 mM) in Tris-HCl buffer (10 mM) and NaCl (150 mM) measured at 70 ˚C

Run	Average Diameter C16-DAPMA (2.60 mM) / nm	Average Diameter C16-DAPMA (2.60 mM) + $H_2AsO_4^-$ (12.82 mM) / nm
1	8.94	47.73
2	7.42	42.04
3	7.69	37.27
4	10.42	36.42
5	8.32	32.57

Figure 2.2.2 and Table 2.2.1 show that when comparing C16-DAPMA micelles with and without the presence of arsenate (12.82 mM) ***(8),*** there is a clear difference in diameter. C16-DAPMA micelles (2.60 mM) without arsenate ***(8)*** have an average diameter of 8.6 ± 1.2 nm. C16-DAPMA micelles (2.60 mM) in the presence of arsenate (12.82 mM) ***(8)*** formed a larger aggregate having an average diameter of 39.2 ± 5.8 nm. The size of the aggregate that formed indicates an elecstratic interaction between cationic C16-DAPMA and anionic arsenate.

Given that this experiment is performed in the presence of 150 mM of NaCl and just 12.82 mM of arsenate these results would suggest C16-DAPMA micelles bind to arsenate ions preferentially to chloride.

The literature value for the diameter of C16-DAPMA micelles in the presence of phosphate anions is 20.9 ± 2.2 nm.[52] The diameter of C16-DAPMA micelles with arsenate was 39.2 ± 5.8 nm. When comparing phosphate and arsenate binding to C16-DAPMA micelles, arsenate forms a larger aggregate compared to phosphate, which might suggest it induces greater aggregation. This maybe be a result of its lower pK_a value and hence it's greater negative charge at the pH of the buffer (pH = 7.4).

2.2.3.2 Zeta potential

Zeta potential was used to investigate the change in charge on the surface of cationic C16-DAPMA micelles. This allowed exploration of the electrostatic interactions within the aggregate formed by C16-DAPMA micelle and anionic arsenate.

Table 2.2.2 Zeta potential of C16-DAPMA (2.60 mM) in the presence and absence of $Na_2HAsO_4.7H_2O$ (12.82 mM) in Tris-HCl buffer (10 mM) measured at 25 ˚C

Run	Zeta potential of C16-DAPMA (2.60 mM) / mV	Zeta potential of C16-DAPMA (2.60 mM) + $H_2AsO_4^-$ (12.82 mM) / mV
1	44.7	12.2
2	39.8	11.0
3	36.8	11.8
4	40.4	12.5
5	46.6	12.5
6	53.2	12.3
7	56.6	12.2
8	53.9	13.0
9	51.7	12.3
10	46.8	12.2

The results in Table 2.2.2 show there is a significant difference between the zeta potential of C16-DAPMA micelles in the absence of arsenate and C16-DAPMA micelles in the presence of arsenate. The average zeta potential of C16-DAPMA micelles (2.60 mM) was + 47.1 ± 6.7 mV and C16-DAPMA micelles (2.60 mM) with arsenate (12.82 mM) was + 12.2 ± 0.5 mV.

The difference between zeta potentials showed that there is an electrostatic interaction between cationic C16-DAPMA micelles and anionic arsenate ions which lead to the partial neutralisation of the surface of the cationic micelles.

The literature reported the zeta potential measured at 25 ˚C of C16-DAPMA micelles with Tris-HCl buffer (10 mM) and NaCl (150 mM), pH 7.4, was + 57.2 mV. In PBS buffer (10 mM) and NaCl (150 mM), pH 7.4, this decreased to just - 0.3 mV. The decrease between the values was due to the strength of ionic interaction between C16-DAPMA and the buffer component.[52]

The most likely reason for the difference is that the zeta potential for C16-DAPMA micelles was recorded in NaCl (150 mM) for PBS buffer, whereas the zeta potential for C16-DAPMA micelles and arsenate was recorded just in Tris-HCl buffer (10 mM), with the absence of NaCl. It is well known that the presence of salt can impact somewhat on the self-assembly of charged micelles by helping screen the surface charge.[54]

2.2.3.3 Minimum Aggregation Concentration

Figure 2.2.2 showed that in the presence of arsenate (12.82 mM), C16-DAPMA micelles form large aggregates with a diameter of 39.2 nm. A new assay was developed to determine the Minimum Aggregation Concentration (MAC). This was defined as the lowest concentration of arsenate required to be present for C16-DAPMA micelle aggregation with arsenate to occur.

A solution of C16-DAPMA (2.60 mM), Tris-HCl buffer (10mM) and NaCl (150 mM) was prepared, sonicated and left in an incubator for 15 minutes at 60 ˚C. An aliquot (1 mL) of the solution containing C16-DAPMA (2.60 mM), Tris-HCl buffer (10mM) and NaCl (150 mM) were added to $Na_2HAsO_4.7H_2O$. This created a solution of C16-DAPMA (2.60 mM), arsenate (19.23 mM), Tris-HCl buffer (10mM) and NaCl (150 mM). Both solutions were then passed through a nylon syringe filter (0.22 μm) and kept in the incubator at 60 ˚C. DLS was used to record the diameter of a solution of C16-DAPMA micelles (2.60 mM), Tris-HCl buffer (10 mM) and NaCl (150 mM), aliquots of the solution containing C16-DAPMA (2.60 mM), arsenate (19.23 mM), Tris-HCl buffer (10mM) and NaCl (150mM) solution were added, and after each addition, the diameter of the aggregate was recorded.

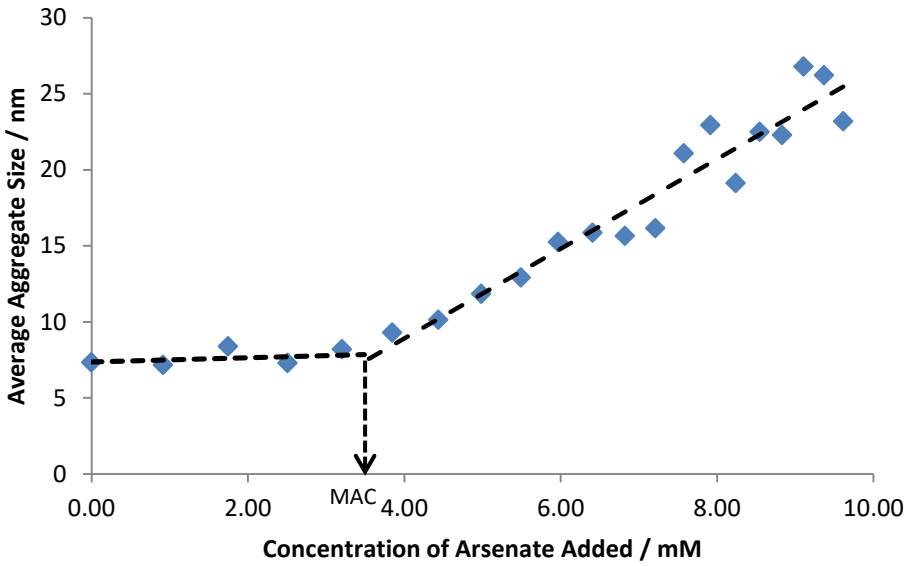

Figure 2.2.3 Average aggregate diameter measured by DLS at 70 ˚C after addition of an aliquot of a solution containing C16-DAPMA (2.60 mM), arsenate (19.23 mM), Tris-HCl buffer (10 mM) and NaCl (150 mM) plotted against concentration of arsenate added.

Monitoring the concentration at which the average aggregate diameter starts to rapidly increase, after each addition of arsenate containing solution gave the MAC as 3.49 mM (Figure 2.2.3). This is the concentration at which the DLS shows that an aggregate was formed, and the average diameter being measured was not just C16-DAPMA micelles (2.60 mM) with NaCl (150 mM). This suggests that 1.34 equivalents of arsenate relative to C16-DAPMA micelles are required to start the micelle aggregation process. We suggest that binding also occurs below this concentration but only once this concentration is exceeded does aggregation become triggered.

2.2.4 TEM of Arsenate Aggregates

TEM images where recorded to produce images of C16-DAPMA micelles (2.60 mM), with arsenate (9.62 mM) in Tris-HCl buffer (10 mM) and NaCl (150 mM). The sample was placed onto a copper grid, washed with ultra-pure water and excess water was removed by gentle blotting using filter paper. A negative stain (1% uranyl acetate) was applied and left to dry for 30 minutes; this process was used to avoid salt crystals being formed.

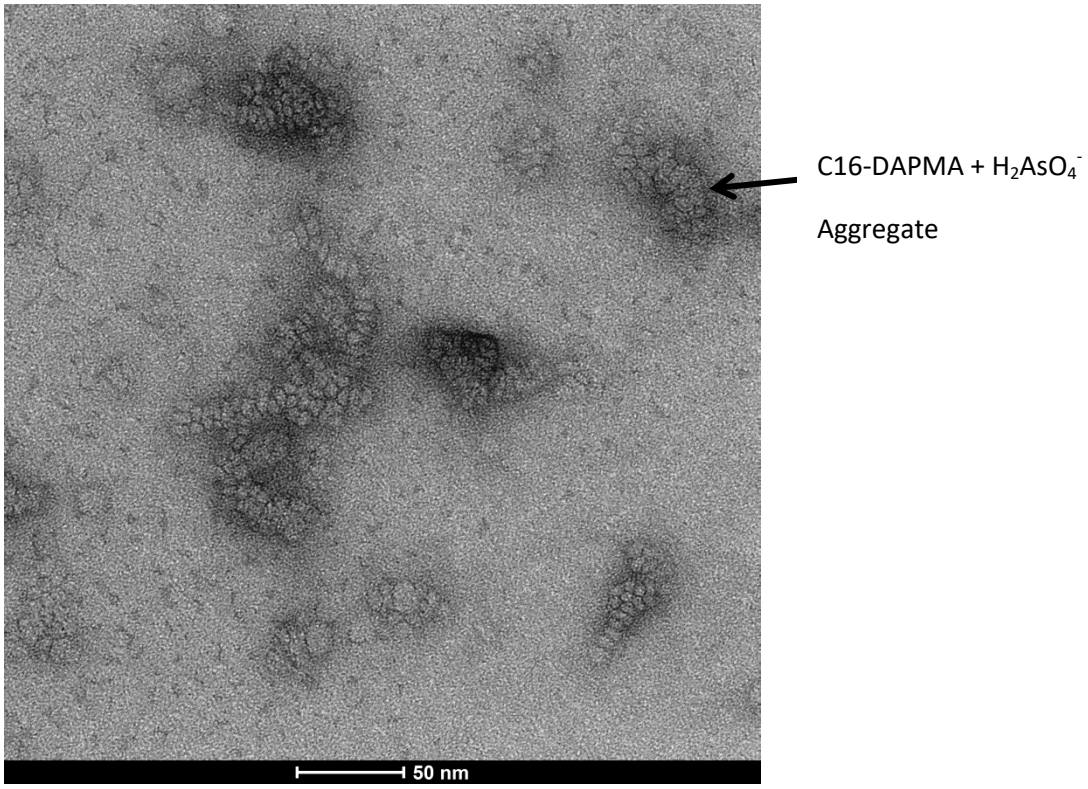

Figure 2.2.4 TEM of C16-DAPMA (2.60 mM) micelles and $Na_2HAsO_4.7H_2O$ (9.62 mM) in Tris-HCl buffer (10mM) at 120k magnification

Figure 2.2.4 shows a TEM images recorded of C16-DAPMA (2.60 mM) micelles and arsenate (9.62 mM). It confirms the presence of C16-DAPMA micelles, as well as larger structure assigned as arsenate / C16-DAPMA aggregates. The average aggregate diameter was calculated using ImageJ by measuring a number of aggregate diameters and averaging them. The average aggregate diameter was 42.9 nm, which is supported the hypothesis that aggregation occurs between C16-DAPMA micelles and arsenate, as demonstrated by the DLS data in Section 2.2.3.1. Given the difference in method, this is in good agreement with the DLS data.

2.3 p,p'-dihydraza-1,3: 2,4-dibenzylidene-D-sorbitol (DBS-CONHNH$_2$)

2.3.1 Synthesis

The DBS-CONHNH$_2$ gelator (Figure 2.3.1) was synthesised, to investigate its ability as a hydrogelator, and the resulting properties.

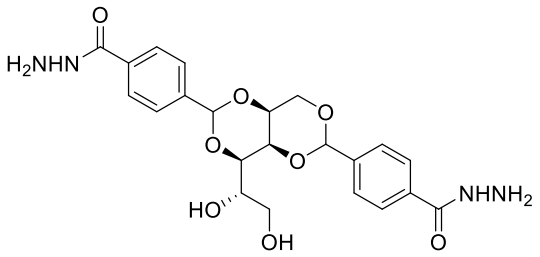

(13)

Figure 2.3.1 Structure of DBS-CONHNH$_2$

DBS-CONHNH$_2$ was synthesised, following the literature procedure, in a two-step process as shown in Scheme 2.3.1.[56] First, 1,3;2,4-dibenzylidene-D-sorbitol-p, p'-dimethylester ***(12)*** (DBS-COOCH$_3$) was prepared by a condensation cyclization reaction of sorbitol ***(10)*** with 2 equivalents of 4-methylformybenzoate ***(11)*** in the presence of p-toluenesulfonic acid using Dean-Stark apparatus. DBS-COOCH$_3$ ***(13)*** was washed thoroughly to remove mono-substituted and tri- substituted by-products and dried to give the target compound in a yield of 20 %. To wash the crude product, water and dichloromethane were each refluxed with crude reaction mixture and filtered to remove mono-substituted (MBS-COOCH$_3$) ***(14)*** and tri-substituted (TBS-COOCH$_3$) ***(15)*** (Figure 2.3.2) respectively.

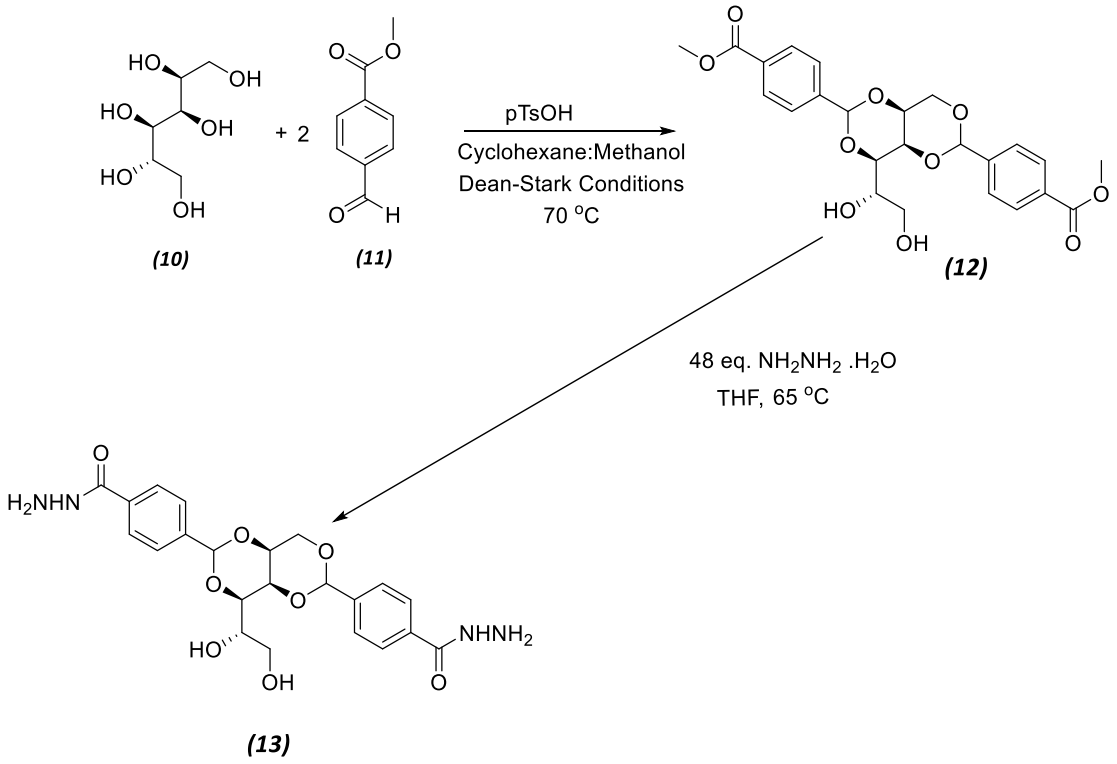

Scheme 2.3.1 Reaction scheme for the synthesis of DBS-CONHNH$_2$

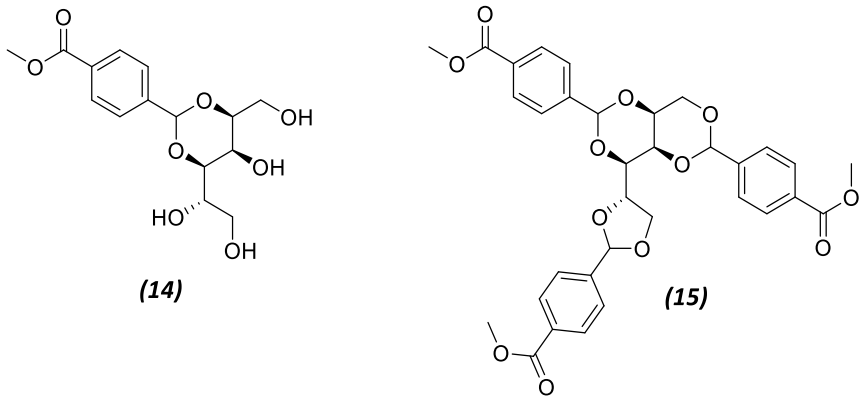

Figure 2.3.2 Showing Structures of MBS-COOCH$_3$ *(14)*, *TBS*-COOCH$_3$ *(15)*

DBS-COOCH$_3$ ***(12)*** was then refluxed overnight with 48 equivalents of hydrazine monohydrate; the reaction was monitored by Thin Layer Chromatography (TLC). DBS-CONHNH$_2$ ***(13)*** was washed and dried to give a yield of 88%.

2.3.2 Minimum Gelation Concentration

The Minimum Gelation Concentration (MGC) was investigated, to confirm whether DBS-$CONHNH_2$ formed hydrogels and the range of concentrations at which this occurred. (Figure 2.3.3)

DBS-$CONHNH_2$ hydrogels formed when a solution of DBS-$CONHNH_2$ is prepared at the desired concentration and then sonicated for 15 minutes. The solution is then heated up using a heat gun until all the solution is dissolved and the solution is boiling. The solution was then left to stand and cool to room temperature.

The tube-inversion test, where the material in a vial is inverted, was used to investigate if gelation had occurred. If the material in question is a hydrogel, it will form a self-supporting network when inverted as seen in Figure 2.3.3 and Figure 2.3.4. If the material in question is not self-supporting, it is not a hydrogel. The inversion test was performed on 0.5 mL of various concentrations of DBS-$CONHNH_2$ hydrogels in a 2.5 mL vial, and on 1 mL of hydrogels in an 8 mL vial (Table 2.3.1).

Table 2.3.1 Results of the gelation test for DBS-CONHNH$_2$ hydrogels at a variety of concentrations in different vials. ✓ - Representing a formation of a self-spanning gel network that passed the tube-inversion test. ✗ - Representing a failure of a self-spanning gel network to form that failed the tube-inversion test.

Concentration of DBS-CONHNH$_2$ / mM	Gel formation of 0.5 mL gel in 2.5 mL vial	Gel formation of 1.0 mL gel in 8.0 mL vial
1.12	✗	✗
1.43	✗	✗
1.62	✗	✗
2.11	✗	✓
2.63	✗	✓
3.16	✗	✓
3.69	✓	✓
4.22	✓	✓
4.74	✓	✓
5.27	✓	✓
5.80	✓	✓
6.32	✓	✓
6.85	✓	✓
7.38	✓	✓
7.90	✓	✓
8.43	✓	✓

When comparing the results of the test between hydrogel in a 2.5 mL vial and an 8.0 mL vial, they both formed hydrogels from 3.69 mM to 8.43 mM but hydrogels form in an 8.0 mL vial at concentrations as low as 2.11 mM.

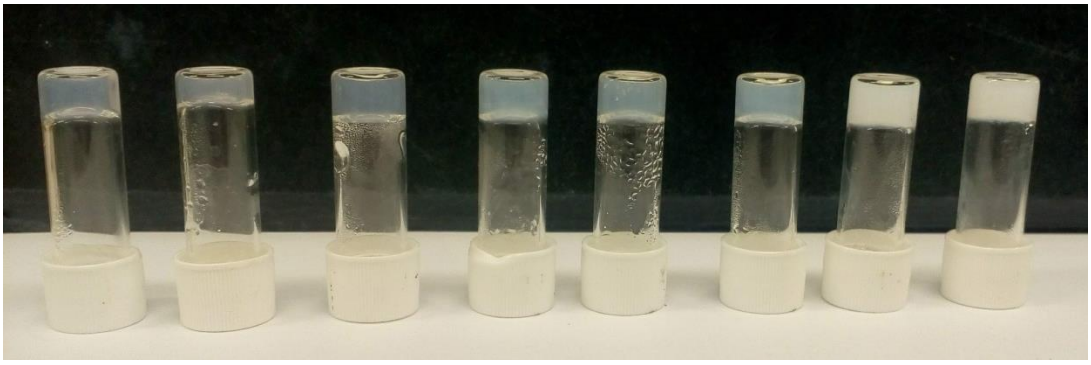

Figure 2.3.3: 0.5 mL DBS-CONHNH$_2$ hydrogels in a 2.5 mL vial, with a variety of concentrations of DBS-CONHNH$_2$ between 3.69 mM to 8.43 mM. Increasing concentrations of DBS-CONHNH$_2$ from left to right.

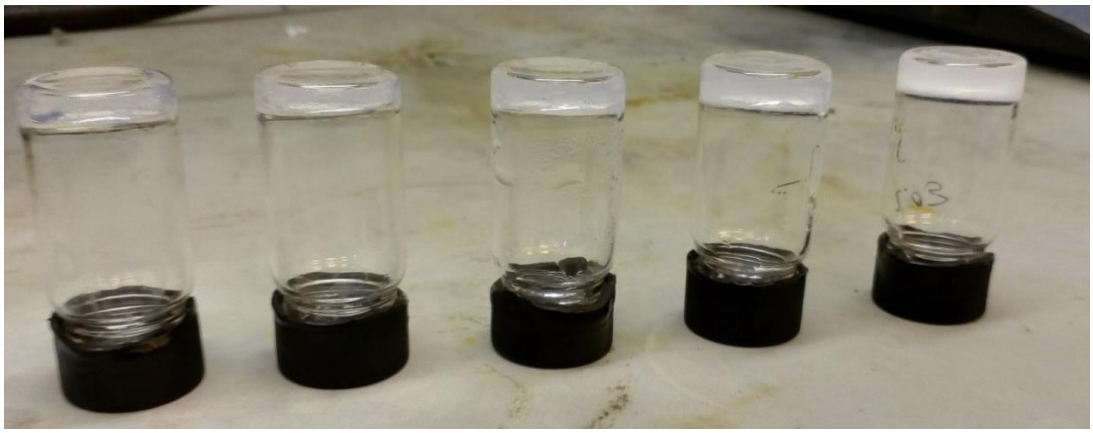

Figure 2.3.4: 1.0 mL DBS-CONHNH$_2$ hydrogels in a 8 mL vial, with a variety of concentrations of DBS-CONHNH$_2$ from 2.11 mM to 8.43 mM. Increasing concentrations of DBS-CONHNH$_2$ from left to right.

All concentrations shown in Figure 2.3.3 and Figure 2.3.4 formed hydrogels. Figure 2.3.3 and Figure 2.3.4 show that with increasing concentrations of DBS-CONHNH$_2$ the transparency of DBS-CONHNH$_2$ hydrogels decreases especially with 7.90 mM and 8.43 mM (Figure 2.3.3). Potentially this could be due to a denser gel network with greater insolubility. Notably at concentrations > 8.43 mM not all the gelator could dissolve and homogenous gels could not form.

2.3.3 T_{Gel}

T_{Gel} was used to investigate the thermal stability of DBS-CONHNH$_2$ hydrogels over a range of temperatures. This was investigated by making of 0.5 mL of DBS-CONHNH$_2$ hydrogels over a variety of concentrations in 2.5 mL vials, as seen in Figure 2.3.3. The DBS-CONHNH$_2$ hydrogels were placed in an oil bath and the temperature was steadily increased at a

controlled rate until 100 ˚C was reached. The inversion test was carried out on the DBS-$CONHNH_2$ hydrogels every 1 ˚C, as the temperature of the oil bath increased. The T_{Gel} value was the temperature which the gel network no longer self-supporting (Table 2.3.2).

Table 2.3.2 T_{Gel} Value for DBS-$CONHNH_2$ hydrogels at variety of concentrations

Concentrations of DBS-$CONHNH_2$ / mM	T_{Gel} Value / ˚C
4.22	98
4.74	> 100
5.27	88
5.80	> 100
6.32	> 100
6.85	> 100
7.38	> 100
7.90	> 100
8.43	> 100

It was shown that across a range of concentrations (except 5.27 mM and 4.22 mM) T_{Gel} was > 100 ˚C. The T_{Gel} value for 5.27 mM DBS-$CONHNH_2$ was 88 ˚C; this could potentially be due to an anomalous result as the immediately higher and lower concentrations of DBS-$CONHNH_2$ had T_{Gel} values of > 100 ˚C.

2.3.4 TEM of DBS-$CONHNH_2$ hydrogels

TEM images were recorded of DBS-$CONHNH_2$ hydrogel (5.90 mM) made using ultra-pure water. The sample was placed onto a copper grid and excess water was removed using filter paper. A negative stain (1% uranyl acetate) was applied and left to dry for 30 minutes.

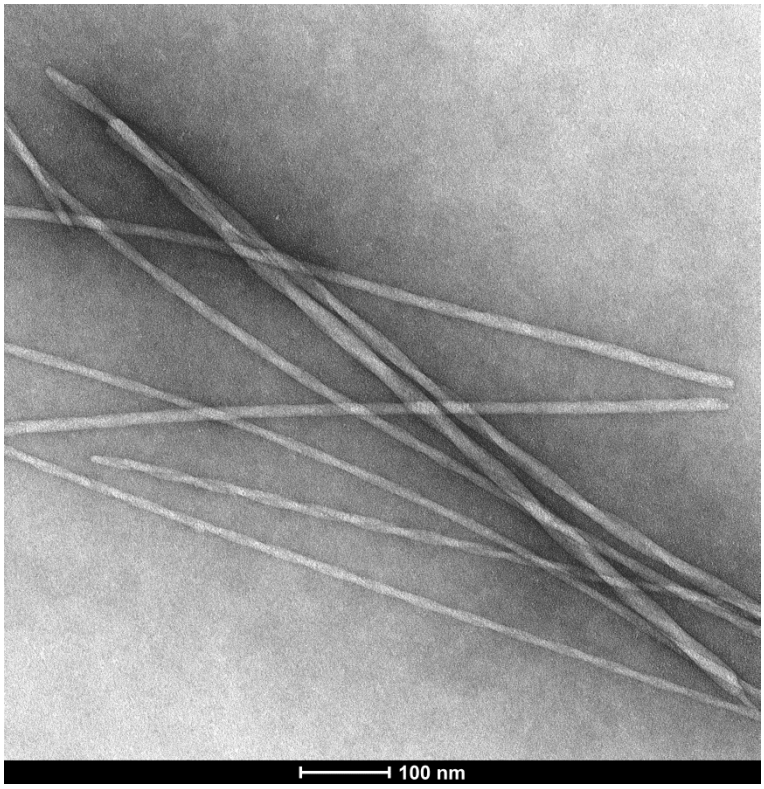

Figure 2.3.5 TEM image of DBS-CONHNH$_2$ hydrogel (5.90 mM) in ultrapure water at 49 k magnification.

Figure 2.3.5 shows a TEM image recorded of DBS-CONHNH$_2$ hydrogel. The image (Figure 2.3.5) showed the presence of hydrogel fibrils, which underpin the supramolecular gel network. The average fibril diameter was calculated using ImageJ by measuring a number of different fibrils and taking an average. The average fibril width for DBS-CONHNH$_2$ hydrogel was 13.9 nm. Figure 2.3.5 also shows that DBS-CONHNH$_2$ hydrogel fibrils have a clear helical twist, which was reported in literature. [53] It was also suggested in literature computer simulations on DBS-CONHNH$_2$ hydrogels. [57]

2.3.5 Rheology of DBS-CONHNH$_2$ hydrogels

The mechanical properties of DBS-CONHNH$_2$ hydrogels were investigated using rheology with parallel plate geometry. The data produced by the rheometer provides information about stiffness and robustness, as well the Linear Viscoelastic Region (LVR). The LVR is the linear region with little or no change to storage modulus (*G'*) or loss modulus (*G''*) with changing shear strain.

A fixed volume (0.5 mL) of DBS-CONHNH$_2$ hydrogels at several concentrations was prepared in an inverted 2.5 mL vial on the rheometer plate. Excess water was removed by blotting with "blue roll"; the rheometer plate was then applied to the gel. DBS-CONHNH$_2$ hydrogels were first tested using an amplitude sweep; this was done by increasing shear strain at a constant frequency as seen in Figure 2.3.6, Figure 2.3.7 and Figure 2.3.8.

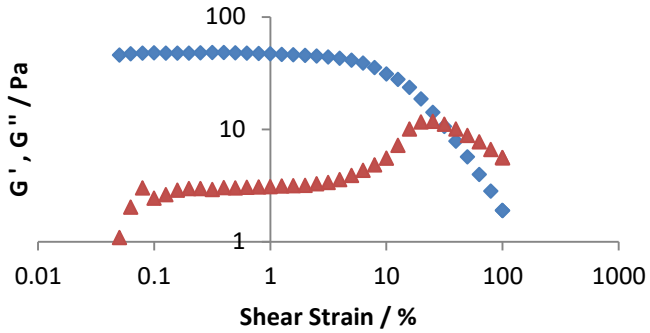

Figure 2.3.6 Amplitude sweep, storage modulus (*G'*, blue diamonds) and loss modulus (*G''*, red triangle) of DBS-CONHNH$_2$ (4.22 mM) hydrogels with varying shear strain (f = 1 Hz)

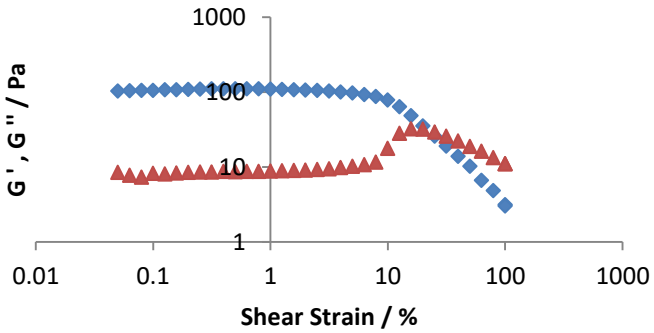

Figure 2.3.7 Amplitude sweep, storage modulus (*G'*, blue diamonds) and loss modulus (*G''*, red triangle) of DBS-CONHNH$_2$ (6.32 mM) hydrogels with varying shear strain (f = 1 Hz)

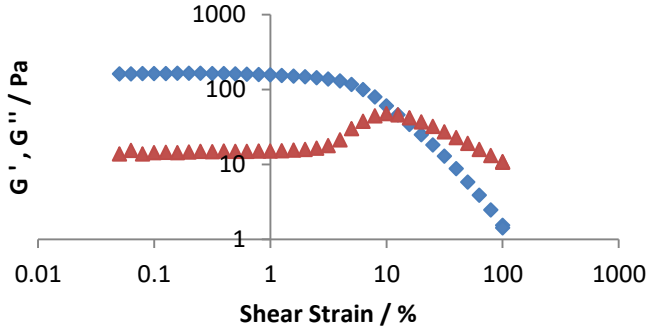

Figure 2.3.8 Amplitude sweep, storage modulus (*G'*, blue diamonds) and loss modulus (*G''*, red triangle) of DBS-CONHNH$_2$ (8.43 mM) hydrogels with varying shear strain (f = 1 Hz)

Figures 2.3.6, 2.3.7 and 2.3.8 show the result of amplitude sweeps of DBS-$CONHNH_2$ hydrogels at 4.22 mM, 6.32 mM and 8.43 mM concentrations respectively. LVRs were located up to 4.0 %, 5.0 % and 3.2 % for samples at 4.22 mM, 6.32 mM and 8.43 mM respectively. The stiffness, *G'* and *G''*, increases with increasing concentrations of DBS-$CONHNH_2$, indicating a more extensive, stiffer, sample spanning gel network.

Table 2.3.3 Showing storage modulus (*G'*) and loss modulus (*G''*) values for DBS-$CONHNH_2$ hydrogels from amplitude sweep in the LVR (f = 0.3155 %)

Concentration of DBS-$CONHNH_2$ / mM	*G'* / Pa	*G''* / Pa
4.22	48.0	2.9
6.32	110.3	8.6
8.43	163.1	14.8

Table 2.3.3 shows storage modulus (*G'*) and loss modulus (*G''*) values for DBS-$CONHNH_2$ hydrogels at various concentrations during the amplitude sweep. Storage modulus and loss modulus are indications of the stiffness of the gel, (i.e. the force required to deform the gel). The higher values of storage modulus and loss modulus can indicate a stiffer material. Table 2.3.3 shows that with increasing concentrations of DBS-$CONHNH_2$, *G'* and *G''* increase in value; the higher the concentrations of DBS-$CONHNH_2$, the stiffer the hydrogel. The increase in *G'* and *G''* between 4.22 mM and 6.32 mM DBS-$CONHNH_2$ concentration resulted in an average percentage increase of 163 %. The increase between 6.32 mM and 8.43 mM DBS-$CONHNH_2$ concentration resulted in an average percentage increase of 60 %. This demonstrated that there isn't a linear increase in stiffness over the full range of concentrations. This suggests that above, a certain concentration, no additional DBS-$CONHNH_2$ was added to the nanofibers in the gel network, hence the smaller increase in stiffness between 6.32 – 8.43 mM.

Critical Shear Stress (CSS) was also calculated, CSS is the shear strain percentage when *G'* and *G''* are equal to each other. CSS values for DBS-$CONHNH_2$ hydrogels at 4.22 mM, 6.32 mM and 8.43 mM were 25.1 %, 25.1 % and 12.6 % respectively. CSS is an important value: if *G'* is greater than *G''* the DBS-$CONHNH_2$ hydrogel has viscoelastic character or gel like behaviour. When *G''* is greater than *G'* the DBS-$CONHNH_2$ hydrogel has liquid-like behaviour. The CSS also gives an indication of the robustness of a gel by providing a

measure of shear strain at which the hydrogel behaviour changes from gel-like to liquid-like. Interestingly the CSS decreases with increasing concentrations of DBS-$CONHNH_2$, indicates that as the hydrogels become stiffer, the gel becomes more sensitive to breakage on application of shear strain.

As well as amplitude sweeps, frequency sweeps were also conducted on the DBS-$CONHNH_2$ hydrogels. A frequency sweep is where constant shear strain was applied to the gel with varying oscillation of frequency. The shear strain which was applied to the gel during the frequency sweep is located in the LVR which was 0.3 % for all samples.

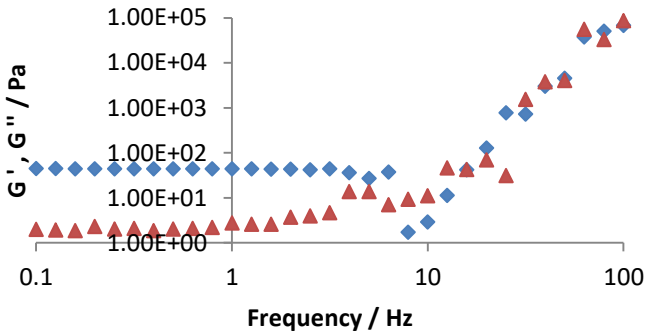

Figure 2.3.9 Frequency sweep, storage modulus (*G'*, blue diamonds) and loss modulus (*G''*, red triangle) of DBS-$CONHNH_2$ (4.22 mM) hydrogels with constant shear strain and varying frequency

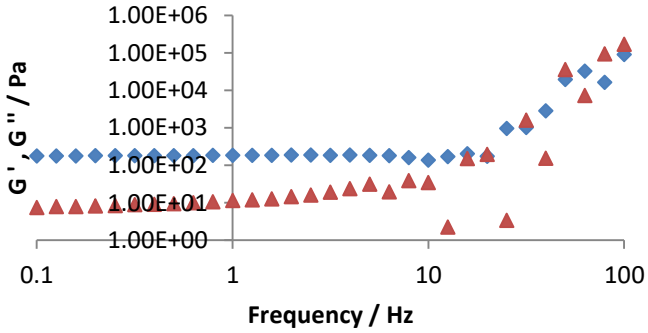

Figure 2.3.10 Frequency sweep, storage modulus (*G'*, blue diamonds) and loss modulus (*G''*, red triangle) of DBS-$CONHNH_2$ (6.32 mM) hydrogels with constant shear strain and varying frequency

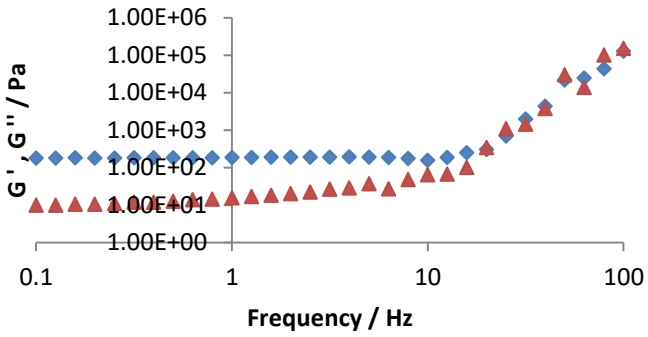

Figure 2.3.11 Frequency Sweep, storage modulus (*G'*, blue diamonds) and loss modulus (*G''*, red triangle) of DBS-CONHNH$_2$ (8.43 mM) hydrogels with constant shear strain and varying frequency

Figures 2.3.9, 2.3.10 and 2.3.11 show the results of frequency sweeps of DBS-CONHNH$_2$ hydrogels at 4.22 mM, 6.32 mM and 8.32 mM respectively. It was shown that with increasing frequency there was no change to *G'* and *G''* up until a critical point. This corresponds to the region of gel-like behaviour. Beyond this point it was seen there was a linear response to *G'* and *G''* with increasing frequency, this shows liquid-like behaviour. The frequency at which the behaviour changes between gel-like and liquid-like behaviour were 5.0 Hz, 15.9 Hz and 20.0 Hz respectively, indicating that increasing the DBS-CONHNH$_2$ concentration leads to a hydrogel that is more resistant to increasing frequency.

2.3.6 NMR spectroscopy of DBS-CONHNH$_2$ hydrogels

NMR spectroscopy was used to investigate DBS-CONHNH$_2$ gels to determine the amount of DBS-CONHNH$_2$ that is involved / not involved in the gel network. A DBS-CONHNH$_2$ (4.64 mM, 1 mL) hydrogel was formed in using D_2O in an NMR tube. Using a 5 µL internal spike of dimethyl sulfoxide (DMSO), an NMR spectrum was acquired and the integration of the internal spike was compared to the integration of the DBS-CONHNH$_2$ aromatic signal. DBS-CONHNH$_2$ molecules involved in the gel network aggregate together to form fibrils as mentioned in Section 1.1. The fibrils have a low mobility and tumble slowly so are not seen in the NMR spectrum; only molecules not involved in the DBS-CONHNH$_2$ gel network are observed in the NMR spectrum, due to not being aggregated together.[58]

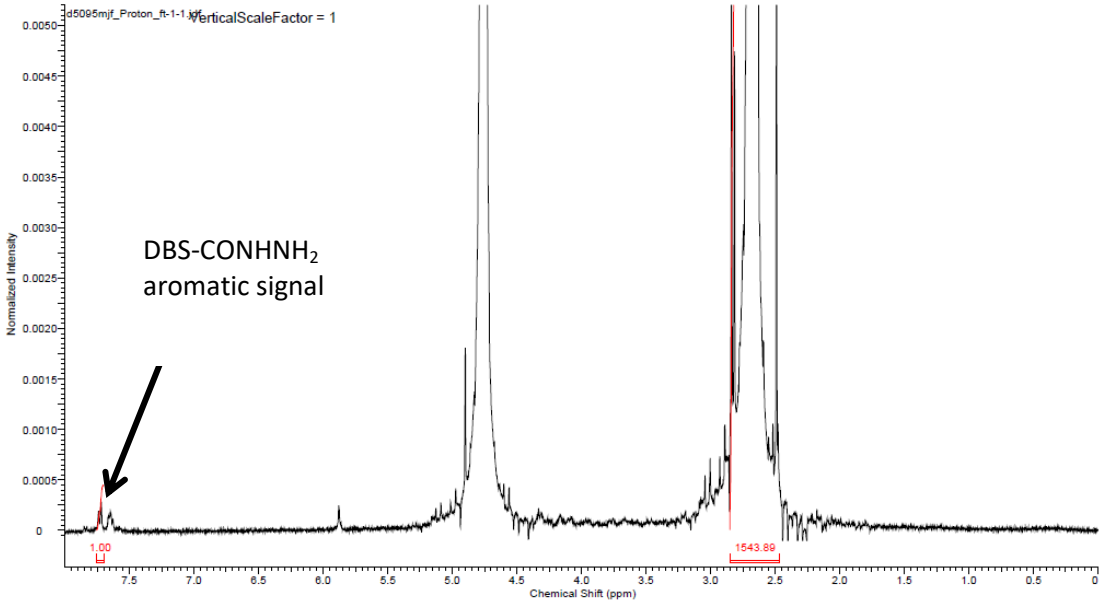

Figure 2.3.12 NMR spectrum of 1 mL DBS-CONHNH$_2$ (4.64 mM) hydrogel.

Figure 2.3.12 shows the NMR spectrum of DBS-CONHNH$_2$ (4.64 mM, 1 mL) hydrogel, it was calculated by comparing integrations of the internal spike and DBS-CONHNH$_2$ aromatic signal, that 0.068 µmol (1.5 %) of DBS-CONHNH$_2$ was not involved the gel network; 4.572 µmol (98.5 %) of DBS-CONHNH$_2$ was included into the gel network.

2.4 DBS-CONHNH$_2$ with C16-DAPMA micelles

The properties of DBS-CONHNH$_2$ hydrogels were investigated in the presence of C16-DAPMA micelles. The incorporation of C16-DAPMA micelles into DBS-CONHNH$_2$ gels made using Tris-HCl buffer (10 mM) and NaCl (150 mM) was reported in literature.[53] The combination of C16-DAPMA micelles and DBS-CONHNH$_2$ was to be investigated here for its potential use as a water filter for arsenic removal from water due to the ability of C16-DAPMA micelles ability to bind arsenate in Tris-HCl buffer (10mM) and NaCl (150 mM) as demonstrated in Section 2.2.

Incorporating C16-DAPMA micelles into the DBS-CONHNH$_2$ gel network was performed by initially forming a solution of C16-DAPMA micelles by sonication, transferring this solution of C16-DAPMA micelles into a vial containing DBS-CONHNH$_2$ and making up to the required concentration. Finally, the hydrogels were formed *via* a heat-cool cycle. Previous studies had shown that components can assemble orthogonally but brief characterization was also performed here.[53]

2.4.1 Minimum Gelation Concentration

The minimum gelation concentration was investigated, to see if C16-DAPMA micelles incorporated into DBS-CONHNH$_2$ hydrogels affected gelation.

Table 2.4.1 Results of the gelation test to investigate if the presence of C16-DAPMA affected the gelation range of DBS-CONHNH$_2$ hydrogels at a variety of concentrations of DBS-CONHNH$_2$ gelator. Hydrogels were 0.5 mL in a 2.5 mL vial. ✓ - Representing a formation of a self-spanning gel network that passed the tube-inversion test. ✗ - Representing a failure of a self-spanning gel network to form that failed the tube-inversion test.

Concentration of DBS-CONHNH$_2$ / mM	Gel formation of DBS-CONHNH$_2$	Gel formation of DBS-CONHNH$_2$ + C16-DAPMA (1000 µM)
2.11	✗	✗
2.63	✗	✗
3.16	✗	✗
3.69	✓	✓
4.22	✓	✓
4.74	✓	✓
5.27	✓	✓
5.80	✓	✓
6.32	✓	✓
6.85	✓	✓
7.38	✓	✓
7.90	✓	✓
8.43	✓	✓

The inversion test as described in Section 2.3.2, was used to investigate if gelation had occurred for DBS-CONHNH$_2$ hydrogel with C16-DAPMA micelles (1000 µM) incorporated into the hydrogel network. Table 2.4.1 shows that DBS-CONHNH$_2$ still can form hydrogels across a variety of concentrations in the presence of C16-DAPMA micelles (1000 µM). The range at which gelation occurs at for DBS-CONHNH$_2$ hydrogels in the presence and absence of C16-DAPMA micelles (1000 µM), showed gelation occurred over the same concertation range and had the same minimum gelation concentration of 3.69 mM of DBS-CONHNH$_2$.

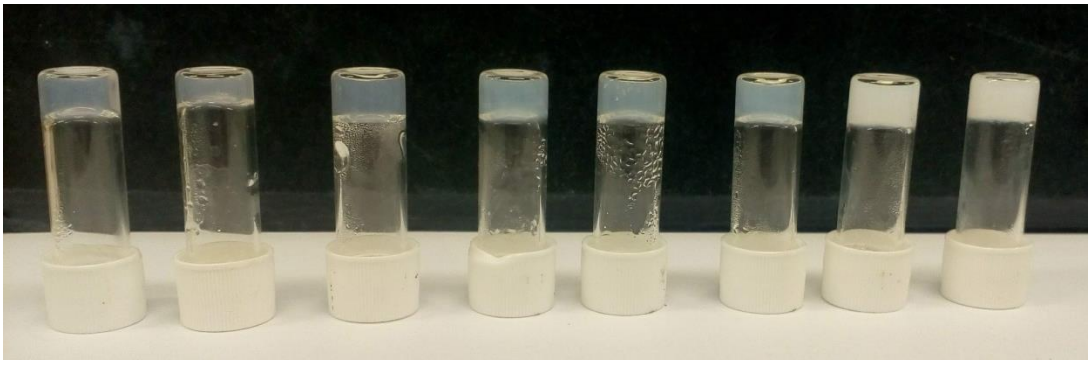

Figure 2.4.1: 0.5 mL DBS-CONHNH$_2$ hydrogels in a 2.5 mL vial, with a variety of concentrations of DBS-CONHNH$_2$ between 3.69 mM and 8.43 mM. Increasing concentrations of DBS-CONHNH$_2$ from left to right

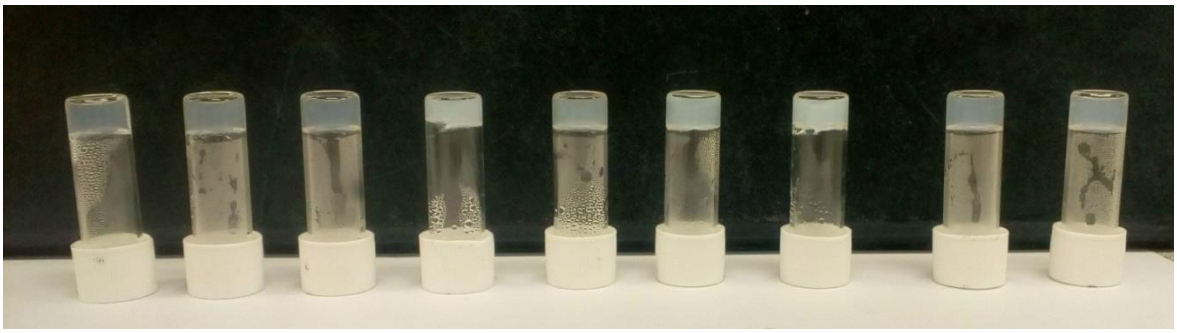

Figure 2.4.2: 0.5 mL DBS-CONHNH$_2$ hydrogels in the presence of C16-DAPMA micelles (1000 µM) in a 2.5 mL vial, with a variety of concentrations of DBS-CONHNH$_2$ between 3.69 mM and 8.43 mM. Increasing concentrations of DBS-CONHNH$_2$ from left to right.

Figures 2.4.1 and 2.4.2 show DBS-CONHNH$_2$ hydrogels at a variety of concentrations in the absence and presence of C16-DAPMA micelles (1000 µM) respectively. In both Figures 2.4.1 and 2.4.2 it is seen that with increasing concentrations of DBS-CONHNH$_2$, the transparency of the hydrogels decreases. As previously mentioned, this is due to a more extensive sample spanning network. This effect is more pronounced in Figure 2.4.1 compared with Figure 2.4.2 when C16-DAPMA is present; potentially the presence of C16-DAPMA micelles in DBS-CONHNH$_2$ hydrogels has an influence on the appearance of the gel, somewhere limiting the aggregation of the gel nanofibers and enhancing the solubility.

2.4.2 Maximum Micelle Concentration

Maximum micelle concentration was investigated to determine the maximum loading of C16-DAPMA micelles which could be incorporated into DBS-$CONHNH_2$ gel network. A variety of concentrations of C16-DAPMA micelles were prepared and 0.5 mL of the C16-DAPMA micelles solution was added into a 2.5 mL vial, to create a solution of DBS-$CONHNH_2$ (5.90 mM). This solution was heated and allowed to cool see if gel formation occurred.

Table 2.4.2: Results of the gelation test to determine the maximum loading of C16-DAPMA micelles that can be incorporated into a DBS-$CONHNH_2$ (5.90 mM) hydrogels. Hydrogels were 0.5 mL in a 2.5 mL vial. ✓ - Representing a formation of a self-spanning gel network that passed the tube-inversion test. ✗ - Representing a failure of a self-spanning gel network to form that failed the tube-inversion test.

C16-DAPMA Concentration / µM	Gel formation?
1000	✓
1250	✓
1500	✓
1750	✓
2000	✓
2250	✗
2500	✗
2750	✗
3000	✗

It was shown (Table 2.4.2) that DBS-$CONHNH_2$ was able to form hydrogels in the presence of C16-DAPMA micelles over a variety of concentrations up until 2000 µM. Beyond the concentration of 2000 µM C16-DAPMA micelles, DBS-$CONHNH_2$ failed to fully dissolve during heat cool cycle, potentially due to saturation of the solution being reached.

2.4.3 T_{Gel}

T_{Gel} measurements were employed to investigate if the presence of C16-DAPMA micelles in DBS-$CONHNH_2$ hydrogels affected the thermal stability. The same procedure as in Section 2.3.3 was used. The inversion test as described in Section 2.3.2, was carried out

on DBS-$CONHNH_2$ hydrogels every 1 ˚C as the temperature of the oil bath increased; the T_{Gel} value is the temperature at which the gel is no longer a self-supporting network.

Table 2.4.3 T_{Gel} values for 0.5 mL DBS-$CONHNH_2$ hydrogels in a 2.5 mL vial, at a variety of concentrations of DBS-$CONHNH_2$ in the presence and absence of C16-DAPMA micelles (1000 µM)

Concentration of DBS-$CONHNH_2$ / mM	T_{Gel} Value for absence of C16-DAPMA / ˚C	T_{Gel} Value for presence of C16-DAPMA / ˚C
4.22	98	86
4.74	>100	>100
5.27	88	61
5.80	>100	>100
6.32	>100	>100
6.85	>100	>100
7.38	>100	>100
7.90	>100	>100
8.43	>100	>100

Table 2.4.3 shows the T_{gel} values for DBS-$CONHNH_2$ hydrogels in the absence and presence of C16-DAPMA micelles (1000 µM). For all concentrations of DBS-$CONHNH_2$ except for 4.22 mM and 5.27 mM of DBS-$CONHNH_2$, the T_{Gel} value for the DBS-$CONHNH_2$ hydrogel was not affected by the presence of C16-DAPMA micelles (1000 µM) as it remained >100 ˚C. At a concentration of 4.22 mM of DBS-$CONHNH_2$, there was a difference between T_{Gel} values in the presence and absence of C16-DAPMA micelles (1000 µM), the values being 86 ˚C and 98 ˚C respectively. The difference may suggest that C16-DAPMA micelles have an effect on thermal stability of hydrogels at low concentration of DBS-$CONHNH_2$, perhaps by limiting the entanglement of the nanofibers.

2.4.4 TEM of DBS-CONHNH$_2$ hydrogel in the presence of C16-DAPMA micelles

TEM images were recorded of DBS-CONHNH$_2$ hydrogels (5.90 mM) in the presence of C16-DAPMA micelles (1000 µM) in ultra-pure water. The sample was placed onto a copper grid and excess water was removed using filter paper. A negative stain (1% uranyl acetate) was applied and left to dry for 30 minutes.

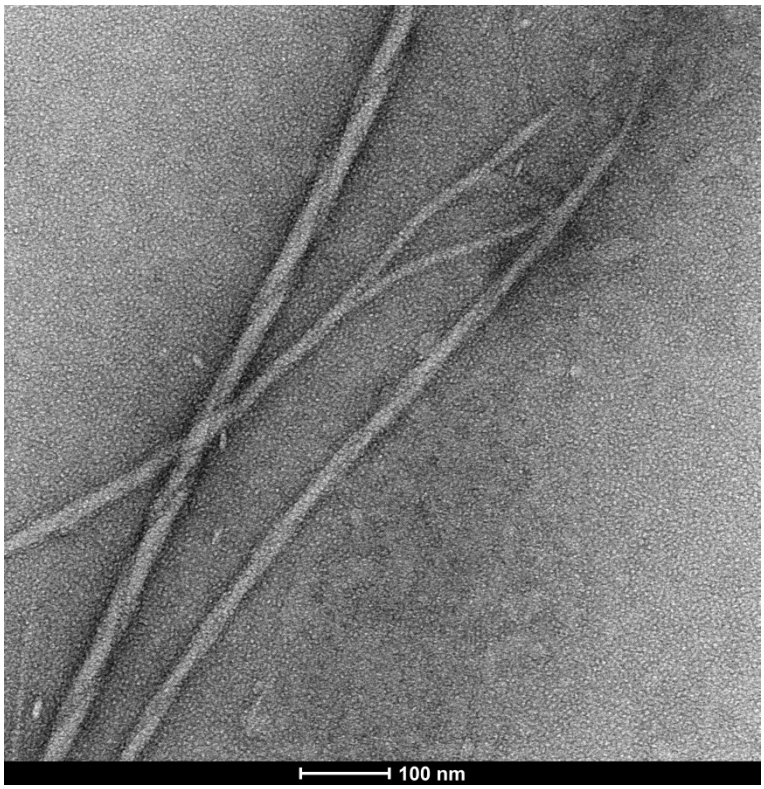

Figure 2.4.3 TEM images of DBS-CONHNH$_2$ (5.90 mM) hydrogel in the presence of C16-DAPMA micelles (1000 µm) in ultrapure water at 49k magnification.

The TEM image of DBS-CONHNH$_2$ hydrogel in the presence of C16-DAPMA micelles (Figure 2.4.3), showed the presence of DBS-CONHNH$_2$ hydrogel fibrils as well as C16-DAPMA micelles. The average fibril width was calculated using ImageJ by measuring a number of different fibril widths and taking an average. This was then compared with the previous values in the absence of C16-DAPMA micelles (Section 2.3.4). The average fibril width of DBS-CONHNH$_2$ in the absence and presence of C16-DAPMA micelles were 13.9 nm and 19.6 nm respectively; this indicates that presence of C16-DAPMA micelles may cause slightly thicker fibrils.

The average C16-DAPMA micelle diameter was calculated using ImageJ by measuring a number of C16-DAPMA micelles and taking an average. The average C16-DAPMA micelle diameter was calculated to be 6.8 nm. This shows that the C16-DAPMA micelles when placed into DBS-$CONHNH_2$ hydrogels still form micelles with the expected diameter. This experiment therefore confirms the view that the assembly of the two different components is largely orthogonal.

2.4.5 Rheology of DBS-$CONHNH_2$ hydrogel in the presence of C16-DAPMA micelles

The mechanical properties of DBS-$CONHNH_2$ hydrogels with C16-DAPMA micelles were investigated to see if the presence of C16-DAPMA micelles affected the mechanical properties of DBS-$CONHNH_2$ hydrogels. Data on stiffness and robustness were compared to results obtained in Section 2.3.5 to determine the influence of C16-DAPMA micelles on the mechanical properties of DBS-$CONHNH_2$ hydrogels. Information about the Linear Viscoelastic Region (LVR) were also obtained, and compared to previous results in Section 2.3.5.

DBS-$CONHNH_2$ hydrogels (0.5 mL) at several concentrations in the presence of C16-DAPMA micelles (1000 μM) were prepared in an inverted 2.5 mL vial on the rheometer plate. Excess water was removed by blotting with “blue roll” paper; the rheometer plate was then applied to the gel.

DBS-$CONHNH_2$ hydrogels in the presence of C16-DAPMA (1000 μM) micelles were first tested by an amplitude sweep; this was performed by increasing shear strain at a constant frequency as seen in Figure 2.4.4 and Figure 2.4.5

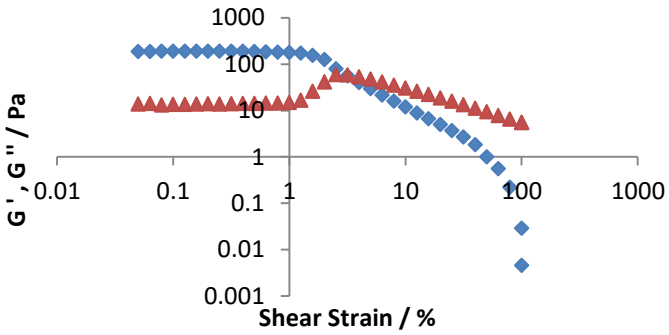

Figure 2.4.4 Amplitude sweep, storage modulus (*G'*, blue diamonds) and loss modulus (*G''*, red triangles) of DBS-CONHNH$_2$ (6.32 mM) hydrogels with C16-DAPMA (1000 µM) with varying shear strain (f = 1 Hz)

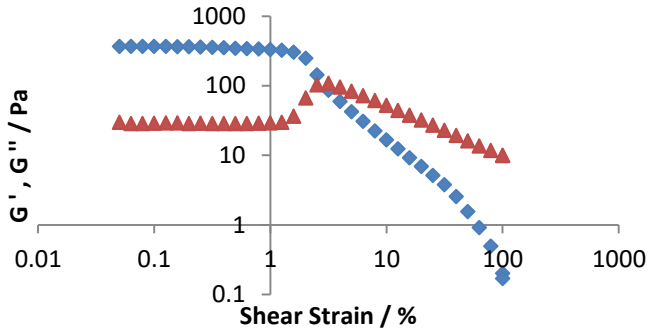

Figure 2.4.5 Amplitude sweep, storage modulus (*G'*, blue diamonds) and loss modulus (*G''*, red triangles) of DBS-CONHNH$_2$ (8.43 mM) hydrogels with C16-DAPMA (1000 µM) with varying shear strain (f = 1 Hz)

Figures 2.4.4 and 2.4.5 show amplitude sweeps of DBS-CONHNH$_2$ hydrogels at varying concentrations in the presence of C16-DAPMA micelles (1000 µM), LVRs were located up to 1.3 % and 1.6 % for DBS-CONHNH$_2$ hydrogels at concentrations of 6.32 mM and 8.43 mM respectively.

Table 2.4.4 Upper limits of LVRs for DBS-CONHNH$_2$ hydrogels at different concentrations in the presence and absence of C16-DAPMA (1000 µM)

Concentration of DBS-CONHNH$_2$ / mM	LVR of DBS-CONHNH$_2$ hydrogel / %	LVR of DBS-CONHNH$_2$ hydrogel with C16-DAPMA (1000 µM) / %
6.32	5.0	1.3
8.43	3.2	1.6

Table 2.4.4 shows LVR values for DBS-CONHNH$_2$ hydrogels at different concentrations in the presence and absence of C16-DAPMA micelles (1000 µM). They demonstrate that

when comparing LVR values for the presence and absence of C16-DAPMA micelles (1000 µM) at the same concentrations of DBS-$CONHNH_2$ hydrogels, the LVR values were lower in the presence of C16-DAPMA micelles. This might suggest that the presence of micelles somewhat limits the entanglement of the self-spanning network.

The CSS from Figures 2.4.4 and 2.4.5 were 3.2 % for each gel respectively. The CSS gives an indication of the robustness of the hydrogel as it quantifies the shear strain at which it breaks down from gel-like behaviour to liquid-like behaviour. The CSS for DBS-$CONHNH_2$ hydrogels in the presence of C16-DAPMA micelles when compared to DBS-$CONHNH_2$ hydrogels in the absence of C16-DAPMA micelles was again much lower.

Frequency sweeps were conducted as well on DBS-$CONHNH_2$ hydrogel in the presence of C16-DAPMA micelles (1000 µM) and compared to previous results in Section 2.3.5. The shear strain applied to the hydrogel during frequency sweep is located within the LVR which was 0.3 %.

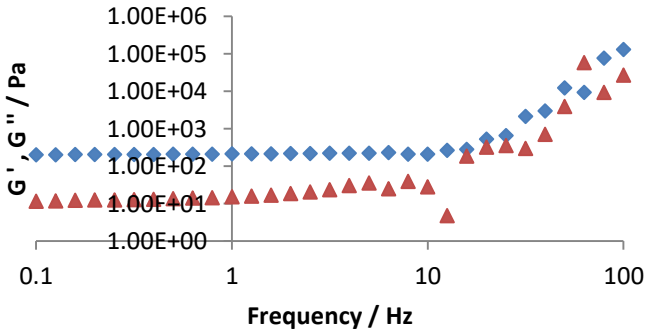

Figure 2.4.6 Frequency sweep, storage modulus (*G'*, blue diamonds) and loss modulus (*G''*, red triangles) of DBS-$CONHNH_2$ (6.32 mM) hydrogels with C16-DAPMA (1000 µM) with constant shear strain and varying frequency

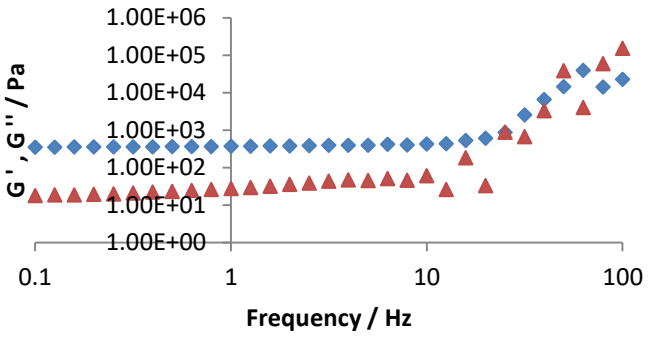

.

Figure 2.4.7 Frequency sweep, storage modulus (*G'*, blue diamonds) and loss modulus (*G''*, red triangles) of DBS-CONHNH$_2$ (6.32 mM) hydrogels with C16-DAPMA (1000 µM) with constant shear strain and varying frequency

Figures 2.4.6 and 2.4.7 show the results of frequency sweeps of DBS-CONHNH$_2$ hydrogels in the presence of C16-DAPMA micelles (1000 µM) at varying concentrations. With increasing frequencies there was no change with *G'* and *G''* up until a point, this corresponds to gel-like behaviour. Beyond this point there is a linear response with *G'* and *G''* with changing frequency, this shows liquid-like behaviour. The frequency values for change between gel-like behaviour and liquid-like behaviour were 15.9 Hz and 25.1 Hz respectively.

Table 2.4.5 Storage modulus (*G'*) and loss modulus (*G''*) values for DBS-CONHNH$_2$ hydrogels in the presence and absence of C16-DAPMA micelles (1000 µM) from frequency sweep in the LVR (f=0.1995 Hz)

	Absence of C16-DAPMA (1000 µM)		Presence of C16-DAPMA (1000 µM)	
Concentration of DBS-CONHNH$_2$ / mM	*G'* / Pa	*G''* / Pa	*G'* / Pa	*G''* / Pa
6.32	177.3	8.1	203.8	12.5
8.43	180.5	10.6	353.9	19.3

Table 2.4.5 shows storage modulus (*G'*) and loss modulus (*G''*) values for DBS-CONHNH$_2$ hydrogels at various concentrations in the presence and absence of C16-DAPMA micelles during the frequency sweep.

Storage Modulus and loss modulus are an indication of the stiffness of a gel, Table 2.4.5 shows at higher concentrations of DBS-CONHNH$_2$ with C16-DAPMA micelles (1000 µM),

the hydrogel was stiffer. When comparing the storage and loss modulus in the presence and absence of C16-DAPMA micelles (1000 μM), the hydrogels containing C16-DAPMA micelles are stiffer hydrogels than those without C16-DAPMA micelles. This suggests a less flexible network probably with micelles limiting fibre flexibility and entanglement.

2.4.6 NMR Spectroscopy of DBS-CONHNH$_2$ hydrogel with C16-DAPMA micelles

1H NMR spectroscopy was used to investigate DBS-CONHNH$_2$ gels to determine whether the presence of C16-DAPMA micelles changes the amount of DBS-CONHNH$_2$ involved / not involved in the gel network. This was compared to the results of Section 2.3.6 NMR spectroscopy of a DBS-CONHNH$_2$ (4.64 mM, 1 mL) hydrogel in the absence of C16-DAPMA micelles.

A DBS-CONHNH$_2$ (4.64 mM, 1 mL) hydrogel was formed in the presence of C16-DAPMA micelles (1000 μM) using D_2O in an NMR tube. Using a 5 μL internal spike of DMSO, an NMR spectrum was acquired and the integrations of the internal spike and a known peak of C16-DAPMA were compared. As before in Section 2.3.6 DBS-CONHNH$_2$ molecules involved in the gel network tumble slowly, so are not seen on an NMR spectrum; only molecules not involved in the DBS-CONHNH$_2$ gel network can be seen on an NMR spectrum.

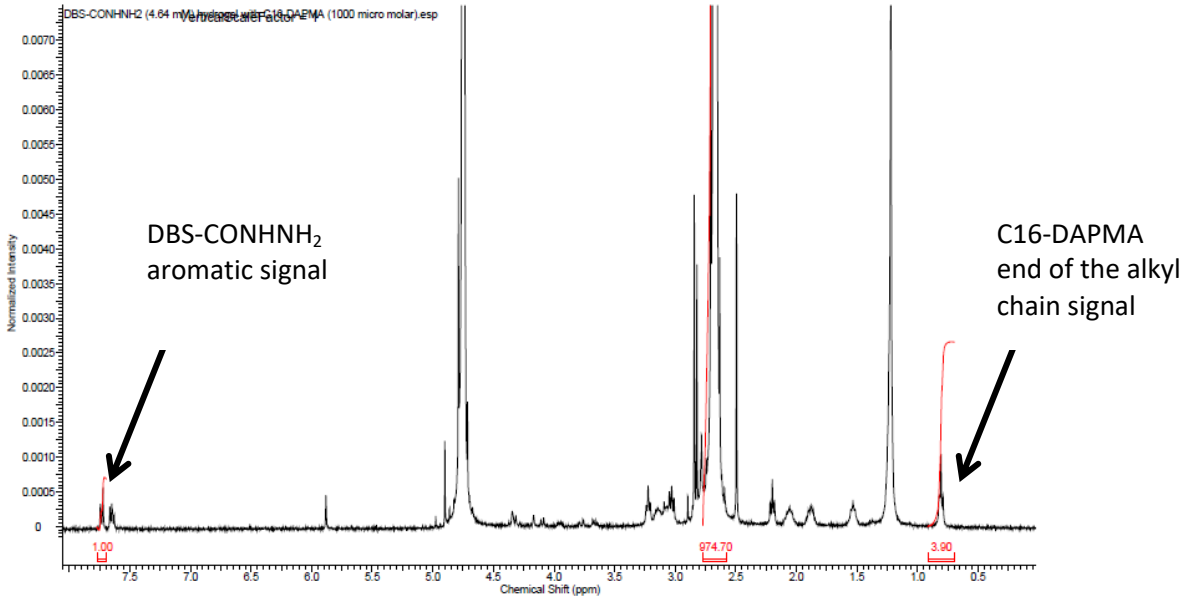

Figure 2.4.8 NMR spectrum of 1 mL DBS-CONHNH$_2$ (4.64 mM) in the presence of C16-DAPMA micelles (1000 µM)

It was found from comparing the integrations of the internal spike to the known NMR peaks of DBS-CONHNH$_2$ and C16-DAPMA, that 0.108 µmol (2.3 %) of DBS-CONHNH$_2$ was not involved in the gel network and 4.532 µmol (97.7 %) was involved in the gel network (Figure 2.4.8).

Comparing the results from Figure 2.4.8 against the results from Section 2.3.6, the absence of C16-DAPMA micelles within DBS-CONHH$_2$ gel network, it was calculated that 0.068 µmol of DBS-CONHNH$_2$ was not involved in the gel network. The presence of C16-DAPMA micelles caused a 59 % increase in DBS-CONHNH$_2$ molecules that are not incorporated into the gel network.

Also shown in Figure 2.4.8, are NMR peaks from C16-DAPMA micelles. It was calculated that 0.563 µmol of C16-DAPMA micelles were not observed, 56.3 % of the 1 µmol of C16-DAPMA micelles initially used to make the DBS-CONHNH$_2$ gel. This indicated that up to 43.7 % of C16-DAPMA micelles may undergo interactions with DBS-CONHNH$_2$ gel network and are consequently not observed by NMR spectroscopy, or are involved in micellar aggregates with sufficiently low tumbling rates that they cannot be observed in a NMR spectrum.

2.5 Arsenate Removal System

The efficiency of DBS-$CONHNH_2$ hydrogel encapsulated with C16-DAPMA micelles for arsenic removal was then investigated, based on the C16-DAPMA micelles ability to bind arsenate (Section 2.3). Arsenic analysis was performed to calculate how much arsenate was removed using DBS-$CONHNH_2$ hydrogel in the presence of C16-DAPMA.

2.5.1 Colorimetric Method

A literature search was conducted for a method for quantitative arsenic analysis. A number of options were considered, such as work by Merargie *et al.* which involved anodic stripping voltammetry and differential pulse anodic stripping voltammetry, using a gold working electrode.[59] The reported arsenic detection limit was 0.02 ppb, below the World Health Organization (WHO) limit of arsenic concentration in drinking water (10 ppb).[60]

Ray *et al.* conducted work into using glutathione, dithiothreitol and cysteine based gold nanoparticles. These had the ability to bind arsenite and a detection limit of 10 ppt using DLS.[41] Neither of these methods was chosen for quantitative arsenic analysis due to their complexity.

Dhar *et al.* reported a colorimetric method for arsenic analysis developed from the Johnston and Pilson method.[61,62] The method reported a detection limit of between 50 – 400 ppb but used a calibration curve of between 10-1000 ppb. For the colour to develop, solutions of; L-ascorbic acid (10.8 %), ammonium molybdate (3 %), antimony potassium tartrate (0.56 %) and sulfuric acid (13.98 %); were mixed together in a ratio of 2:2:1:5 to form the indicator solution. Samples were acidified with HCl so the final concentration was 1 %. This method was investigated further for its suitability in this study.

A number of solutions were prepared containing different concentrations of arsenic between 20 – 2000 ppb for use on a calibration curve, then acidified using HCl (2 %). The indicator solution (0.5 mL) was added to the standard solutions (5 mL), and an ultraviolet – visible (UV-Vis) spectrum was recorded. The UV-Vis spectra showed no colour development and the method could not be taken further here.

However it was noticed, when adding the indicator solution to higher concentrations of arsenate solutions (7.10 mM), a blue colour was produced which could be monitored by

UV-visible spectroscopy. A calibration curve was constructed using a number of solutions containing arsenate up to 7.10 mM; the indicator solution (0.5 mL) was added to each of the arsenate solutions and a UV-Vis spectrum was recorded.

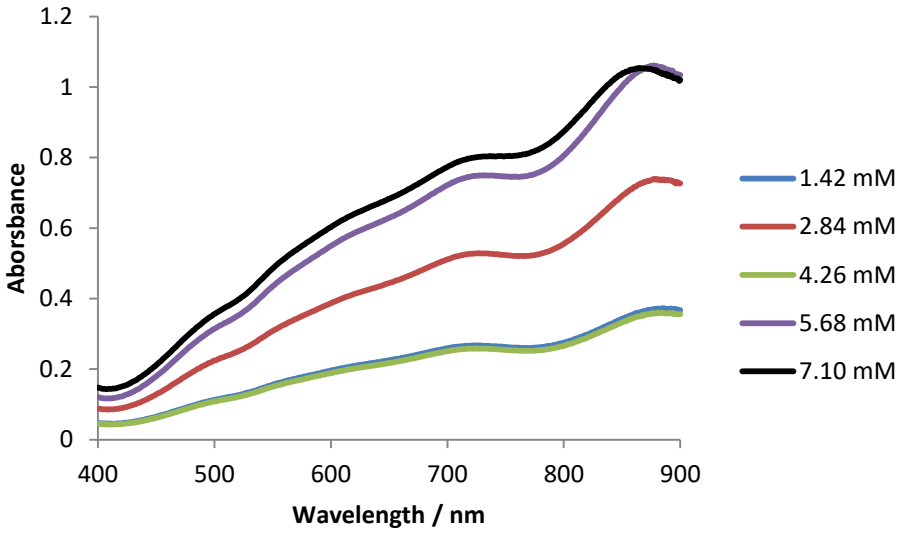

Figure 2.5.1 UV-Vis Spectrum for arsenate solutions at different concentrations after 0.5 mL of indicator solution being added for a calibration curve.

Figure 2.5.1 shows a series of UV-Vis spectra of arsenate solutions at different concentrations after the indicator solution (0.5 mL) were added. It was determined that, even though at all concentrations of arsenate a coloured solution had formed, the data produced for the calibration curve was uncorrelated and therefore not useable. As an example, the response of the 2.84 mM solution of arsenate was higher than the absorbance values for the 4.26 mM solution. Based on these results, the method was determined to be unsuitable for this work.

2.5.2 Arsenic Test Kit

Reconsidering arsenic analysis work by Sarkar *et al.*, we considered a method that could be used as a field test kit for arsenic detection in water.[42] Detection was based on the production of arsine gas using potassium permanganate, a mixture of sulfamic acid and L-ascorbic acid and a mixture of zinc dust and sodium borohydride. The arsine gas produced was detected by a mercuric bromide paper strip, which changed colour depending on the concentration of arsine gas. Figure 2.5.2 shows the different yellow colours that mercuric bromide paper develops with different concentrations of arsine.

Figure 2.5.2 Colour mercuric bromide paper turns with different concentrations of arsenic.[42]

The use of potassium permanganate in the test kit prevents the interference of sulphides such as hydrogen sulphide with the measurements. The mixture of acids and zinc was used to produce in-situ hydrogen. The zinc and sodium borohydride are thus used to produce arsine. The work by Sarkar *et al.* shows an alternative method for arsenic analysis by the production of arsine gas which could be used more easily than other methods mentioned above due to quantifying the amount of arsenic present by colour comparison.

$$As_4O_6 + 12\ Zn + 24\ H^+ \longrightarrow 4\ AsH_3 + 12\ Zn^{2+} + 6\ H_2O$$

Figure 2.5.3 Chemical equation for the production of arsine gas

It was decided for initial work a commercial version of this arsenic test kit was suitable and could be used in this study. Indeed, this is the way arsenic levels are determined in the field and hence seemed suitable for use. It was purchased from Simplex Health. The chosen test kit used a modified Gutzeit method, which usually uses zinc and hydrochloric acid to generate arsine gas (Figure 2.5.3).[63, 64] The test kit instead used L-tartaric acid in place of hydrochloric acid, due to its safer handling. It also used potassium peroxymonosulfate to prevent interference from hydrogen sulphide.

To quantify the arsenic present in solution, mercuric bromide paper turned coloured in the presence of arsine gas. This was compared against a colour chart (Figure 2.5.4). The arsenic test kit required 100 mL of a solution to quantify the concentration of arsenic present in the sample.

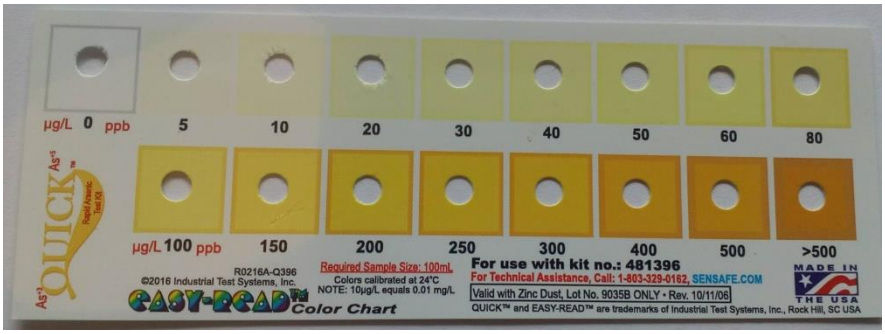

Figure 2.5.4 Image of arsenic test kit colour scale

The commercial test kit was verified using a solution of arsenate at 298 ppb. Figure 2.5.5 shows the mercuric bromide paper strip turned the correct colour when exposed to this solution, and was therefore fit for purpose.

Figure 2.5.5 The arsenic test kit results on a solution of arsenate (298 ppb) placed on top of the colour scale provided

Figure 2.5.5 shows the results of the arsenic test kit on a solution of arsenate calculated to contain 298 ppb of arsenate. It was shown that due to the similarity in colours between arsenic concentrations it was hard to identify a particular arsenic concentration present; this resulted in a higher potential for uncertainty in the indication of arsenic concentration present. Figure 2.5.5 gave an estimated arsenate concentration of between 250 to 300 ppb from the colour of the mercuric bromide paper strip turned compared against the colour scale.

Literature has reported that DBS-$CONHNH_2$ forms stable hydrogels in the presence of C16-DAPMA micelles in a vial. These hydrogels are still relatively weak rheologically and easily break down from gel-like behaviour to liquid-like behaviour as seen in the CSS values in Section 2.4.5. Additional mechanical strength is therefore needed to improve the strength and robustness of the DBS-$CONHNH_2$ hydrogels in the presence of C16-

DAPMA micelles to give sufficient robustness to be removed from water for the arsenate removal experiments. On their own, the DBS-$CONHNH_2$ hydrogels in the presence of C16-DAPMA micelles would fall apart when placed into such a large amount of water. Agarose (2.36 mg mL^{-1}) was used to increase the mechanical strength of the DBS-$CONHNH_2$ hydrogels in the presence of C16-DAPMA micelles, as agarose can form polymeric hydrogels *via* a heat-cool cycle. Literature has already reported the incorporation of agarose into DBS-$CONHNH_2$ hydrogels in the presence of C16-DAPMA micelles as a simple strengthening technique.[53]

The quantification of arsenate uptake by DBS-$CONHNH_2$ and agarose hydrogels in the presence and absence of C16-DAPMA (1000 µM) was investigated by forming a hydrogel (2 mL) in an upturned syringe (10 mL) with the nozzle cut off and the plunger in place. Once gelation had occurred this was placed into a solution (100 mL) containing $Na_2HAsO_4.7H_2O$ (0.213 µmol), calculated to be 298 ppb of $HAsO_4$. (Figure 2.5.6).

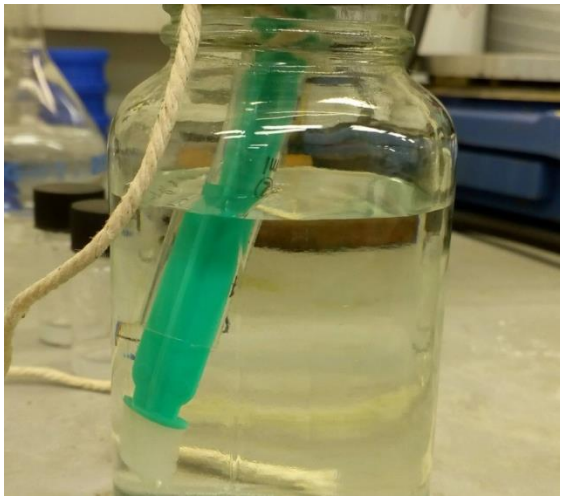

Figure 2.5.6 Image of 2 mL hydrogel of C16-DAPMA (1000 µM), DBS-$CONHNH_2$ (4.68 mM) and agarose (2.36 mg mL^{-1}) made in a 10 mL syringe and placed in 100 mL solution of arsenate (298 ppb)

Initial studies were conducted for arsenic removal efficiency using the hydrogel (2 mL) in the presence of C16-DAPMA micelles (1000 µM). The time dependence of arsenic removal was also investigated by leaving a hydrogel (2 mL) in the solution containing arsenate (298 ppb) for 24 and 72 hours. After 24 and 72 hours the hydrogels were removed and an arsenic test kit was carried out on the solutions.

It should be noted that this is a qualitative approach and there are therefore errors associated with colour detection. However, this methodology is used in the field for arsenic detection, and the focus here was on looking for significant differences induced by C16-DAPMA rather than determining precise quantities of arsenic. It is estimated the errors associated with this approach as being equivalent to one colour either side of the specified colour on the test strip (e.g. 250 ppb = 200-300 ppb, 50 ppb = 40-60 ppb).

It is important to note that the thesis printing process affected the apparent colour identification given the similarities between the yellow and orange colours inherent within the test kit. Colour matching was therefore performed on original samples under laboratory lighting conditions and was not performed based on the printed images.

In summary, this is considered to be a useful indicative approach to consider large changes in arsenic concentration, which is hoped, would be induced by these gel-phase materials. Clearly, other strategies, such as ICP-MS (see below) are required for more quantitative conclusions to be made.

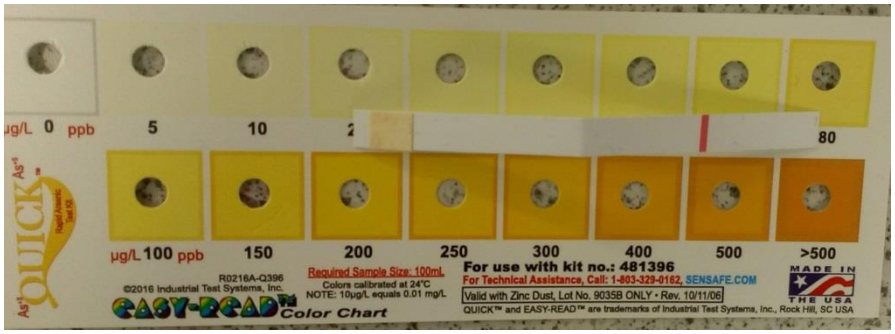

Figure 2.5.7 Shows the mercuric bromide paper colour after arsenic test kit on a solution that had a 2 mL hydrogel of C16-DAPMA (1000 µM), DBS-CONHNH$_2$ (4.68 mM) and agarose (2.36 mg mL^{-1}) placed in it for 24 hours

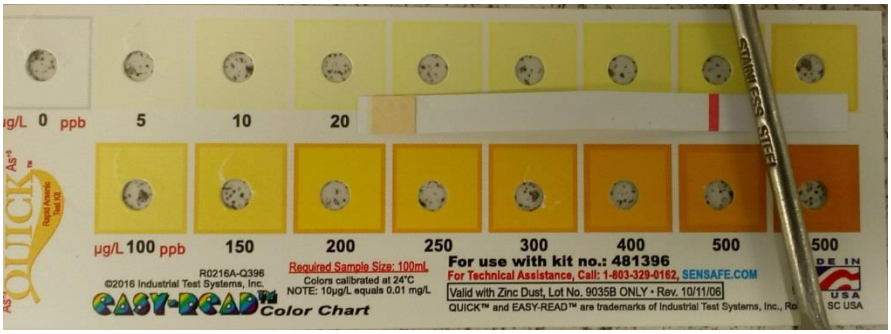

Figure 2.5.8 Shows the mercuric bromide paper colour after arsenic test kit on a solution that had a 2 mL hydrogel of C16-DAPMA (1000 µM), DBS-CONHNH$_2$ (4.68 mM) and agarose (2.36 mg mL^{-1}) placed in it for 72 hours

Figures 2.5.7 and 2.5.8 show the results from the arsenic removal experiment after 24 and 72 hours respectively. The hydrogel (2 mL) containing C16-DAPMA micelles (1000 µM), DBS-CONHNH$_2$ (4.68 mM) and agarose (2.36 mg mL^{-1}) was shown to have extracted arsenate from the solution. When comparing the bromide paper colour to the colour scale (Figures 2.5.7 and 2.5.8) it was determined that the solution decreased in arsenate concentration from 298 ppb of arsenate to an estimated value of between 80 to 100 ppb from the colour of the mercuric bromide paper strip turned compared against the colour scale. Although the above Figures indicate an arsenate concentration of between 200 to 250 ppb, this is not a true reflection of the sample due to the thesis printing process. The estimated arsenate concentration of 80 to 100 ppb was concluded on the original samples under laboratory lighting conditions.

When the colour of mercuric bromide paper after 24 and 72 hours were compared, it was demonstrated that the colours were similar. This indicated the maximum amount of arsenate adsorption was probably reached within the first 24 hours of being placed into the solution.

An investigation into whether C16-DAPMA micelles were the only component of the hydrogel system that had the ability to adsorb arsenic was investigated. A hydrogel (2 mL) of DBS-CONHNH$_2$ (4.64 mM) and agarose (2.36 mg mL^{-1}) was prepared in the absence of C16-DAPMA micelles (1000 µM) and placed in a solution (100 mL) of arsenate (298 ppb).

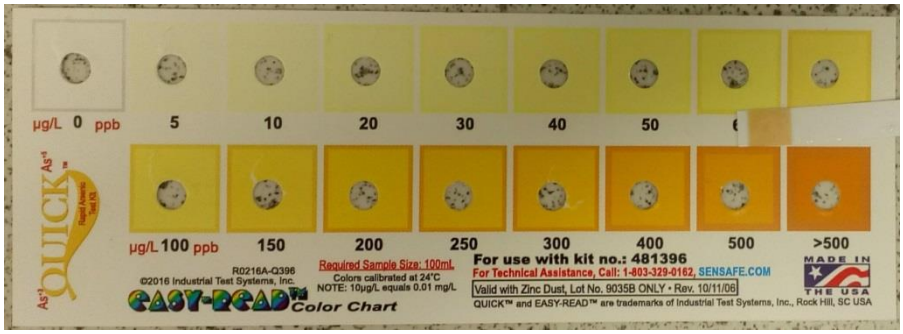

Figure 2.5.9 Shows the mercuric bromide paper colour after arsenic test kit on a solution that had a 2 mL hydrogel of DBS-CONHNH$_2$ (4.68 mM) and agarose (2.36 mg mL^{-1}) placed in it for 72 hours

Figure 2.5.9 shows the results of the of arsenic removal experiment using DBS-CONHNH$_2$ and agarose hydrogel. The concentration of arsenate present after the hydrogel was removed after 72 hours was estimated to be between 250 to 300 ppb from the colour of the mercuric bromide paper strip turned compared against the colour scale. When the colour of the mercuric bromide paper was compared between this experiment (Figure 2.5.9) and a known solution of 298 ppb arsenate (Figure 2.5.5) it was seen they were very similar. This demonstrated that the of DBS-CONHNH$_2$ and agarose components of the hydrogel has small or negligible amount of arsenate adsorbed compared to the C16-DAPMA micelles within DBS-CONHH$_2$ and agarose hydrogel.

Further study used an agarose hydrogel without DBS-CONHNH$_2$ was conducted. The concentration of arsenate present after the hydrogel was removed after 72 hours was estimated to be between 250 to 300 ppb from the colour of the mercuric bromide paper strip turned compared against the colour scale. When using an original sample under laboratory lighting conditions. When the colour of the mercuric bromide paper was compared between this experiment (Figure 2.5.10) and a known solution of 298 ppb arsenate (Figure 2.5.4) it was seen they were similar. Demonstrating that the agarose hydrogel alone had negligible amount of arsenate adsorbed compared to C16-DAPMA micelles within DBS-CONHNH$_2$ and agarose hydrogel.

Figure 2.5.10 Shows the mercuric bromide paper colour after arsenic test kit on a solution that had a 2 mL hydrogel of Agarose (2.36 mg mL^{-1}) placed in it for 72 hours

As such this study suggested that DBS-CONHNH$_2$ loaded with C16-DAPMA micelles was able to significantly reduce the loading of arsenate in solution. However it was not possible to reduce the concentration to below the WHO level of 10 ppb.

2.5.3 Inductively Coupled Plasma - Mass Spectrometry (ICP-MS)

ICP-MS was used to provide quantitative arsenic analysis after arsenic removal. It was suitable as the limit of detection of ICP-MS is below 1 ppb for arsenic. This was also conducted as a follow on assay after using the arsenic test kit into the investigation to the impact on the individual components into arsenic removal system. Three hydrogels samples (2 mL) were prepared as mentioned in Section 2.5.2; C16-DAPMA (1000 µM), DBS-CONHNH$_2$ (4.68 mM) and agarose (2.36 mg mL^{-1}) hydrogel, DBS-CONHNH$_2$ (4.68 mM) and agarose (2.36 mg mL^{-1}) hydrogel and agarose (2.36 mg mL^{-1}) hydrogel. These were then placed into a solution for 72 hours calculated to contain 298 ppb of arsenate. Aliquots (10 mL) of the resulting solutions were sent off for ICP-MS analysis at the University of Hull, in addition to an additional control sample of stock solution, calculated to be 298 ppb of arsenate. The results are shown in Table 2.5.1.

Table 2.5.1 ICP-MS results for arsenic extraction

Hydrogel Components	Arsenate Concentration / ppb
C16-DAPMA (1000 µM), DBS-$CONHNH_2$ (4.68 mM) and agarose (2.36 mg mL^{-1}) -1	198.486
C16-DAPMA (1000 µM), DBS-$CONHNH_2$ (4.68 mM) and agarose (2.36 mg mL^{-1}) -2	302.405
DBS-$CONHNH_2$ (4.68 mM) and agarose (2.36 mg mL^{-1})	272.296
Agarose (2.36 mg mL^{-1})	382.393
Stock solution (calculated to be 298 ppb)	242.900

Table 2.5.1 shows the ICP-MS results from the arsenic removal system using C16-DAPMA, DBS-$CONHNH_2$ and Agarose. As seen in Table 2.5.1, the ICP-MS results were inconclusive due to the fact that the, the extraction results for C16-DAPMA, DBS-$CONHNH_2$ and agarose hydrogel not being of similar values; for one sample the arsenate concentration was 198.486 ppb and the other sample the arsenate concentration was 302.405 ppb. It is not clear why these ICP-MS results are inconsistent. Further work would be required, with greater use of control samples, and focus on sample preparation to understand this in more detail.

Due to time constraints after the inconsistent results from the ICP-MS results, it was not possible to obtain further ICP-MS results; further study will be needed to obtain accurate results.

2.6 Leaching of C16-DAPMA micelles from DBS-CONHNH$_2$ Hydrogels

An investigation into the leaching of C16-DAPMA out of DBS-CONHNH$_2$ hydrogels into water was conducted. This could be problematic for industrial use, as C16-DAPMA is cytotoxic. If leaching occurs out of the DBS-CONHNH$_2$ hydrogel, this is a potential issue which could prevent its use in an arsenic removal system as it will be present in water.[53] A hydrogel (2 mL) of C16-DAPMA (1000 µM), DBS-CONHNH$_2$ (4.68 mM) and agarose (2.36 mg mL^{-1}) was prepared *via* a heat-cool cycle in a syringe (10 mL) and placed in deionised water (100 mL) (Figure 2.6.1).

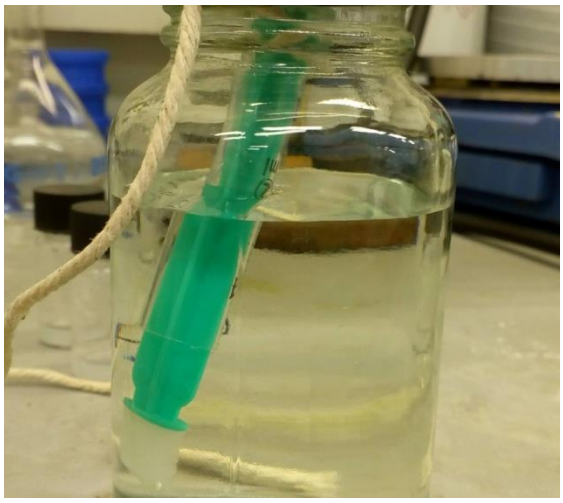

Figure 2.6.1 Image of 2 mL hydrogel of C16-DAPMA (1000 µM), DBS-CONHNH$_2$ (4.68 mM) and agarose (2.36 mg mL^{-1}) made in a 10 mL syringe and placed in 100 mL of deionised water.

Literature has reported that DBS-CONHNH$_2$ forms stable hydrogels in the presence of C16-DAPMA micelles in a vial. These hydrogels are still relatively weak rheologically and easily break down from gel-like behaviour to liquid-like behaviour as seen in the CSS values in Section 2.4.5. Additional mechanical strength is therefore needed to improve the strength and robustness of the DBS-CONHNH$_2$ hydrogels in the presence of C16-DAPMA micelles to give sufficient robustness to be removed from water for the arsenate removal experiments. On their own, the DBS-CONHNH$_2$ hydrogels in the presence of C16-DAPMA micelles would fall apart when placed into such a large amount of water. Agarose (2.36 mg mL^{-1}) was used to increase the mechanical strength of the DBS-CONHNH$_2$ hydrogels in the presence of C16-DAPMA micelles, as agarose can form polymeric

hydrogels *via* a heat-cool cycle. Literature has already reported the incorporation of agarose into DBS-$CONHNH_2$ hydrogels in the presence of C16-DAPMA micelles as a simple strengthening technique.[53] Deionised water (100 mL) was used for this study to mirror the arsenic removal experimental in Section 2.5.2.

After 3 days the gel was removed and deionised water removed in *vacuo*. The residue was dissolved in deuterated dimethyl sulfoxide (DMSO-d_6) with an internal spike of chloroform (10 µL) and an NMR spectrum was recorded. Comparing integrals of chloroform and the known peaks of C16-DAPMA, an average of three measurements was calculated. It was shown that 1.14 µmol of C16-DAPMA leaches out of the hydrogel (2 mL) which initially contained 2 µmol of C16-DAPMA (57 % of C16-DAPMA was lost through leaching). This highlighted a potential problem for to commercial use of this system to remove arsenic using the combination of DBS-$CONHNH_2$ hydrogel in the presence of C16-DAPMA.

3.0 Conclusion and Future work

3.1 C16-DAPMA micelles with arsenic

In this work, C16-DAPMA, which has been reported in literature was synthesised.[51] C16-DAPMA molecules were shown by DLS and TEM images to form micelles, the micelle diameter (7.1 ± 0.2 nm) and critical micelle concentration (42 ± 2 μM) was shown to be consistent with literature values. The surface of C16-DAPMA micelles were determined to be positively charged by measuring the zeta potential. Due to the positive surface charge of the C16-DAPMA micelles, the investigation between C16-DAPMA micelles and anionic arsenate (As (V)) was able to be conducted.

Studies were conducted with arsenate, which exists as an anion at certain pH values. Large aggregate of arsenate and C16-DAPMA micelles formed and was observed using DLS and TEM. By measuring the zeta potential, it was found that the presence of arsenate with C16-DAPMA decreased the surface charge of the C16-DAPMA micelles compared with the absence of arsenate. This indicated the interactions between C16-DAPMA micelles and arsenate were electrostatic interactions and therefore they were suitable for arsenate removal studies.

3.2 DBS-$CONHNH_2$ with C16-DAPMA micelles

DBS-$CONHNH_2$ was synthesised following literature procedures.[56] It was found that DBS-$CONHNH_2$ formed hydrogels at concentrations as low as 2.11 mM. The thermal stability of the hydrogels were investigated and it was observed that the DBS-$CONHNH_2$ hydrogels at all concentrations had good thermal stability. The mechanical properties of the DBS-$CONHNH_2$ hydrogels were investigated and it was found that with increasing concentration of DBS-$CONHNH_2$, the stiffness of the hydrogel increased. This increase in stiffness with increase in concentration of DBS-$CONHNH_2$ was not linear. This was due to the fact that above 6.32 mM no more DBS-$CONHNH_2$ was added to the nanofibers in the gel network. This would result in the gel fibres becoming thicker up until a point above 6.32 mM, after this point the additional DBS-$CONHNH_2$ added was not involved in the gel

network. This dual trend was also observed with the appearance of the gel; the decrease of transparency of the gel was observed up until a point. From NMR spectroscopy data at 4.64 mM of DBS-$CONHNH_2$, it was calculated that 1.5 % of DBS-CONHNH molecules were not involved in the gel network. These values were measured for the comparison of the properties of DBS-$CONHNH_2$ hydrogels in the presence and absence of C16-DAPMA micelles.

The presence of C16-DAPMA micelles embedded in the gel network was shown not to affect the gelation range or the thermal stability of DBS-$CONHNH_2$ hydrogels. DBS-$CONHNH_2$ formed hydrogels with embedded C16-DAPMA micelle concentrations as high as 2000 μM; beyond this concentration DBS-$CONHNH_2$ failed to fully dissolve, potentially due to saturation of the solution. The mechanical properties of the DBS-$CONHNH_2$ hydrogels in the presence of embedded C16-DAPMA micelles were investigated. It was found that the presence of C16-DAPMA micelles caused stiffening of the DBS-$CONHNH_2$ hydrogel when compared with the absence of C16-DAPMA micelles. The increase in the stiffness is likely to be due to the presence of C16-DAPMA micelles limiting the entanglement of the self-supporting network, leading to less flexibility. TEM images were recorded of DBS-$CONHNH_2$ hydrogel in the presence and absence of C16-DAPMA; it was found that the presence of C16-DAPMA micelles leads to thicker DBS-$CONHNH_2$ hydrogel fibres, compared to the absence of C16-DAPMA within the gel network. The images of DBS-$CONHNH_2$ hydrogel in the presence of C16-DAPMA micelles showed the presence of micelles within the hydrogel with the correct diameter for C16-DAPMA micelles. NMR spectroscopy studies found that 2.3 % of DBS-$CONHNH_2$ molecules (from a starting concentration of 4.64 mM of DBS-$CONHNH_2$) were not involved in the gel network, this is higher than the amount of DBS-$CONHNH_2$ not involved in the gel network in the absence of C16-DAPMA micelles. It was also found using NMR spectroscopy that 46.7 % of the C16-DAPMA was not observed when embedded in the gel network. This indicated that C16-DAPMA had potentially interacted with DBS-$CONHNH_2$ fibres or they were involved in micellar aggregates with sufficiently low tumbling rates that they could not be observed in a ^{1}H NMR spectrum.

3.3 Arsenate Removal System

The combination of C16-DAPMA micelles, DBS-$CONHNH_2$ and agarose hydrogel was investigated for its ability to remove arsenate from water. It was found the combination of Agarose, DBS-$CONHNH_2$ and embedded C16-DAPMA micelles had the ability to reduce the concentration of arsenate in water from 298 ppb to be an estimated value of between 80 to 100 ppb from the colour of the mercuric bromide paper strip turned compared against the colour scale in laboratory conditions. In comparison, when using the DBS-$CONHNH_2$ and agarose hydrogel without the embedded C16-DAPMA micelles, it was found that only a small reduction of arsenate concentration was observed. This proves that C16-DAPMA micelles had the biggest influence in the removal of arsenate within the hydrogel system. ICP-MS results were not useable due to unknown reasons; therefore further study is needed to investigate for the adsorption capacity and for quantitativearsenic analysis.

It was found that 57 % of the C16-DAPMA micelles leached from the combination of C16-DAPMA, DBS-$CONHNH_2$ and Agarose hydrogel into water. The leaching of C16-DAPMA is an issue due to C16-DAPMA being cytotoxic.[53] This makes it currently unsuitable in the use of an arsenic removal system but further work may be conducted to solve this issue.

3.4 Future Work

In this work, the removal of arsenate was studied; further investigation of the removal of both arsenite and arsenate simultaneously is recommended, as arsenite and arsenate are both present in groundwater. Work by Okesola and Smith showed that DBS-$CONHNH_2$ had the ability for the removal of arsenite.[34] Work using C16-DAPMA did not show any potential to remove arsenite but has demonstrated the ability of C16-DAPMA to remove arsenate.

DBS-$CONHNH_2$ hydrogels were previously shown to have the ability to adsorb cations such as Hg^{2+} and this work has demonstrated they are able to remove anionic species. In countries such as Indonesia, where illegal gold mining occurs, both mercury and cyanide are present in water due to the gold mining process.[65] Mercury exists as a cation in water and cyanide exists as an anion in water. Therefore, the combination of DBS-$CONHNH_2$ and C16-DAPMA could be investigated for the removal of mercury and cyanide from water in addition to arsenic.

4.0 Experimental

4.1 General Experimental

All reagents were purchased from commercial sources and used directly without further purification. Proton and carbon NMR spectra were recorded on a Jeol 400 spectrometer (^{1}H 400 MHz, ^{13}C 100 MHz). Thin Layer Chromatography (TLC) was performed on Merck aluminium-backed plates coated with 0.25 nm silica gel 60. Preparative Gel Permeation Chromatography (GPC) was performed on Biobeads SX-1 supplied by Bio-Rad. ESI mass spectra were recorded on a Bruker Daltonics Micro-TOF mass spectrometer. Fluorescence spectra were obtained with a Hitachi F-4500 fluorimeter. UV-Vis absorbance was recorded on a Shimadzu UV-2401PC spectrophotometer. TEM images were obtained by Meg Stark at the Biology Technology Faculty, University of York using an FEI Tecnai 12 Bio TWIN operated at 120 kV. Thermal stability was recorded on a Huber Ministat 230 circulator oil bath. DLS and zeta potential measurements were recorded on a Zetasizer Nano ZS. Rheology studies were performed on a Kinexus Pro+ rheometer from Malvern instruments using parallel plate geometry. ICP-MS results were obtained by Bob Knight at Trace Elemental Analysis laboratory, University of Hull.

4.2 Synthesis

4.2.1 Synthesis of tert-butyl 3-((3-aminopropyl)(methyl)amino) propyl carbamate (Mono-Boc DAPMA).[51]

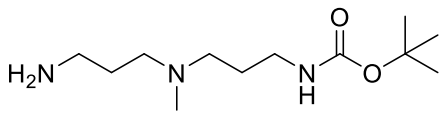

Figure 4.2.1 Structure of Mono-Boc DAPMA

3,3-di-(3-aminopropyl)-*N*-methylamine (DAPMA) (10 mL, 62 mmol) was added to THF (40 mL) and cooled to 0 ˚C. Di-(*tert*-butyl) dicarbonate (Boc_2O) (2.5 g, 11.5 mmol) was dissolved in THF (10 mL) and added dropwise to the stirring amine solution over 2 hours, then stirred for a further 15 minutes. The reaction was then quenched with H_2O (5 mL). The mixture was dried *in vacuo,* the residue taken up in aqueous NaOH (1M) and washed with dichloromethane (20 mL). The organic layer was washed with citric acid solution (1M, 20 mL). The aqueous layers were combined and made alkaline with NaOH (pH > 10, 4M). The product was then extracted using dichloromethane (20 mL). The organic phases were combined and dried with $MgSO_4$ and solvent removed *in vacuo,* to yield a yellow oil. Yield 0.37 g (13 %).^{1}H NMR (400 MHz, MeOD-d_4): δ 3.06 (t, C*H*$_2$NHCO, *J*= 6.6 Hz, 2H); 2.69 (t, C*H*$_2$NH$_2$, J= 7.3 Hz, 2H); 2.41 (m, C*H*$_2$N(CH$_3$), 4H); 2.23 (s, N(C*H*$_3$), 3H); 1.66 (m, C*H*$_2$CH$_2$CO and C*H*$_2$CH$_2$NH$_2$, 4H); 1.43 (s, CC*H*$_3$, 9H). ^{13}C NMR (100 MHz, MeOD-d_4) : δ 158.64 (*C*=O); 79.99 (*C*CH$_3$); 56.56 (*C*H$_2$N(CH$_3$)); 56.38 (*C*H$_2$N(CH$_3$)); 42.40 (N(*C*H$_3$)); 41.05 (*C*H$_2$NHCO); 39.80 (*C*H$_2$NH$_2$); 30.45 (*C*H$_2$CH$_2$NHCO); 28.94 (C*C*H$_3$); 28.32 (*C*H$_2$CH$_2$NH$_2$). ESI-MS; Calcd. [M+H$^+$] ($C_{12}H_{28}O_2N_3$), m/z = 246.2103; Found [M+H$^+$] m/z =246.2179.

4.2.2 Synthesis of Mono-Boc C16-DAPMA.[51]

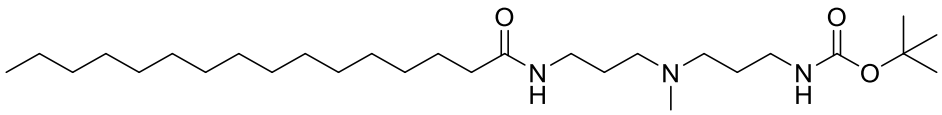

Figure 4.2.2 Structure of Mono-Boc C16-DAPMA

Palmitic acid (0.64 g, 2.50 mmol) was dissolved in dichloromethane (65 mL) and TBTU (0.80 g, 2.56 mmol) and NEt_3 (5 mL) were added to the mixture, which was stirred for 20 minutes. Mono-Boc DAPMA (0.61 g, 2.50 mmol) was dissolved in dichloromethane (10 ml) and added to the mixture, which was left to stir overnight. The solvent was removed in *vacuo* and the product re-dissolved in ethyl acetate (50 mL), then washed three times with 5% potassium bisulphate solution (15 mL), twice with saturated sodium bicarbonate (15 mL), three times with water (15 mL) and twice with saturated brine (15 mL). The solvent was removed *in vacuo* and Mono-Boc C16-DAPMA (0.45 g) was dissolved in a minimum amount of dichloromethane then purified by GPC (dichloromethane), to yield an off white solid. Yield 0.37 g (81 %). ^{1}H NMR (400 MHz, $CDCl_3$): δ 6.74 (br s, CON*H*, 1H); 5.10 (br s, N*H*Boc, 1H); 3.31 (app q, C*H*$_2$NHCO, *J*= 5.8 Hz, 2H); 3.18 (app q, C*H*$_2$NHBoc, *J*= 6.0 Hz, 2H); 2.46 (m, C*H*$_2$N(CH_3), 4H); 2.25 (s, N(C*H*$_3$), 3H); 2.16 (t, C*H*$_2$CONH, *J*= 7.6 Hz, 2H); 1.66 (m, C*H*$_2$CH$_2$N(CH_3) + C*H*$_2$CH$_2$CONH, 6H); 1.44 (s, C(C*H*$_3$)$_3$, 9H); 1.26 (m, CH_3(C*H*$_2$)$_{12}$CH$_2$, 24H); 0.88 (t, C*H*$_3$CH$_2$, *J*= 6.9 Hz, 3H). ^{13}C NMR (100 MHz, $CDCl_3$) : δ 173.35 (*C*=O); 155.97 (*C*=OBoc); 79.07 (*C*(CH_3)$_3$); 55.23 (*C*H$_2$N(CH_3)); 41.31 (N(*C*H$_3$)); 38.91 (*C*H$_2$NHBoc); 37.88 (*C*H$_2$NHCO); 36.74 (*C*H$_2$CONH); 31.82 (*C*H$_2$CH$_2$CH$_3$); 29.59 (*C*H$_2$); 29.44 (*C*H$_2$); 29.38 (*C*H$_2$); 29.31 (*C*H$_2$); 29.26 (*C*H$_2$); 28.31 (*C*H$_2$); 25.82 (*C*H$_2$CH$_2$N(CH_3)); 25.77 (*C*H$_2$CH$_2$CONH); 22.58 (*C*H$_2$); 14.02 (*C*H$_3$CH$_2$). ESI-MS; Calcd. [M+H$^+$] ($C_{28}H_{58}O_3N_3$), m/z = 484.4400; Found [M+H$^+$] m/z =484.4486.

4.2.3 Synthesis of C16-DAPMA.[51]

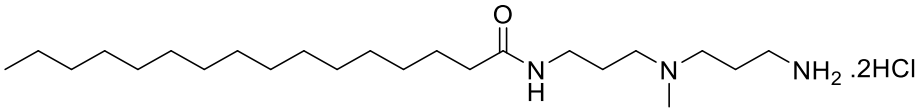

Figure 4.2.3 Structure of C16-DAPMA

Mono-Boc C16-DAPMA (45 mg, 93 µmol) was added to 4M HCl in dioxane (0.35 mL, 1.4 mmol), and the solution was left to stir for 1.5 hours. The solvent was removed *in vacuo* and the product dried under vacuum, to yield a pale orange solid. Yield 35 mg (83 %).^{1}H NMR (400 MHz, MeOD- d_4): δ 3.21 (m, C*H*$_2$NH$_2$ + C*H*$_2$NHCO, 4H); 3.07 (t, C*H*$_2$N(CH$_3$), *J*= 7.6 Hz, 4H); 2.90 (s, NC*H*$_3$, 3H); 2.23 (t, C*H*$_2$CONH, *J*= 7.8 Hz, 2H); 2.15 (app quin, C*H*$_2$CH$_2$N(CH$_3$), *J*= 7.6 Hz, 2H); 1.97 (quin, C*H*$_2$CH$_2$NH$_2$, *J*= 6.9 Hz, 2H); 1.61 (app quin, C*H*$_2$CH$_2$CONH, *J*= 6.9 Hz, 2H); 1.31 (m, CH$_3$(C*H*$_2$)$_{12}$, 24H); 0.90(t, C*H*$_3$CH$_2$, *J*= 6.9 Hz, 3H). ^{13}C NMR (100 MHz, MeOD-d_4) : δ 177.47 (*C*ONH); 55.49, 54.47 (*C*H$_2$N(CH$_3$)); 40.46 (N(*C*H$_3$)); 37.96 (*C*H$_2$CO); 37.18 (*C*H$_2$NHCO); 36.06 (*C*H$_2$NH$_2$); 33.21 (*C*H$_2$CH$_2$CH$_3$); 30.93, 30.62 (*C*H$_2$CH$_2$CH$_2$); 30.54 (*C*H$_2$CH$_2$CH$_2$CO); 27.11 (*C*H$_2$CH$_2$NH); 25.90 (*C*H$_2$CH$_2$CO); 23.88 (*C*H$_2$CH$_2$NH$_2$); 23.67 (*C*H$_2$CH$_3$); 14.58 (*C*H$_3$CH$_2$). APCI-MS; Calcd. [M+H$^+$] ($C_{23}H_{50}ON_3$), m/z = 384.3948; Found [M+H$^+$] m/z =384.3939.

.

4.2.4 Synthesis of 1,3;2,4-dibenzylidene-D-sorbitol-p, p'-dimethylester (DBS-COOCH$_3$). [56]

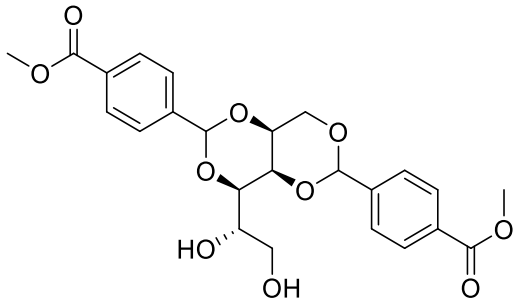

Figure 4.2.4 Structure of DBS-COOCH$_3$

D-sorbitol (4.90 g, 25.3 mmol) was weighed into a three neck round bottom flask fitted with Dean-Stark apparatus. Cyclohexane (35 mL) and methanol (10 mL) were added to the flask, the mixture was stirred with a mechanical stirrer under nitrogen for 20 mins, then heated to 50 ˚C and stirred for a further 20 mins. Methyl 4-formylbenzoate (7.5 g, 45.7 mmol) and p-toluene sulfonic acid hydrate (1.0 g, 52.6 mmol) was dissolved in methanol (20 mL) and the solution was added dropwise to the mixture. The mixture was then heated to 70 ˚C and stirred with a mechanical stirrer for 3 hours; topping up with cyclohexane: methanol solvent mixture when required. The mixture was then cooled to room temperature and washed with ice cold ethanol to remove unreacted starting material. The crude product was then washed with boiling water (3 x 100 mL), and boiling dichloromethane (3 x 100 mL) then filtered after each wash. The resulting white powder was dried under vacuum until the weight became constant, to yield a white powder. Yield 2.43 g (20%). ^{1}H NMR (400 MHz, DMSO-d$_6$): δ 7.98 (m, Ar*H*, 4H); 7.61 (m, ArH, *J*= 8.7 Hz, 4H); 5.76 (s, ArC*H*, 2H); 4.94 (d, CHO*H*, *J*= 6.0 Hz, 1H); 4.48 (t, CH$_2$O*H*, *J*= 6.0 Hz, 1H); 4.22 (m, sugar, 3H); 4.01 (s, sugar, 1H); 3.90 (m, sugar, 1H); 3.85 (m, OC*H$_3$*, 6H); 3.79 (m, sugar, 1H); 3.60 (m, sugar, 1H); 3.47(m, sugar, 1H). ^{13}C NMR (100 MHz, DMSO-d$_6$) : δ 166.04 (*C*OO); 143.36 (Ar-*C*); 143.09 (Ar-*C*); 129.80 (Ar-*C*); 129.74 (Ar-*C*); 129.07 (Ar-*C*H); 128.98 (Ar-*C*H); 126.54 (Ar-*C*H); 98.55 (Acetal-*C*); 98.48 (Acetal-*C*); 77.60 (*C*H); 70.21 (*C*H); 69.34 (*C*H$_2$); 68.55 (*C*H); 67.60 (*C*H); 62.85 (*C*H$_2$); 52.24 (*C*H$_3$). ESI-MS; Calcd. [M+Na$^+$] ($C_{24}H_{26}O_{10}$), m/z = 497.1418; Found [M+Na$^+$] m/z = 497.1432.

4.2.5 Synthesis of p,p'-dihydraza-1,3: 2,4-dibenzylidene-D-sorbitol (DBS-CONHNH$_2$). [56]

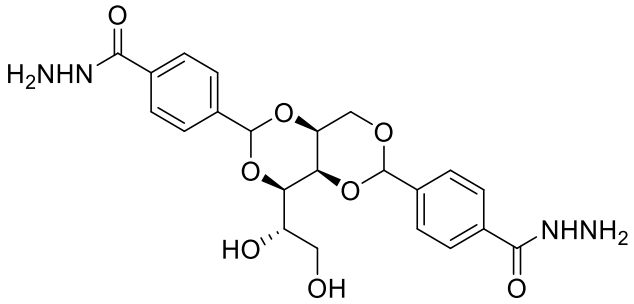

Figure 4.2.5 Structure of DBS-CONHNH$_2$

DBS-COOCH$_3$ (1.10 g, 2.32 mmol) was added to a round bottom flask with THF (50 mL) and hydrazine monohydrate (6 mL, 120 mmol) was added to the reaction mixture. The reaction mixture was heated to 65 ˚C and refluxed overnight. The reaction mixture was filtered and the crude product washed with water (100 mL x 4). This was dried under vacuum to a constant mass, to yield a white powder. Yield 0.97 g (88%). ^{1}H NMR (400 MHz, DMSO-d$_6$): δ 9.81 (s, CON*H*NH$_2$, 2H); 7.83 (d, Ar*H*, *J*= 6.9 Hz, 4H); 7.52 (m, Ar*H*, *J*= 9.2 HZ, 4H); 5.71 (s, ArC*H*, 2H); 4.93 (d, CHO*H*, *J*= 5.3 Hz 1H); 4.47 (m, CONHN*H*$_2$ + CH$_2$O*H*, 5H); 4.19 (m, sugar, 3H); 3.98 (s, sugar, 1H); 3.87 (d, sugar, *J*= 10.0 Hz, 1H); 3.77 (m, sugar, 1H); 3.61 (m, sugar, 1H); 3.45 (m, sugar, 1H). ^{13}C NMR (100 MHz, DMSO-d$_6$) : δ165.60 (*C*=O); 141.24 (Ar-*C*); 140.97 (Ar-*C*); 133.51 (Ar-*C*); 133.43 (Ar-*C*); 126.75 (Ar-*C*H); 126.66 (Ar-*C*H); 126.07 (Ar-*C*H); 98.75 (Acetal-*C*); 98.67 (Acetal-*C*); 77.54 (*C*H); 70.11 (*C*H); 69.31 (*C*H$_2$); 68.46 (*C*H); 67.46 (*C*H); 62.59 (*C*H$_2$). ESI-MS; Calcd. [M+H$^+$] ($C_{22}H_{26}O_8N_4$), m/z = 497.1751; Found [M+H$^+$] m/z = 497.1822.

4.3 Characterisation and Experimental Methods

4.3.1 Section 2.1 C16-DAPMA Micelles

4.3.1.1 Micelle Formation of C16-DAPMA micelles

C16-DAPMA micelles were formed by weighing the appropriate amount of C16-DAPMA and then adding the appropriate amount of solvent or buffer solution, to give the required concentration. Each solution was then sonicated for 15 minutes.

4.3.1.2 DLS diameter Measurement of C16-DAPMA micelles

C16-DAPMA micelles (2.60 mM) were prepared in Tris-HCl buffer (10 mM) and NaCl (150 mM), pH 7.4, by the method mentioned in Section 4.3.1.1 and then filtered using a nylon syringe filter (0.22 μm). The suspension was placed in a disposable cuvette and then recorded at 70 ˚C. Each recorded measurement was an average of 11-15 runs.

4.3.1.3 Zeta potential Measurement of C16-DAPMA micelles

C16-DAPMA micelles (2.60 mM) were prepared in Tris-HCl buffer (10 mM) by the method mentioned in Section 4.3.1.1 and then filtered using a nylon syringe filter (0.22 μm) and placed in a zeta capillary cell (DTS1070), which had been washed with methanol and then four times with water, ensuring the electrodes were fully covered and no air bubbles formed. An electric field was applied using a 4 mW He-Ne laser at 633 nm and each suspension recorded at 25 ˚C. Each recorded measurement was an average of 11-15 runs.

4.3.1.4 TEM Image of C16-DAPMA micelles

C16-DAPMA (2.60 mM) micelles were prepared in Tris-HCl buffer (10 mM) and NaCl (150 mM) by the method mentioned in Section 4.3.1.1 and then filtered using a nylon syringe filter (0.22 μm). The solution was then placed onto a copper grid with Formvar and carbon support film. It was then washed with ultra-pure water and excess water was

removed using filter paper. A negative stain (1% uranyl acetate) was applied and left to dry for 30 minutes; this was to avoid salt crystals being formed.

4.3.1.5 Nile Red Assay of C16-DAPMA micelles

Nile Red Solution (2.5 mM) was prepared in ethanol. A stock solution of C16-DAPMA (100 µM) micelles was prepared in Tris-HCl buffer (10 mM) and NaCl (150 mM) by the method in Section 4.3.1.1. A variety of C16-DAPMA concentrations were prepared by diluting the stock solution with Tris-HCl buffer (10 mM) and NaCl (150 mM). Nile Red (1 µL) was added to each cuvette to give a Nile Red concentration of (2.5 µm) and final volume of 1 mL. The fluorescence emission was measured using excitation wavelength 550 nm. Fluorescence intensity was recorded at 635 nm. This experiment was performed in duplicate.

4.3.1.6 NMR Spectroscopy of C16-DAPMA micelles

A solution of C16-DAPMA (1000 µM, 1 mL) was prepared in D_2O by the method in Section 4.3.1.1. A 5 µL internal spike of dioxane was added to the solution. A proton NMR spectrum was then recorded of the solution.

4.3.2 Section 2.2 C16-DAPMA Micelles with arsenic

4.3.2.1 Aggregate size Measurement

A solution of C16-DAPMA micelles (2.60 mM) was prepared in Tris-HCl buffer (10 mM) and NaCl (150 mM) and sonicated for 15 minutes. Then the solution was filtered using a nylon syringe filter (0.22 µm) and placed in a disposable cuvette. The aggregate diameter of this solution was recorded at 70 ˚C. An aliquot (1 mL) of this solution was added to $Na_2HAsO_4.7H_2O$ to form an arsenate (12.82 mM) solution and then sonicated for 15 minutes. This was filtered using a nylon syringe filter (0.22 µm) and placed in a disposable cuvette. The aggregate diameter of this solution was recorded at 70 ˚C. Each recorded measurement was an average of 11-15 runs.

4.3.2.2 Zeta potential Measurement

C16-DAPMA micelles (2.60 mM) were prepared in Tris-HCl buffer (10 mM) and arsenate (12.82 mM) then sonicated for 15 minutes. Then the solution was filtered using a nylon syringe filter (0.22 µm) and placed in a zeta capillary cell (DTS1070), which had been washed with methanol and then four times with water. It was ensured that the electrodes were fully covered and no air bubbles formed. An electric field was applied using a 4 mW He-Ne laser at 633 nm and each measurement was recorded at 25 ˚C. Each measurement recorded had 11-15 runs per single measurement.

4.3.2.3 Minimum Aggregation Concentration

A solution of C16-DAPMA (2.60 mM) micelles was prepared in Tris-HCl buffer (10 mM) and NaCl (150 mM) and sonicated for 15 minutes. Then the solution was filtered using a nylon syringe filter (0.22 µm) and placed in a disposable cuvette. The aggregate diameter of this solution was recorded at 70 ˚C. An aliquot (1 mL) of this solution was added to $Na_2HAsO_4.7H_2O$ to create an arsenate (19.23 mM) containing solution. This was sonicated for 15 minutes and left in an incubator at 60 ˚C for 15 minutes. The solution was filtered using a nylon syringe filter (0.22 µm) and placed back into the incubator at 60 ˚C.

An aliquot (50 µL) of the arsenate containing solution was then added to the solution in the disposable cuvette of which the aggregate diameter had previously been recorded by DLS. After each addition of the arsenate containing solution, the solution in the disposable cuvette which the aggregate diameter had been previously recorded was shaken and then the new aggregate diameter rerecorded. This was repeated until 1 mL of the arsenate containing solution had been added to the solution in the disposable cuvette of which the aggregate diameter had previously been recorded. Five measurements were taken after each addition of the arsenate containing solution; each measurement recorded had 11-15 runs per single measurement. This was done in duplicate.

4.3.2.4 TEM Images

C16-DAPMA (2.60 mM) micelles were prepared in Tris-HCl buffer (10 mM), NaCl (150 mM) and arsenate (9.62 mM). Then the solution was sonicated and then filtered using a nylon syringe filter (0.22 μM). The solution was then placed onto a copper grid with Formvar and carbon support film, then washed with ultra-pure water and the excess water was removed using filter paper. A negative stain (1% uranyl acetate) was applied and left to dry for 30 minutes; this was to avoid salt crystals being formed.

4.3.3 Section 2.3 and 2.4 DBS-CONHNH$_2$ and DBS-CONHNH$_2$ with C16-DAPMA micelles

4.3.3.1 Formation of DBS-CONHNH$_2$ Hydrogel

A known mass of DBS-CONHNH$_2$ was weighed into a vial and a known amount of water was pipetted into the vial. The vial was then sonicated for 15 minutes; the solution was heated up using a heat gun until complete dissolution occurred of DBS-CONHNH$_2$. The solution was then left to cool to room temperature.

Gel formation was confirmed using the tube inversion test, where the material in a vial is inverted. If the material in question was a hydrogel, it formed a self-supporting network when inverted. If the material in question did not have a self-supporting network it was not a hydrogel.

4.3.3.2 T_{Gel}

DBS-CONHNH$_2$ hydrogels of fixed volumes (0.5 mL) over a variety of concentrations were prepared in glass vials (2.5 mL) by the process in Section 4.3.3.1 and placed in an oil bath. The temperature was steadily increased at a controlled rate of 1 ˚C per minute until 100 ˚C. The inversion test was carried out on the DBS-CONHNH$_2$ hydrogels every 1 ˚C. T_{Gel} value was the temperature the gel network was observed to be no longer self-supporting.

4.3.3.3 TEM Images of DBS-CONHNH$_2$

DBS-CONHNH$_2$ (5.90 mM) gels were made in ultra-pure water by the process described in Section 4.3.3.1. Images were obtained taking one microspatula of each gel, placed onto a copper grid with Formvar and carbon support film. The excess water was removed with filter paper and a negative stain (1% uranyl acetate) was applied to the grid while wet to allow the stain to run across the grid. The grid was left to rest for 30 minutes before taking the images.

4.3.3.4 Rheology of DBS-CONHNH$_2$ hydrogel

DBS-CONHNH$_2$ hydrogels (0.5 mL) at a variety of concentrations were prepared on the rheometer plate by heating up a solution of DBS-CONHNH$_2$ in a vial until the solution was completely dissolved. The hot solution was pipetted into an inverted glass vial (2.5 mL) was held on to the rheometer plate by tape, and left to gel for 30 minutes. After 30 minutes, the tape and vial were removed and excess water removed using blue roll. The rheometer plates had diameter of 20 mm and a gap width of 1.5 mm was applied to the hydrogel. Amplitude sweeps were conducted first using varying shear strain of 1 Hz from 0.05 to 100 %. Frequency sweeps were conducted using shear strain of 0.3 % from 100 to 0.1 Hz.

4.3.3.5 Proton NMR Spectroscopy of DBS-CONHNH$_2$ hydrogel

A DBS-CONHNH$_2$ hydrogel was prepared by the process in Section 4.3.3.1 but substituting H_2O with D_2O. The hot solution was transferred to an NMR tube using a glass pipette. Gelation occurred within the NMR tube.

4.3.3.6 Formation of DBS-CONHNH$_2$ hydrogels with C16-DAPMA micelles

The formation of DBS-CONHNH$_2$ hydrogels containing C16-DAPMA micelles was achieved using a solution of C16-DAPMA micelles prepared as described in Section 4.3.1.1. These were transferred into a vial containing DBS-CONHNH$_2$. This vial was then heated as described in Section 4.3.3.1 then left to cool to room temperature.

All other experimental methods used to investigate the properties of the C16-DAPMA micelles incorporated into DBS-$CONHNH_2$ hydrogels were the same as previously described.

4.3.4 Section 2.5 Arsenate Removal system

4.3.4.1 Colorimetric Method

Solutions of L-ascorbic acid (10.8 %), ammonium molybdate (3 %), antimony potassium tartrate (0.56 %) and sulfuric acid (13.98 %) were prepared in water and then were mixed together in a ratio of 2:2:1:5 to form an indicator solution.

A number of solutions were prepared, each containing different concentrations of arsenate between 20 – 2000 ppb and 1.42 – 7.10 mM, then acidified using HCl (2 %). These were used to construct a calibration curve. An aliquot (0.5 mL) of the indicator solution was added to standard solutions (5 mL), and then left for 15 minutes. An ultraviolet – visible (UV-Vis) spectrum was recorded between 400 – 900 nm.

4.3.4.2 Larger scale hydrogel preparation

A larger quantity of hydrogel (2 mL) was prepared as described in Section 4.3.3.1, by combining two hot gel solutions (each 1 mL) from different vials. These vials (1 mL) contained DBS-$CONHNH_2$ (2.2 mg) and agarose (2.36 mg) and in some cases C16-DAPMA (0.38 mg) and deionised water (1 mL). The first vial was heated after complete dissolution had occurred, and placed in an oil bath at 85 ˚C to stop gelation occurring. This process was repeated for the second vial. The contents of both glass vials were then added simultaneously into an upturned syringe (10 mL) with the nozzle cut off and the plunger in place. This yielded the gel which could then be simple removed if needed using the plunger.

4.3.4.3 Arsenic Removal Experiments

A stock solution of 14.10 µM of arsenate was prepared by adding arsenate dibasic heptahydrate (1.10 mg) to deionised water (250 mL). An aliquot of the arsenate solution (14.10 µM, 15.2 mL) was then removed using a Gilson pipette and made up to 100 mL using deionised water to form an arsenate solution at 298 ppb.

Hydrogel (2 mL) was placed into an arsenate solution (298 ppb, 100 mL) as described in Section 2.5.2.

4.3.4.4 Arsenic Test Kit

Once the hydrogel was removed, the arsenate containing solution (100 mL) was quantified using an arsenic test kit (481396-5) purchased from Simplex Health.

The solution (100 mL) described above for arsenate removal was transferred to a reaction bottle, L-tartaric acid (full quantity included in the test kit) was added and the reaction bottle was shaken for 15 seconds. The potassium peroxymonosulfate (full quantity included in the test kit) was then added and the reaction bottle was shaken for 15 seconds and stood for 2 minutes. The zinc (full quantity included in the test kit) was then added and the reaction bottle was shaken again for 5 seconds. The cap was then replaced with another cap that had a turret, which meant it was possible to inset the mercuric bromide paper into the reaction bottle. The turret was then closed and left for 10 minutes. After 10 minutes, the mercuric bromide paper was then removed. The colour of the mercuric bromide was measured against a colour chart that was then used to quantify the amount of arsenate present in the solution.

4.3.4.5 ICP-MS

Arsenate solution (298 ppb, 100 mL) was prepared by the method described in Section 4.3.4.3 (a glass pipette was used instead of a Gilson pipette). Hydrogel (2 mL) was prepared as described in Section 4.3.4.2 and placed into a solution of arsenate (100 mL,

298 ppb). After 3 days the hydrogel was removed, and 10 mL of the samples were sent for ICP-MS analysis.

4.3.5 Section 2.6 Leaching of C16-DAPMA micelles from DBS-$CONHNH_2$ Hydrogels

A hydrogel (2 mL) of C16-DAPMA (1000 μM), DBS-$CONHNH_2$ (4.68 mM) and agarose (2.36 mg mL^{-1}) was prepared as mentioned in Section 4.3.4.2 and placed in deionised water (100 mL) for 72 hours.

The gel was removed and deionised water removed in *vacuo*. The residue was dissolved in DMSO-d_6 (0.75 mL) with an internal spike of chloroform (10 μL) and a ^1H NMR spectrum was recorded.

5.0 Abbreviations

^{1}H	Proton NMR
^{13}C	Carbon-13 NMR
δ	Delta
µM	Micromolar
µm	Micrometre
µmol	Micromole
APCI	Atmospheric Pressure Chemical Ionisation
As (III)	Arsenite
As (V)	Arsenate
Boc	*Tert*-butyl dicarbonate
Boc_2O	Di-*tert*-butyl dicarbonate
br	Broad (NMR)
CMC	Critical Micelle Concentration
CSS	Critical Shear Stress
d	Doublet (NMR)
DAPMA	3,3'-diamino-*N*-methyldipropylamine
$DBS\text{-}CONHNH_2$	p,p'-dihydraza-1,3: 2,4-dibenzylidene-D-sorbitol
$DBS\text{-}COOCH_3$	1,3;2,4-dibenzylidene-D-sorbitol-p, p'-dimethylester
DLS	Dynamic Light Scattering
DMSO	Dimethyl sulfoxide
$DMSO\text{-}d_6$	Deuterated dimethyl sulfoxide
ESI	Electronic Spray Ionisation
G'	Storage modulus
G''	Loss modulus
GPC	Gel Permeation Chromatography

Hz	Hertz
ICP-MS	Inductively Coupled Plasma - Mass Spectrometry
kV	Kilovolt
LMWGs	Low Molecular Weight Gelators
LVR	Linear Viscoelastic Region
m	Multiplet (NMR)
MAC	Minimum Aggregation Concentration
MBS-$COOCH_3$	Mono-substituted
MeOD-d_4	Deuterated methanol
mg	Milligram
mg g^{-1}	Milligrams of pollutant adsorbed per gram of adsorbent
MGC	Minimum Gelation Concentration
MHz	Megahertz
mL	Millilitre
mM	Millimolar
mmol	Millimole
MOF	Metal-Organic Framework
MOG	Metal-Organic Gel
Mono-Boc DAPMA	*Tert*-butyl 3-((3-aminopropyl)(methyl)amino) propyl carbamate
MS	Mass Spectrometry
mV	Millivolt
mW	Milliwatt
nm	Nanometre
NMP	*N*-methylpyrrolidine
NMR	Nuclear Magnetic Resonance
ppb	Parts per billion
ppm	Parts per million

ppt	Parts per trillion
q	Quartet (NMR)
s	Singlet (NMR
quin	Quintet (NMR)
t	Triplet (NMR)
TBS-$COOCH_3$	Tri-substituted
TBTU	O-(Benzotriazol-1-yl)-N,N,N’,N’-tetramethyluronium
TEM	Transmission Electron Microscopy
THF	Tetrahydrofuran
TLC	Thin Layer Chromatography
TOF	Time of Flight
UV-Vis	Ultraviolet – Visible
WHO	World Health Organisation

6.0 References

1 J. W. Steed and J. L. Atwood, *Supramolecular Chemistry, Second Edition*, Wiley, Chichester, 2009.

2 C. Hao, J. Gao, Y. Wu, X. Wang, R. Zhao, S. Mei, J. Yang, X. Zhai and H. Qiu, *React. Funct. Polym.*, 2018, **122**, 140–147.

3 The Nobel Prize in Chemistry 1987, https://www.nobelprize.org/prizes/chemistry/1987/summary/, (accessed 27 November 2018).

4 The Nobel Prize in Chemistry 2016, https://www.nobelprize.org/prizes/chemistry/2016/summary/, (accessed 27 November 2018).

5 J.M. Lehn, *Angew. Chemie Int. Ed. English*, 1990, **29**, 1304–1319.

6 P. Atkins, T. Overton, J. Rourke, M. Weller and F. Armstrong, *Shriver & Atkins' Inorganic Chemistry*, Oxford University Press, Oxford, 2010.

7 Jean-Marie Lehn Biographical, https://www.nobelprize.org/prizes/chemistry/1987/lehn/biographical/, (accessed 28 December 2018).

8 D. K. Chand, P. Ghosh, R. Shukla, S. Sengupta, G. Das, P. Bandyopadhyay and P. K. Bharadwaj, *Proc. Indian Acad. Sci. Chem. Sci.*, 1996, **108**, 229–233.

9 P. Atkins and J. De Paula, *Atkins' Physical Chemistry*, Oxford University Press, Oxford, 2009.

10 J. N. Israelachvili, D. J. Mitchell and B. W. Ninham, *J. Chem. Soc. Faraday Trans. 2*, 1976, **72**, 1525.

11 A. Aggeli, M. Bell, N. Boden, J. N. Keen, P. F. Knowles, T. C. B. McLeish, M. Pitkeathly and S. E. Radford, *Nature*, 1997, **386**, 259–262. 102

12 D. J. Cornwell and D. K. Smith, *Materials Horizons*, 2015, **2**, 279-293.

13 N. M. Sangeetha and U. Maitra**,** *Chem. Soc. Rev.*, 2005, **34**, 821-836.

14 V. S. Sajisha and U. Maitra, *Chem. Int. J. Chem.*, 2013, **67**, 44–50.

15 J. W. Steed, *Chem. Commun*, 2011, **47**, 1379-1383.

16 P. R. A. Chivers and D. K. Smith, *Chem. Sci.*, 2017, **8**, 7218–7227.

17 E. R. Draper and D. J. Adams, *Chem*, 2017, **3**, 390–410.

18 D. K. Smith, in *Molecular Gels: Structure and Dynamics*, ed. R. G. Weiss, Royal Society Chemistry, London, 2018, ch. 9, pp. 300-371.

19 F. Rodríguez-Llansola, J. F. Miravet and B. Escuder, *Chem. A Eur. J.*, 2010, **16**, 8480–8486.

20 E. J. Howe, B. O. Okesola and D. K. Smith, *Chem. Commun.*, 2015, **51**, 7451–7454.

21 Rajkamal, N. P. Pathak, D. Chatterjee, A. Paul and S. Yadav, *RSC Adv.*, 2016, **6**, 92225–92234.

22 S. Panja, S. Bhattacharya and K. Ghosh, *Langmuir*, 2017, **33**, 8277–8288.

23 C. Rizzo, S. Marullo, P. R. Campodonico, I. Pibiri, N. T. Dintcheva, R. Noto, D. Millan and F. D'Anna, *ACS Sustain. Chem. Eng.*, 2018, **6**, 12453–12462.

24 D. Li, Q. Li, N. Bai, H. Dong and D. Mao, *ACS Sustain. Chem. Eng.*, 2017, **5**, 5598–5607.

25 S. Basak, N. Nandi, S. Paul, I. W. Hamley and A. Banerjee, *Chem. Commun.*, 2017, **53**, 5910–5913.

26 L. Yan, M. Lv, C. Su, L. Zheng, J. Li and Z. Ye, *Soft Matter*, 2017, **13**, 8772–8780.

27 S. Ray, A. K. Das and A. Banerjee, *Chem. Mater.*, 2007, **19**, 1633–1639.

28 J. Wang, H. Wang, Z. Song, D. Kong, X. Chen and Z. Yang, *Colloids Surfaces B Biointerfaces*, 2010, **80**, 155–160. 103

29 F. Rodríguez-Llansola, B. Escuder, J. F. Miravet, D. Hermida-Merino, I. W. Hamley, C. J. Cardin and W. Hayes, *Chem. Commun.*, 2010, **46**, 7960–7962.

30 X. Han, J. Liu, C. Zhao, B. Zhang, X. Xu and J. Song, *J. Colloid Interface Sci.*, 2018, **525**, 177–186.

31 K. K. Carter, H. B. Rycenga and A. J. McNeil, *Langmuir*, 2014, **30**, 3522–3527.

32 B. O. Okesola, S. K. Suravaram, A. Parkin and D. K. Smith, *Angew. Chemie Int. Ed.*, 2016, **55**, 183–187.

33 P. Slavík, D. W. Kurka and D. K. Smith, *Chem. Sci.*, 2018, **9**, 8673-8681.

34 B. O. Okesola, PhD thesis, Univesity of York, 2015.

35 P. L. Smedley and D. G. Kinniburgh, *Appl. Geochemistry*, 2002, **17**, 517–568.

36 A. J. Bora, S. Gogoi, G. Baruah and R. K. Dutta, *J. Environ. Chem. Eng.*, 2016, **4**, 2683–2691.

37 S. D. Richardson and T. A. Ternes, *Anal. Chem.*, 2005, **77**, 3807–3838.

38 J. Yang, H. Zhang, M. Yu, I. Emmanuelawati, J. Zou, Z. Yuan and C. Yu, *Adv. Funct. Mater.*, 2014, **24**, 1354–1363.

39 A. Bora, S. Gogoi, G. Baruah and R. Dutta, *Journal of Environmental Chemical Engineering*, 2016, **4**, 2683-2691.

40 A. K. Shakya and P. K. Ghosh, *J. Clean. Prod.*, 2018, **186**, 304–312.

41 J. R. Kalluri, T. Arbneshi, S. Afrin Khan, A. Neely, P. Candice, B. Varisli, M. Washington, S. McAfee, B. Robinson, S. Banerjee, A. K. Singh, D. Senapati and P. C. Ray, *Angew. Chemie Int. Ed.*, 2009, **48**, 9668–9671.

42 J. Das, P. Sarkar, J. Panda and P. Pal, *J. Environ. Sci. Heal. Part A*, 2014, **49**, 108–115.

43 H. Atallah, M. ELcheikh Mahmoud, A. Jelle, A. Lough and M. Hmadeh, *Dalt. Trans.*, 2018, **47**,799–806.

44 Arsenic, http://www.who.int/en/news-room/fact-sheets/detail/arsenic, (accessed 14 May 2018).

45 K. Cho, B. Y. Shin, H. K. Park, B. G. Cha and J. Kim, *RSC Adv.*, 2014, **4**, 21777–21781.

46 A. F. D. de Namor, N. Al Hakawati, W. A. Hamdan, R. Soualhi, S. Korfali and L. Valiente, *J. Hazard. Mater.*, 2017, **326**, 61–68.

47 J. Sui, L. Wang, W. Zhao and J. Hao, *Chem. Commun.*, 2016, **52**, 6993–6996.

48 Z. Gao, J. Sui, X. Xie, X. Li, S. Song, H. Zhang, Y. Hu, Y. Hong, X. Wang, J. Cui and J. Hao, *AIChE J.*, 2018, **64**, 3719–3727.

49 J. Carter, C. Viviano-Beck, D. Loizeau, J. Bishop and L. Le Deit, *Icarus*, 2015, **253**, 296–310.

50 I. Ali, *Chem. Rev.*, 2012, **112**, 5073–5091.

51 L. E. Fechner, B. Albanyan, V. M. P. Vieira, E. Laurini, P. Posocco, S. Pricl and D. K. Smith, *Chem. Sci.*, 2016, **7**, 4653–4659.

52 A. C. Rodrigo, E. Laurini, V. M. P. Vieira, S. Pricl and D. K. Smith, *Chem. Commun.*, 2017, **53**, 11580–11583.

53 V. M. P. Vieira, A. C. Lima, M. de Jong and D. K. Smith, *Chem. A Eur. J.*, 2018, **24**, 15112–15118.

54 S. M. Bromfield, P. Posocco, C. W. Chan, M. Calderon, S. E. Guimond, J. E. Turnbull, S. Pricl and D. K. Smith, *Chem. Sci.*, 2014, **5**, 1484-1492

55 M. C. A. Stuart, J. C. Van De Pas and J. B. F. N. Engberts, *J. Phys. Org. Chem.*, 2005, **18**, 929–934.

56 B. O. Okesola and D. K. Smith, *Chem. Commun.*, 2013, **49**, 11164.

57 D. Knani and D. Alperstein, *J. Phys. Chem. A*, 2017, **121**, 1113-1120.

58 M. Wallace, J. A. Iggo and D. J. Adams, *Soft Matter*, 2015, **11**, 7739.

59 G. Forsberg, J. W. O'Laughlin, R. G. Megargle and S. R. Koirtyihann, *Anal. Chem.*, 1975, **47**, 1586–1592.

60 S. D. Richardson and T. A. Ternes, *Anal. Chem.*, 2005, **77**, 3807–3838.

61 R. K. Dhar, Y. Zheng, J. Rubenstone and A. Van Geen, *Anal. Chim. Acta*, 2004, **526**, 203–209.

62 D. L. Johnson and M. E. Q. Pilson, *Anal. Chim. Acta*, 1972, **58**, 289–299.

63 A. Baghel, B. Singh, P. Pandey and K. Sekhar, *Anal. Sci.*, 2007, **23**, 135–137.

64 N. I. Goldstone, *Ind. Eng. Chem. Anal. Ed.*, 1946, **18**, 797–799.

65 N. Hidayati, T. Juhaeti and F. Syarif, *HAYATI J. Biosci.*, 2009, **16**, 88–94.